INSIGHTS INTO PATHWAYS OF NITROUS OXIDE GENERATION FROM NOVEL ISOTOPOLOGUE MEASUREMENTS

Thesis by

Paul Macdonald Magyar

In Partial Fulfillment of the Requirements for
the Degree of
Doctor of Philosophy

CALIFORNIA INSTITUTE OF TECHNOLOGY
Pasadena, California

2017
(Defended May 12, 2017)

Paul Macdonald Magyar
ORCID: 0000-0003-0234-247X

ACKNOWLEDGEMENTS

Spending eight years in a place like Caltech and GPS makes it nearly impossible to make a comprehensive accounting of all the amazing people who I have had the opportunity to know and work with. First, I would like to thank my co-advisors, John Eiler and Victoria Orphan for their continuous support for my work, their enthusiasm for it at even the least promising points, and their inspiring example for how to perform science with a great sense of adventure and exploration, while maintaining a high level of rigor. I also want to particularly thank three other GPS professors: George Rossman, who always has a question for every student he encounters; Dianne Newman, for opening the doors of her lab for performing many experiments reported here, and for a boundless enthusiasm; and Joe Kirschvink, whose Ge 136 trips provide such a foundation for the student experience in the Division. Amongst the many GPS students I have had the joy of knowing, I want to specifically mention my classmates Daniel Stolper, Joel Scheingross, Alison Piasecki, Megan Newcombe, Jeff Marlow, and Erika Swanson; my officemates Brooke Dallas and Maggie Osburn; and Sebastian Kopf, who was essential and fun collaborator on experiments in both chapters 3 and 4 of this thesis. Finally, I want to thank my family—my brothers Andrew and John, and especially my parents Elaine and Jim—for setting me on the course into science and through live that has led me here, and for their seemingly infinite love and support in all things.

ABSTRACT

The accumulation of nitrous oxide (N_2O) in the atmosphere is a significant manifestation of human perturbations of the nitrogen cycle. This thesis reports the development and first applications of a novel isotopic technique for characterizing nitrous oxide sources. Chapter 1 describes the development of methods to use the newly available technology of high-resolution dual-inlet multi-collector mass spectrometry to measure six isotopic parameters in nitrous oxide. It reports the standardization and initial biological application of these methods. Chapter 2 presents a model for the generation of isotope effects in an important N_2O generating enzyme, the bacterial nitric oxide reductase; this model and published isotopic constraints are used to provide insights into the mechanism of that enzyme. Chapter 3 describes the six-dimensional isotopic characterization of nitrous oxide from bacterial denitrifiers, while Chapter 4 describes nitrous oxide generated by ammonia oxidizing bacteria.

PUBLISHED CONTENT AND CONTRIBUTIONS

Magyar, P. M, Orphan V. J., and Eiler J. M. (2016). "Measurement of rare isotopologues of nitrous oxide by high-resolution multi-collector mass spectrometry". In: *Rapid Communications in Mass Spectrometry* **30** (17), pp. 1923–1940. doi: 10.1002/rcm.7671.

P.M.M participated in the conception of the project, performed the experiments, prepared the data and analysis, and wrote the manuscript.

TABLE OF CONTENTS

C h a p t e r 1

Measurement of rare isotopologues of nitrous oxide by high-resolution multi-collector mass spectrometry

Paul M. Magyar*, Victoria J. Orphan, and John M. Eiler

Division of Geological and Planetary Sciences, California Institute of Technology, Pasadena, CA 91125, USA

*corresponding author (magyar@caltech.edu)

Published in *Rapid Communications in Mass Spectrometry,* **30,** 1923–1940 (2016), doi:10.1002/rcm.7671

Abstract

RATIONALE: Bulk and position-specific stable isotope characterization of nitrous oxide represents one of the most powerful tools for identifying its environmental sources and sinks. Constraining $^{14}N^{15}N^{18}O$ and $^{15}N^{14}N^{18}O$ will add two new dimensions to our ability to uniquely fingerprint N_2O sources. **METHODS:** We describe a technique to measure six singly and doubly substituted isotopic variants of N_2O, constraining the values of $\delta^{15}N$, $\delta^{18}O$, $\Delta^{17}O$, ^{15}N site preference, and the clumped isotopomers $^{14}N^{15}N^{18}O$ and $^{15}N^{14}N^{18}O$. The technique uses the Thermo MAT 253 Ultra, a high-resolution multi-collector gas source mass spectrometer. It requires 8-10 hours per sample and ~10 micromoles or more of pure N_2O. **RESULTS:** We demonstrate the precision and accuracy of these measurements by analyzing N_2O brought to equilibrium in its position specific and clumped isotopic composition by heating in the presence of a catalyst. Finally, an illustrative analysis of biogenic N_2O from a

denitrifying bacterium suggests its clumped isotopic composition is controlled by kinetic isotope effects in N_2O production. **CONCLUSIONS:** We developed a method for measuring six isotopic variants of N_2O and tested it with analyses of biogenic N_2O. The added isotopic constraints provided by these measurements will enhance our ability to apportion N_2O sources.

Introduction

Nitrous oxide (N_2O) is a trace component of Earth's atmosphere (currently ~328 ppb), acts as a greenhouse gas,[1] and is the main source of reactive nitrogen species that contribute to depletion of stratospheric ozone.[2] Its concentration in tropospheric air is increasing at an average rate of 0.8 ppb/year, which motivates the study of its budget and its environmental biogeochemistry. N_2O is produced mainly by biological processes and consumed by both biological and stratospheric reactions.[3] The biological sources are believed to be primarily associated with the microbial processes of denitrification and nitrification, but the balance of these sources in the environment is poorly constrained.

In denitrification, the anaerobic respiration of nitrate and nitrite by bacteria, fungi, and archaea yields N_2O as an intermediate or final product.[4] Microorganisms capable of complete denitrification can further reduce N_2O to N_2. The aerobic oxidation of ammonia to nitrite by archaeal and bacterial nitrifiers also leads to to leakage of trace amounts of N_2O as a side product,[5-7] likely by different pathways in the bacteria and archaea.[8-11] Nitrifier-denitrification by ammonia oxidizing bacteria has also been shown to produce N_2O during the reduction of nitrite by the denitrification pathway.[12] In addition, abiotic chemical pathways have also been shown to produce N_2O under environmentally relevant conditions

from a variety of nitrogen compounds, including some intermediates of nitrogen-cycling microbes.[13-16] Increases in atmospheric nitrous oxide are thought to be linked to the stimulation of some or all environmental N_2O sources, especially through the fertilization of agricultural fields.[17] Understanding the relative importance of each of these biological sources to environmental N_2O is a critical component for biogeochemical modeling and future mitigation of this greenhouse gas.

Stable isotope measurements can constrain the sources and sinks of N_2O. Because of the asymmetric structure of N_2O, there are three distinct sites for isotopic substitution: terminal N, central N, and O. The incorporation of the stable isotopes of nitrogen (^{14}N and ^{15}N) and oxygen (^{16}O, ^{17}O, and ^{18}O) into these three molecular sites yields twelve distinct isotopic variants of N_2O (see Table 1). All of the singly substituted isotopologues of N_2O have been measured in natural samples, yielding $\delta^{15}N$ (bulk $^{15}N/^{14}N$ ratio, averaged across both positions), $\delta^{18}O$, and $\Delta^{17}O$ values, and the position specific ^{15}N incorporation (site preference)[1]. Each of these parameters constrains different aspects of the natural budget of N_2O. For example, measurements of $\delta^{15}N$ combine information about metabolism and source of N;[18, 19] measurements of $\delta^{18}O$ values have been used to characterize substrate sources and exchange of N_2O precursors with water,[20-22] and measurements of $\Delta^{17}O$ values reflect the influence of mass-independent isotope effects in atmospheric reactions on O incorporated into N_2O.[23] These parameters have been used to characterize N_2O from microbial cultures, soils, waters, and in the atmosphere.[24]

[1] $\delta = (R/R_{ref} - 1)$, where $R = {}^{15}N/{}^{14}N$, $^{17}O/^{16}O$, or $^{18}O/^{16}O$, and R_{ref} refers to N_2 in air for $\delta^{15}N$ and VSMOW for $\delta^{17}O$ and $\delta^{18}O$.

Perhaps the most sophisticated stable isotope constraint on the biogeochemistry of N_2O arises from measurements of differences in $^{15}N/^{14}N$ ratio between the two distinct N sites.[25, 26] Position specific ^{15}N incorporation is typically reported as the site preference (SP; commonly expressed as $\delta^{15}N^{\alpha} - \delta^{15}N^{\beta}$, where α and β denote the central and outer nitrogen atoms, respectively). We will report the site preference as

$$SP = \left(\frac{^{15}R^{\alpha}_{SA}}{^{15}R^{\beta}_{SA}} - 1 \right) = \left(\frac{\delta^{15}N^{\alpha} + 1}{\delta^{15}N^{\beta} + 1} - 1 \right) \cong \delta^{15}N^{\alpha} - \delta^{15}N^{\beta} . \quad (1)$$

This expression is close to equality at values of site preference near 0‰. The site preference in natural and equilibrated samples can potentially vary by tens of per mil. When both site preference and $\delta^{15}N$ values are far from 0‰, such variations can lead to deviations from equality in equation 1 of several per mil. The isotopic composition of the α nitrogen is determined by measuring the ratio of $^{15}N^{16}O$ to $^{14}N^{16}O$ in the NO^+ ions produced by fragmentation of N_2O in the ion source of a mass spectrometer; $^{15}N/^{14}N$ of the β nitrogen is then calculated by mass balance based on an independent measurement of the bulk $\delta^{15}N$ value of the full N_2O molecule,[26] using the relationship

$$^{15}R = \frac{^{15}R^{\alpha} + ^{15}R^{\beta}}{2}. \quad (2)$$

Site preference measurements have provided the most useful isotopic constraints on the microbial sources of N_2O. In particular, measurements of pure cultures suggest that N_2O produced by archaeal[6] and bacterial[27-29] nitrification can be distinguished from that produced by bacterial denitrification.[28, 30] However, ^{15}N site preference (as well as other stable isotope proxies measured to date) cannot distinguish between archaeal and bacterial

nitrification, nor between nitrification and fungal denitrification[31] nor between denitrification and nitrifier-denitrification.[27, 29] Nevertheless, site preference has been deployed as a tool for estimating the contributions of particular microbes to environmental samples.[30, 32-34] In addition, site preference measurements of atmospheric N_2O have been used to describe the contributions of stratospheric sinks and biological sources to regional and global budgets.[35, 36]

There are seven isotopic variants of N_2O that have not been measured previously, all of which contain two or more rare isotopes. Such species are referred to as 'clumped' or 'multiply-substituted' isotopologues.[37, 38] Measurements of the clumped isotope composition of CO_2,[39] methane,[40] and oxygen[41] have been used for geothermometry[42, 43] and for studying kinetic processes such as carbonate mineral growth forced by CO_2 degassing,[44] the formation and cracking of ethane,[45] and the biologically-mediated generation of O_2[46] and methane.[40, 47] A previous theoretical study has suggested that the multiply-substituted isotopologue $^{15}N_2{}^{16}O$ could be used as a tracer of stratospheric processing.[48] In principle, such arguments could be raised for all seven clumped isotopologues of N_2O because each has unique vibrational properties and thus unique thermodynamic stability and chemical-kinetic rates. However, we are not aware of any prior measurement of a clumped isotopologue of N_2O at natural abundances and useful precision.

We describe here the development of mass spectrometric techniques to measure all singly substituted N_2O isotopologues, plus the clumped isotopomers $^{14}N^{15}N^{18}O$ and $^{14}N^{15}N^{18}O$, on a single sample of gas and in a single analytical procedure. This set of measurements is enabled by high resolution gas source mass spectrometry using the Thermo MAT 253 Ultra.[49] We report precision, accuracy, and standardization techniques for this

method, and preliminary measurements of biogenic N_2O from a cultured denitrifying bacteria. A forthcoming paper will present measurements of the compositions of diverse natural, cultured and synthetic N_2O samples.

Systematics of clumped and position-specific isotope effects

A common basis for standardization in clumped isotope geochemistry is a state in which rare isotopes are randomly distributed among all possible isotopic variants of a molecule. (An alternative approach for compounds that are not easily randomized or equilibrated in the laboratory is to instead standardize relative to an arbitrary reference material; e.g., ethane[45]) For an isotopic variant of N_2O, *i*, deviations from a random distribution re reported as Δ_i values:

$$\Delta_i = \left(\frac{{}^i\mathrm{R}}{{}^i\mathrm{R}^*} - 1 \right) \tag{3}$$

where ${}^i\mathrm{R} = [i]/[{}^{14}\mathrm{N}_2{}^{16}\mathrm{O}]$ and ${}^i\mathrm{R}^*$ denotes the value of ${}^i\mathrm{R}$ predicted for that sample if rare isotopes are randomly distributed among all twelve possible isotopic variants. For the clumped isotopomers considered in this study, ${}^{14}\mathrm{N}{}^{15}\mathrm{N}{}^{18}\mathrm{O}$ and ${}^{15}\mathrm{N}{}^{14}\mathrm{N}{}^{18}\mathrm{O}$, the random distribution can be calculated from the ${}^{15}\mathrm{R}$ and ${}^{18}\mathrm{R}$ values of the sample:

$$\mathrm{R}^*_{{}^{14}\mathrm{N}{}^{15}\mathrm{N}{}^{18}\mathrm{O}} = \mathrm{R}^*_{{}^{15}\mathrm{N}{}^{14}\mathrm{N}{}^{18}\mathrm{O}} = {}^{15}\mathrm{R}\,{}^{18}\mathrm{R}\,. \tag{4}$$

Likewise, for position-specific ${}^{15}\mathrm{N}$ incorporation, a randomized distribution of ${}^{15}\mathrm{N}$ is defined to be a 'site preference' of 0‰, that is, $\delta^{15}\mathrm{N}^{\alpha} = \delta^{15}\mathrm{N}^{\beta}$.

At equilibrium, both clumping and position-specific isotope effects are described by homogeneous exchange reactions among isotopic variants of N_2O.[50, 51] As described by

Wang et al.,[50] all position specific and clumped isotope effects for N_2O can be described by a set of eight such homogeneous isotope equilibria. Position specific ^{15}N incorporation is described by the reaction:[50-52]

$$^{15}N^{14}N^{16}O \rightleftharpoons {}^{14}N^{15}N^{16}O. \quad (5)$$

The equilibrium constant for this reaction is

$$K_{\alpha\text{-}\beta} = \frac{\left[{}^{14}N^{15}N^{16}O\right]}{\left[{}^{15}N^{14}N^{16}O\right]} = \frac{{}^{15}R^{\alpha}}{{}^{15}R^{\beta}}. \quad (6)$$

This equilibrium constant can be directly determined from measurements of the values of $\delta^{15}N^{\alpha}$ and $\delta^{15}N^{\beta}$, and can be related to the commonly reported measure of site preference as follows:

$$\ln K_{\alpha-\beta} \cong \left(K_{\alpha-\beta} - 1\right) \quad (7)$$

and, through the Taylor expansion of $\ln K_{\alpha-\beta}$:

$$\delta^{15}N^{\alpha} - \delta^{15}N^{\beta} \cong \left(K_{\alpha-\beta} - 1\right). \quad (8)$$

In this work, we will report site preference as calculated by equation 1, which means that for an equilibrated sample

$$\mathrm{SP} = \left(K_{\alpha-\beta} - 1\right). \quad (9)$$

The values for equilibrium constants such as equation 6 can be calculated through principles of statistical thermodynamics and are dependent only on temperature and the vibrational properties of the relevant isotopologues.[53, 54] Because the vibrational energy for $^{14}N^{15}N^{16}O$ is lower than that of $^{15}N^{14}N^{16}O$ at any given temperature, $^{14}N^{15}N^{16}O$ is favored at equilibrium and is enriched over $^{15}N^{14}N^{16}O$ by 45.7‰ at 300K.[51]

The species that contain one ^{15}N and one ^{18}O can be described by the following reactions:

$$^{14}N^{15}N^{16}O + ^{14}N^{14}N^{18}O \rightleftharpoons ^{14}N^{15}N^{18}O + ^{14}N^{14}N^{16}O \quad (10)$$

$$^{15}N^{14}N^{16}O + ^{14}N^{14}N^{18}O \rightleftharpoons ^{15}N^{14}N^{18}O + ^{14}N^{14}N^{16}O. \quad (11)$$

Each of these reactions corresponds to an equilibrium constant that depends on a concentration of a clumped isotopic species:

$$K_{^{14}N^{15}N^{18}O} = \frac{\left[^{14}N^{15}N^{18}O\right]\left[^{14}N^{14}N^{16}O\right]}{\left[^{14}N^{15}N^{16}O\right]\left[^{14}N^{14}N^{18}O\right]} \quad (12)$$

$$K_{^{15}N^{14}N^{18}O} = \frac{\left[^{15}N^{14}N^{18}O\right]\left[^{14}N^{14}N^{16}O\right]}{\left[^{15}N^{14}N^{16}O\right]\left[^{14}N^{14}N^{18}O\right]}. \quad (13)$$

The values of $\Delta(^{14}N^{15}N^{18}O)$ and $\Delta(^{15}N^{14}N^{18}O)$ can be determined from the three equilibrium constants in equations 6, 12, and 13 as described by Wang et al.[50] For all these reactions, the random distribution, or a Δ_i value of 0‰, is approached at elevated temperatures and reached as an infinite temperature limit.[50] The measurement of the sum of $^{14}N^{15}N^{18}O$ and $^{15}N^{14}N^{18}O$ at mass 47 can be described by

$$\Delta_{^{14}N^{15}N^{18}O + ^{15}N^{14}N^{18}O} = \left(\frac{R_{^{14}N^{15}N^{18}O + ^{15}N^{14}N^{18}O}}{R^{*}_{^{14}N^{15}N^{18}O + ^{15}N^{14}N^{18}O}} - 1\right). \quad (14)$$

For the isotopomers $^{14}N^{15}N^{18}O$ and $^{15}N^{14}N^{18}O$ we define a parameter analogous to ^{15}N site preference, which we call ^{18}O site preference ('SP_{18}'):

$$SP_{18} = \left(\frac{R_{^{14}N^{15}N^{18}O}}{R_{^{15}N^{14}N^{18}O}} - 1\right) = \left(\frac{\Delta\left(^{14}N^{15}N^{18}O\right) + 1}{\Delta\left(^{15}N^{14}N^{18}O\right) + 1} - 1\right). \quad (15)$$

The ^{18}O site preference is equivalent to the equilibrium constant for the reaction

$$^{15}N^{14}N^{18}O \rightleftharpoons {}^{14}N^{15}N^{18}O. \quad (16)$$

In most other isotopic systems where the measurement of clumped isotopologues have been reported (CO_2, carbonate, O_2 and methane), equilibrium exchange reactions comparable to those reviewed above form the basis for both calibrated geothermometers and an absolute reference frame for reporting clumped species.[39, 40, 42, 55] It is likely that the major natural processes that form N_2O do not permit attainment of homogeneous equilibrium with respect to the proportions of isotopologues. Nevertheless, the predicted variation of equilibrium constants with temperature represents a potential reference frame for both clumped and position specific isotope effects, useful as means both of establishing an experimentally verifiable scale for reporting isotopic variations (e.g., Dennis et al.[56]) and of recognizing and quantifying kinetic isotope effects (e.g., Daeron et al.,[44] Stolper et al.,[45, 57] Wang et al.,[47] Yeung et al.,[46]). The most common experimental procedure for equilibrating CO_2, the most commonly-studied clumped isotope system, is heating at low pressures and a temperature of 1000°C. Under these conditions N_2O decomposes rapidly. It is not clear that there is any lower temperature at which gaseous N_2O will exchange isotopes quickly enough to reach a homogeneous isotopic equilibrium but not decompose due to thermal instability. For this reason, we exposed N_2O vapor to high-surface area alumina (Al_2O_3) at 200˚C in an attempt to catalyze isotopic equilibration. Alumina has been shown to be a relatively poor catalyst for the decomposition of N_2O into N_2 and O_2, and it has been suggested that the mechanism for this decomposition proceeds through an adsorbed complex.[58, 59] We hypothesized that this mechanism might allow for the exchange of isotopes on reversible adsorption. The results section of this paper reports experiments confirming this hypothesis.

Another way to produce gases with predictable abundances of every isotopologue is through gas-phase diffusion at low pressures and temperatures, which we expect should follow relatively simple predictions of the kinetic theory of gases. Diffusive fractionations through low density gases can be described by either of two mass laws. When the mean free path of a molecule of diffusing gas is longer than the width of an aperture through which it diffuses, diffusion is described by the Knudsen diffusion law, where the fractionation factor for an isotopologue of mass m_i relative to some reference isotopologue with a different mass is a function of just the masses of the diffusing isotopologues:

$$\alpha_i = \frac{{}^{i}\mathrm{R}_{\mathrm{diffused}}}{{}^{i}\mathrm{R}_{\mathrm{residual}}} = \sqrt{\frac{m_{^{14}\mathrm{N}_2{}^{16}\mathrm{O}}}{m_i}}. \quad (17)$$

Alternatively, at higher gas densities, where the mean free path is shorter, diffusion of N_2O isotopologues through N_2O (mostly composed of $^{14}N_2{}^{16}O$, assuming natural isotope abundances) is described by the mass law for gas-phase interdiffusion:[60, 61]

$$\alpha_i = \frac{{}^{i}\mathrm{R}_{\mathrm{diffused}}}{{}^{i}\mathrm{R}_{\mathrm{residual}}} = \sqrt{\frac{m_i + m_{^{14}\mathrm{N}_2{}^{16}\mathrm{O}}}{2m_i}}. \quad (18)$$

For either Knudsen or gas-phase interdiffusion, the relationship between diffusive mass laws for two isotopologues, *i* and *j,* can be described by its 'mass law', or λ value, where

$$\alpha_{m_i} = \left(\alpha_{m_j}\right)^{\lambda_{m_j/m_i}}. \quad (19)$$

Diffusive mass laws for N_2O predict modest but predictable increases in the clumped isotopic anomaly (Δ_i value) of diffused gas relative to residual gas.[37] Because isotopomers

of N_2O, like $^{14}N^{15}N^{16}O$ and $^{15}N^{14}N^{16}O$, have identical masses, the kinetic theory of gases predicts that diffusive fractionations will not produce any site-preference isotope effects.

Both equilibration and diffusion produce predictable compositions of various isotopologues of nitrous oxide. Together they provide methods for producing predictable abundances of each isotopologue measured in this study, and thus a basis for evaluating the accuracy of our methods. In the results section, we will report the results for N_2O diffused through a small aperture and equilibrated at temperatures ≤200°C.

Sample Preparation

We purified samples of N_2O prior to mass spectrometric analysis by cryogenic distillation on a glass vacuum line. First, N_2O was frozen into a glass trap immersed in liquid nitrogen and exposed to a vacuum pump. This procedure removed non-condensable contaminants like O_2, N_2, and Ar. Second, the trap containing the sample was thawed to room temperature and water was removed by passage over a glass trap immersed in a slurry of dry ice and ethanol, which has a temperature of -60°C to -70°C. Third, biogenic samples and other gases with large amounts of CO_2 were purified by passage over Ascarite (Ascarite-II, Thomas Scientific, Swedesboro, NJ, USA); water generated by the reaction of CO_2 with Ascarite was continually removed by a trap immersed in a dry ice-ethanol slurry. Finally, samples that contain ethanol, methanol, and other organic contaminants were cleaned by passage over a glass trap immersed in an ethanol liquid/ice slurry, which was monitored to ensure that it has a temperature below -110°C.

To produce equilibrated N_2O, we heated samples in quartz breakseals at 200°C in the presence of high surface area alumina (Sigma-Aldrich, St. Louis, MO, USA). About 200 mg

of alumina was placed in each breakseal and capped with quartz wool. The alumina was heated with a natural gas torch under vacuum until the pressure in the system dropped to below 10 millitorr. Once the alumina cooled back to room temperature, about 80 micromoles of N_2O was condensed into the tube by immersing its end in liquid nitrogen, and the tube was then flame sealed with a torch. These tubes were then heated to 200°C for between 3 and 72 hours in a Lindberg furnace, with temperatures monitored by a calibrated thermocouple. On removal from the furnace, tubes were quenched by moving them through the air or placed in the flow of air from an electric fan.[40] Once cooled to room temperature, the tubes were then attached to a vacuum line using a tube-cracker device and broken to release N_2O. This N_2O was purified cryogenically to remove any N_2 and O_2 that may have formed from N_2O; typical recovery of N_2O was 90-100% of the amount condensed in the tube before heating. To generate N_2O equilibrated at lower temperatures, we followed the preceding procedure, but with a first stage at 200°C for 12 hours followed by a second stage of 119 hours to 7 weeks duration, either in an oven (93°C) or a constant-temperature water bath (either 25°C or 50°C). N_2O heated at a lesser temperature without treatment at 200°C first does not exchange in timescales of hours to days; a sample heated at 150°C for ~1 day exhibited unchanged values of all isotopic parameters and 100% of the initial N_2O was recovered. The initial heating step at 200°C appears to be necessary for low-temperature catalysis. A possible explanation for this phenomenon is that the catalyst becomes activated, either by sustained heating at 200°C or by the presence of the small amounts of N_2 and O_2 evolved from the decomposition of N_2O (typically ~5% of the initial N_2O).

To fractionate gases by diffusion, we created a reservoir of N_2O gas (2 L; ≤10 torr) and let it leak to an evacuated vacuum line through a bellows-sealed needle valve (SS-

4BMG; Swagelok, Solon, OH, USA) that was opened the least amount that permitted an appreciable flow of gas. Once gas passed through the valve it was immediately frozen into a glass trap immersed in liquid nitrogen. In each experiment, about 10% of the N_2O in the system was collected, over the course of about an hour, until ~20 micromoles of gas was obtained. Then, the needle valve was sealed and a similar amount of gas was sub-sampled from what remained in the reservoir and vacuum line, for determination of the isotopic composition of the residual N_2O. Both samples were cleaned cryogenically after collection, and were then flame sealed into Pyrex tubes for storage before analysis.

Biogenic N_2O was produced by cultures of the denitrifying bacterium *Pseudomonas aeruginosa* strain PA14, with a genetic knockout (Δ*nosZ*) of the gene for N_2O reduction, making N_2O the final product of denitrification. Triplicate cultures were grown in autoclaved 200 mL bottles containing 150 mL autoclaved, amended Luria-Bertani (LB) medium with 20 mM sodium nitrate (in one liter: 25 g LB mix, Difco, Sparks, MD, USA; 0.78 g KH_2PO_4; 2.50 g K_2HPO_4; and 1.72 g $NaNO_3$, Sigma-Aldrich). Each culture was inoculated with 1 mL aerobic liquid culture and grown until growth ceased, as determined by optical density measurements at 500 nm. At the end of growth, the gas in the headspace was expanded into an evacuated glass sampling volume connected to the bottle and separated from both the bottle and a vacuum line by Teflon vacuum valves. The gas in this sampling volume was then expanded into a vacuum line, where noncondensible gases, CO_2, water, and hydrocarbons were removed as described above.

Measurement Techniques

The measurement technique described below builds on previously published methods for site-specific ^{15}N analysis of N_2O[26] and clumped isotope analysis of CO_2,[39] and makes use of a recently developed high resolution gas source isotope ratio mass spectrometer—the Thermo MAT 253 Ultra (Thermo Scientific, Bremen, Germany).[49] In particular, our method involves three separate analyses of singly and doubly substituted isotopologues of NO^+ fragment ions and N_2O^+ molecular ions, all done at mass resolutions of ~15,000-18,000 (using a 16 μm entrance slit), sufficient to mass resolve species of interest from contaminants (i.e., isotopologues of CO_2 or O_2 that are nearly isobaric with those of N_2O or NO, respectively) or nearly isobaric interferences among isotopologues of N_2O or NO (e.g., $^{15}N^{14}N^{16}O^+$ from $^{14}N_2{}^{17}O^+$).

The measurement of all isotopologues of interest of a single sample requires 8-10 hours, divided between instrument tuning, background measurements, analyses of isotopologues of NO, and analyses of isotopologues of N_2O. Figure 1 presents a summary of the steps required for the measurement. At the start of each day, the Ultra is tuned for sensitivity and resolution, using a 16 μm entrance slit and generally achieving a mass resolving power (M/ΔM, 5/95 % definition) of 15,000-18,000. The most sensitive and important mass resolution problems we encounter are the separation of $^{15}N^{18}O$ from $^{17}O^{18}O$ at mass 33, which requires a mass resolution of ~6100; ($^{14}N^{15}N^{16}O$+$^{15}N^{14}N^{16}O$) from $^{14}N_2{}^{17}O$ at mass 45, which requires a mass resolution of ~6300; $^{14}N_2{}^{18}O$ from $^{15}N_2{}^{16}O$ at mass 46, which requires a mass resolution of ~4500; and ($^{14}N^{15}N^{18}O$+$^{15}N^{14}N^{18}O$) from $^{13}C^{18}O^{16}O$ at mass 47, which requires a mass resolution of ~9600. For each set of measurements, detectors are positioned so that the flat tops of every peak of interest are aligned. This requires moving

detectors between collection of NO^+ and N_2O^+ ions, as well as moving a single collector during the collection of N_2O to collect both ($^{14}N^{15}N^{16}O$+$^{15}N^{14}N^{16}O$) and $^{14}N_2{}^{17}O$ at mass 45. Unless otherwise noted, all measurements described below are collected in dual inlet mode (i.e., repeated comparison of a sample to a standard by cycling a changeover valve block), and every sample/standard comparison ('acquisition') is divided into 10 measurements of a sample, each of which is preceded and followed by a standard measurement. The integration time for each individual sample or standard measurement is 8 seconds.

For the first set of acquisitions, the magnet current and detector positions are set to simultaneously detect four isotopologues of NO, including $^{14}N^{16}O$, $^{15}N^{16}O$, $^{14}N^{18}O$, and $^{15}N^{18}O$. Masses 30, 31, and 32 are detected by Faraday cups (10^{10} Ω, 10^{12} Ω, and 10^{12} Ω amplifiers, respectively) and mass 33 by a secondary electron multiplier (see Figure 2). Under the assumption that all nitrogen in NO^+ fragment ions comes form the interior, α, site in N_2O, the measurements of $^{15}N^{16}O$ and $^{15}N^{18}O$ constrain the proportions of $^{14}N^{15}N^{16}O$ and $^{14}N^{15}N^{18}O$ respectively. This assumption will be tested and refined to account for fragmentation/recombination effects in a subsequent section. The measurement of $^{14}N^{18}O$ provides a constraint on the molecular $\delta^{18}O$ value. Eight acquisitions are collected in this configuration.

Second, the magnet current and detector positions are adjusted so that the detector array collects isotopologues of molecular N_2O^+, including $^{14}N_2{}^{16}O$, $^{14}N_2{}^{17}O$, $^{14}N_2{}^{18}O$, and the sum of $^{14}N^{15}N^{18}O$ and $^{15}N^{14}N^{18}O$. These measurements constrain the bulk molecular $\delta^{17}O$ value; provide a second, redundant constraint on the molecular $\delta^{18}O$ value; and constrain the total abundance of both ^{15}N-^{18}O clumped species. Masses 44, 45, and 46 are detected by

Faraday cups (10^{10} Ω, 10^{12} Ω, and 10^{11} Ω amplifiers, respectively) and mass 47 by a secondary electron multiplier, as shown in Figure 3. Six acquisitions are typically collected in this configuration.

Finally, the position of the mass 45 detector is slightly adjusted to measure the sum of $^{14}N^{15}N^{16}O$ and $^{15}N^{14}N^{16}O$, constraining the bulk molecular $\delta^{15}N$ value. The mass 45 ion beam is detected by a Faraday cup (10^{11} Ω or 10^{12} Ω amplifier). In this configuration, the measurement of $\delta^{18}O$ and the ^{15}N-^{18}O clumped species continues at masses 46 and 47. Two acquisitions are typically collected in this configuration, bringing the total number of acquisitions for $^{18}O/^{16}O$ and the ^{15}N-^{18}O clumped species to eight.

Before each acquisition, a 'mass scan' is collected by varying the magnetic field of the mass spectrometer to cover the region of the image plane where peaks of interest overlap and a magnet setting that is in the flat region for each peak is chosen for the measurement. Sample and reference bellows are pressure balanced manually to be at the same pressure as that scan. Immediately after each acquisition, a series of sixty-second background scans are collected for both sample and reference gases. Because ion beams are narrower than the detectors, it is possible to have two peaks that are formally resolved but are detected at the same time (see Figures 2-3). Therefore, CH_2F, methanol, ethanol, and/or other organic isobars can be collected with the NO or N_2O peaks, depending on exactly where peaks are positioned relative to collectors during analysis. To correct for the contributions of these contaminants that are formally resolved from but collected with the peak of interest, as well as for scattered ions and dark noise detected by electron multipliers, we collect scans just off the main peak, typically ~0.01-0.05 u from the measurement position, with the exact position

chosen based on the mass scan collected before an acquisition. The signal associated with the interference is then subtracted from the measured counts per second for each of the sample and reference measurements from the previous acquisition. The size of this correction is typically between 15% and 20% of the total signal measured at mass 33 and ~1% of the total signal measured at mass 47. At least once per cup configuration, scans are also collected to account for the non-zero baseline and dark noise observed on Faraday cups when gas is flowing but no ion beams are focused on a given detector. These scans are collected by choosing a magnet setting above and below the peaks for masses 30-32 and 44-46 (typically 0.1-0.15 u away from the measurement position) are averaged, and the results are subtracted from the observed voltage at the appropriate Faraday cup. These baseline corrections are typically between -2 and 2 mV, for voltages that range from ~100 mV ($^{14}N_2{}^{17}O$ measured using a 10^{12} Ω amplifier) to ≥10000 mV ($^{14}N_2{}^{16}O$ measured using a 10^{10} Ω amplifier).

There are two potentially significant interferences that are not mass resolved or accounted for by our background corrections: At mass 45, $^{13}C^{16}O_2$ is not resolved from ($^{14}N^{15}N^{16}O$+$^{15}N^{14}N^{16}O$). Therefore, it is necessary to monitor the relative amounts of CO_2 in the sample and reference gases, especially for biogenic gases, where N_2O and CO_2 are produced simultaneously. To estimate the amount of CO_2 in each sample, we measure the ratio of $^{12}C^{16}O_2$ to $^{14}N_2{}^{16}O$ at mass 44. The CO_2 signal is typically 0.6-0.8% of the N_2O signal for both sample and standard, and a given sample-standard pair is typically the same to within 2%. Offsets in pressure between sample and standard lead to an apparent variation in the contribution of CO_2 to the observed $\delta^{15}N$ value of 0.02‰ per percent change in the ratio $^{44}N_2O_{SA}/^{44}N_2O_{REF}$. As described above, CO_2 is removed from samples before they are

introduced to the mass spectrometer by repeated passage over Ascarite. Therefore, it is likely that CO_2 endogenous to the mass spectrometer is the main contributor to the observed N_2O/CO_2 ratios. The measurement of standards described below constrain the accuracy and precision for $\delta^{15}N$ measurements, including any potential contribution from CO_2. Any sample with larger than-usual amounts of CO_2 can be re-scrubbed with Ascarite and reanalyzed; CO_2 can typically be lowered to the level observed in standard gases. In addition, the hydride $^{14}N_2{}^{16}OH$, produced by reaction of N_2O with water in the ion source, is not fully resolved from $^{14}N_2{}^{17}O$. Therefore, it is necessary to dry samples cryogenically before introduction into the mass spectrometer, and to monitor the background levels of water.

Reproducibility and Standardization

Precision

The standard error of each individual measurement (the set of acquisitions described above) typically follows the expectation of counting statistics; Figure 4 shows the observed internal precision relative to the counting-statistics limit calculated for each of the measurements made on N_2O and the NO fragment. The number of counts varies with sample size, and precision varies correspondingly. For measurements of $\delta^{15}N$, $\delta^{17}O$, $\delta^{18}O$, and $\delta^{15}N^{\alpha}$, precision is typically better than 0.1‰. For measurements of $\Delta(^{14}N^{15}N^{18}O+^{15}N^{14}N^{18}O)$, typical values are between 0.1‰ to 0.4‰; and for SP_{18}, between 0.7‰ and 1.3‰. Replicate measurements of standard gases provide a measure of the external precision of the measurements. These values are reported in Tables 2 and 3 and are discussed further in in a subsequent section.

Calculation of 'scrambling factor' for $^{14}N^{15}N^{16}O$ and $^{15}N^{14}N^{16}O$

It has been established that reactions in the ion source scramble isotopes among isotopologues and isotopomers, leading to an interconversion of $^{14}N^{15}N^{16}O$ and $^{15}N^{14}N^{16}O$[25, 26, 62, 63] We follow the approach of Toyoda and Yoshida[26] in correcting for this rearrangement by using a coefficient, y, to represent the fraction of ^{15}N atoms that switch positions in singly substituted isotopomers:

$$^{15}R^{\alpha}_{measured} = \left(1 - y\right)^{15}R^{\alpha}_{true} + y^{15}R^{\beta}_{true}. \quad (20)$$

This expression can be rearranged as

$$^{15}R^{\alpha}_{measured} = 2y\left(^{15}R - {}^{15}R^{\alpha}_{true}\right) + {}^{15}R^{\alpha}_{true} \quad (21)$$

where y varies from 0 for the case of no rearrangement among isotopomers, to 0.5 for the complete randomization of ^{15}N between $^{14}N^{15}N^{16}O$ and $^{15}N^{14}N^{16}O$, to 1 for the physically-unlikely scenario in which every $^{14}N^{15}N^{16}O$ becomes $^{15}N^{14}N^{16}O$ and vice-versa.

We constrained the value of 'y' for our instrument and method by analyzing two previously characterized interlaboratory standards: the Massachusetts Institute of Technology (MIT; Cambridge, MA, USA) reference gas, provided by Shuhei Ono, and our intralaboratory reference gas, for which the values of $\delta^{15}N$ and $\delta^{15}N^{\alpha}$ were measured at the Tokyo Institute of Technology (Yokohama, Japan) by Sakae Toyoda and Naohiro Yoshida. Comparison of our intralaboratory reference standard with the MIT reference gas, which has a preferred $\delta^{15}N$ of -0.24±0.01‰ and $\delta^{15}N^{\alpha}$ of -0.78±0.04‰, yields an apparent $\delta^{15}N^{\alpha}$ value for our reference gas of 6.80±0.16‰, 1 s.d. This measurement constrains the value of

$^{15}R^{\alpha}_{measured}$. The independent analysis of our intralaboratory reference gas by the Tokyo Institute of Technology provides values of $\delta^{15}N^{\alpha}$ = 7.53‰ and $\delta^{15}N^{\beta}$ = 0.89‰ that imply corresponding values of $^{15}R^{\alpha}_{true}$ and $^{15}R^{\beta}_{true}$. Insertion of these three values into equation 20 allows us to solve for *y* on the Ultra at the tuning conditions used for this study as 11.0±0.2% (1 s.d.); all site preference results reported in this study use this value. Repeating this procedure by comparing our intralaboratory standard to the Michigan State University (MSU; East Lansing, MI, USA) reference gas, provided by Nathaniel Ostrom, yields y = 10.8±0.3%. For comparison, previous observations of the scrambling factor range from 8.0% to 10.8%.[25, 26, 29, 64, 65]

Measurement of $\delta^{18}O$, $\delta^{15}N$ and $\delta^{15}N^{\alpha}$ values for interlaboratory standards

We tested the accuracy and full procedural reproducibility of our methods for isotopic properties that have been previously studied using other methods ($\delta^{18}O$, $\delta^{15}N$ and $\delta^{15}N^{\alpha}$) by repeated measurements of intra-laboratory and inter-laboratory N_2O standards. Our intra-laboratory standard, or 'working reference gas' was characterized for $\delta^{15}N$, $\delta^{15}N^{\alpha}$, and $\delta^{18}O$ values (4.21‰, 7.53‰, and 39.96‰, respectively) by S. Toyoda and N. Yoshida at the Tokyo Institute of Technology; their laboratory reference gas is itself standardized against inter-laboratory standards as described in Toyoda and Yoshida[26] and thus can be thought of as a secondary reference material. We also analyzed inter-laboratory standard gases provided by Stanford, MIT, and Michigan State University. The results of these measurements are reported in Table 2.

We find that $\delta^{15}N$ and $\delta^{18}O$ values for all standards match the reported values within the error of the two relevant measurements (i.e., ours and the independent constraint). In

contrast, observed and reported $\delta^{15}N^{\alpha}$ values for interlaboratory standards that were not part of our calibration of the 'scrambling factor' (above) disagree with independently reported values by more than analytical precision (0.44 to 1.08 ‰ average discrepancy, vs. average external errors of 0.2 ‰). We do not have a conclusive explanation for these discrepancies, but in the subsequent section we describe one possibility that arises from our study of thermodynamically equilibrated samples. We also note that similar and greater disagreements in interlaboratory comparisons are a common feature of the current study of ^{15}N site preference in N_2O. A recent community round-robin study determined the site preference of a single N_2O standard in eleven labs and found it to range from 16.6‰ to 25.4‰ (recalculated according to equation 1), even when the measurement of this gas was standardized to accepted reference gases and all data were subjected to a common correction procedure.[66] This inconsistency among laboratories is arguably the greatest challenge to current studies of the stable isotope geochemistry of N_2O, and motivated us to include in this work two experiments that offer some prospect for independent experimental verification of the accuracy of measurements of site preference and clumped isotope properties of N_2O, preferably through some procedure that could be repeated in all laboratories working in this field (i.e., by analogy with the use of heating and water-equilibration experiments to calibrate clumped isotope measurements of CO_2 by Dennis and coworkers[56]). The following sections describe two such experiments: equilibration over a heated catalyst, and diffusive fractionation.

Thermodynamically equilibrated samples and an absolute reference frame

One of the challenges of establishing new methods for measuring intramolecular isotopic distributions, such as site preference and clumping, is determining an absolute reference frame for reporting isotopic variations. In the cases of CO_2 (including CO_2 from carbonate), O_2 and methane, this has been done by driving these compounds to an equilibrated state at known temperature, and assuming that state corresponds to the isotopic distribution predicted by statistical thermodynamic theory. We have attempted the same approach with N_2O by heating gases over alumina, in the hope that this will drive them to equilibrium in their position specific and clumped isotope compositions with minimal disproportionation.

These experiments provide three tests of the attainment of equilibrium. First, as shown in Figures 5-7, we established that gases that differ from one another in initial SP, SP_{18}, and $\Delta(^{14}N^{15}N^{18}O+^{15}N^{14}N^{18}O)$ converge to common values of each of these parameters after heating in the presence of alumina catalyst, and then maintain that value irrespective of the amount of time at that temperature. The experiments performed at 200°C demonstrate both bracketing and time-independence—key benchmarks for proving a thermodynamically equilibrated state has been reached. Second, while we have not shown that the experiments performed at lower temperatures meet these criteria for equilibrium, Table 4 shows that they achieve even larger values of the site preference index, consistent in direction and order of magnitude with theoretical predictions. Notably, the difference between the sample heated to 93°C and the bracketed value at 200°C, after correction for the 'scrambling' effect described above, is 10.7±0.4‰, indistinguishable from the predicted difference at equilibrium of 10.65‰.[50, 51] The samples exposed to alumina at 25°C and 50°C approach but do not reach the predicted composition; we infer this to simply reflect the failure of these

lower temperature experiments to fully reach equilibrium due to the greater kinetic inhibitions to exchange reactions (though perhaps longer time-series studies could document eventual equilibration at these lower temperatures). Finally, a less direct but still relevant observation is that the measurement of triple oxygen isotope compositions of heated samples are consistent with an equilibrium that involves exchange of oxygen between the N_2O and some component of the experimental apparatus. As is shown in Figure 7, N_2O samples with unusual oxygen isotope compositions ($\Delta^{17}O > 0$) evolve on heating toward a $\Delta^{17}O$ of 0‰ (although they do not quite reach 0‰). This suggests N_2O is exchanging oxygen with alumina, adsorbed water and/or glass during heating. If, instead, the changes in isotopic composition these samples undergo during heating were caused by some kinetic isotope effect (say, associated with minor amounts of N_2O disproportionation), they would instead evolve along a line in $\delta^{17}O$-$\delta^{18}O$ space controlled by the mass law of that fractionation (likely with a slope of ~0.515). In that case, $\Delta^{17}O$ would remain approximately constant. The fact that an equilibrium is reached in intramolecular isotopic distribution without achieving a $\Delta^{17}O$ of exactly 0‰ suggests that the reservoir of exchangeable oxygen in the experimental apparatus is large, but not large enough to completely buffer the oxygen in the N_2O.

If we are correct that heating N_2O when exposed to alumina drives it to thermodynamic equilibrium with respect to the SP index on laboratory timescales, this procedure may provide a basis for resolving (or at least exploring) interlaboratory discrepancies in SP measurements. That is, each lab should be capable of generating N_2O equilibrated at two or more known temperatures (and thus known values of the SP index); measurement of these standards should permit the construction of lab-specific transfer

functions relating measured to absolute values of that index (much as for the absolute reference frame for clumped isotope analyses of CO_2).[56] Based on the results of this study, the principal limitation of this approach would be the relatively poor experimental reproducibility of our exchange experiments (e.g., corrected values of SP for long-duration, 200°C experiments have a standard deviation of ±0.4‰). Nevertheless, it seems possible to us that a concerted effort to refine this experiment could improve its reproducibility to levels similar to the nominal state of the art for SP measurements (as good as ±0.05‰, omitting the several-per-mil systematic errors that seem to affect interlaboratory comparisons).

Standardizing $\Delta(^{14}N^{15}N^{18}O+^{15}N^{14}N^{18}O)$ and SP_{18} with equilibrated N_2O

Having demonstrated that heating in the presence of a catalyst drives N_2O to internal equilibrium with respect to the independently calibrated, conventional site preference, we use the same experiments to establish an absolute reference frame for the new measurements of $\Delta(^{14}N^{15}N^{18}O+^{15}N^{14}N^{18}O)$ and SP_{18}. In particular, we assume that N_2O heated in the presence of alumina catalyst until it reaches a time-invariant composition has achieved equilibrium with respect to all of the isotope exchange homogeneous equilibria presented in Wang et al.[50]

A measurement of either of our new measured properties may be compromised by the same 'scrambling' effect described above for conventional site preference. This effect is expected to be small for $\Delta(^{14}N^{15}N^{18}O+^{15}N^{14}N^{18}O)$, where interconversion between $^{14}N^{15}N^{18}O$ and $^{15}N^{14}N^{18}O$ will not be detected because it involves no change in the total abundance of species with this mass. Only ion source scrambling reactions that change the relative abundance of the other 10 isotopologues will effect the observed $\Delta(^{14}N^{15}N^{18}O+^{15}N^{14}N^{18}O)$.

We have no evidence indicating this occurs to measureable extents: the $\Delta(^{14}N^{15}N^{18}O+^{15}N^{14}N^{18}O)$ values of our equilibrated samples are within error of one another and broadly within the limited range of equilibrium values (Figure 8). Therefore, while we develop a correction for the effect of ion source 'scrambling' on SP_{18}, we provisionally assume measurements of $\Delta(^{14}N^{15}N^{18}O+^{15}N^{14}N^{18}O)$ are accurate once standardized against a gas equilibrated to 200°C, using the predicted thermodynamic result from Wang et al.[50] (see Table 4). It seems unlikely to us that this assumption could be in error by more than the analytical precision in this variable, but this issue should be re-visited in future work as we discover materials that vary more widely in this index.

It seems likely to us that the scrambling factor for SP_{18} is indistinguishable from that for SP, simply because it is difficult to think of a reason why the ^{18}O–^{16}O substitution would substantially change the rate of this interconversion. In principle, it should be possible to correct the scrambling effect for both SP and SP_{18} using equilibrated samples because if we have N_2O that has been equilibrated at two or more temperatures, we can solve for the values of a scrambling correction coefficient that results in the theoretically predicted difference in composition between those temperatures.[50, 51] We cannot perform such a calibration with any confidence here because we have only demonstrated bracketing and time-invariance at one temperature (200°C). However, we illustrate the principles behind such a calibration, and examine whether our experimental data at lower temperatures are broadly consistent with the assumption that scrambling occurs at the same rate for SP and SP_{18}.

A linear array of samples with expected and measured compositions (see Figure 9) is described by

$$\Delta_i^{\text{measured}} = f \cdot \Delta_i^{\text{expected}} - \Delta_i^{\text{reference}}, \quad (22)$$

where the factor *f* describes the sample process of scrambling as the factor y described above, and $\Delta_i^{\text{reference}}$ is the difference between the Δ_i of the reference gas and the Δ_i of a random distribution. The slope, *f*, in this space is related to scale compression (*f* > 1) or expansion (*f* < 1) due to rearrangement of atoms among isotopomers; a slope of 1 corresponds to no rearrangement, a slope of 0 to randomization of ^{15}N between α and β positions. To correct isotopomeric composition for scrambling, we use the expression

$$\Delta_i^{\text{corrected}} = \frac{\Delta_i^{\text{measured}}}{f} + \Delta_i^{\text{reference}} \quad (23)$$

.

This correction procedure is presumed to account for the same ion source rearrangement process as the correction of Toyoda and Yoshida,[26] although we have adopted a mathematical formalism based on the Dennis et al.[56] absolute reference frame for CO_2 clumped isotope analysis. To demonstrate the relationship between these alternative approaches, we use our equilibrated samples to describe the rearrangement of $^{14}N^{15}N^{16}O$ and $^{15}N^{14}N^{16}O$. First, to describe these samples, we introduce a parameter Δ_α, which is related to $\delta^{15}N^{\alpha}$ and is analogous to a clumped-isotope Δ value as defined in equation 3:

$$\Delta_\alpha = \left(\frac{^{15}R^{\alpha}}{^{15}R} - 1 \right). \quad (24)$$

The bulk isotopic composition of a sample, ^{15}R, is also the composition that will be observed for both the α and β in the case of a random distribution of ^{15}N among the sites.

Taking equations 22 and 24 together, we find that

$$f = \frac{{}^{15}R^{\alpha}_{measured} - {}^{15}R}{{}^{15}R^{\alpha}_{expected} - {}^{15}R}, \quad (25)$$

and by substituting equation 21 for ${}^{15}R^{\alpha}_{measured}$ in equation 25 (${}^{15}R^{\alpha}_{expected}$ in equation 25 is equivalent to ${}^{15}R^{\alpha}_{true}$ in equation 25) we can solve for *f* in terms of y:

$$f = 1 - 2y. \quad (26)$$

This factor varies from 1 when there is no rearrangement of isotopes among isotopologues (y=0) to 0 when there is a complete scrambling between $^{14}N^{15}N^{16}O$ and $^{15}N^{14}N^{16}O$.

Equilibrated samples at 200°C and 93°C offer an independent test of our estimation of the scrambling factor y. As shown in Figure 9, we find that *f* = 0.770±0.011, which corresponds to y = 11.5±0.6%, consistent with the value estimated from measurements of interlaboratory reference gases, as explained above. It is also shown in Figure 9 that when the equilibrated samples are corrected using the procedure described above, which is independent of the equilibration experiments, they approach a slope of 1, corresponding to no rearrangement.

Another point of comparison for this result comes from measurements of Δ_{47} in carbon dioxide, where the slope of the empirical transfer function described in Dennis et al.[56] is analogous to the inverse of the compression factor *f*. The range of slopes reported for various laboratories performing Δ_{47} measurements is 0.87 to 0.99; all of these values are consistent with less scrambling of mass 47 carbon dioxide isotopologues than of nitrous oxide isotopomers. We also observe a y-intercept of -0.53±0.15, which can be interpreted as an offset between the expected and observed $\delta^{15}N^{\alpha}$ composition of the reference gas of 0.53±0.15‰.

When we follow an analogous procedure for SP_{18}, we observe a value of $f_{14N15N18O}$ of 0.48±0.10, which suggests a much larger likelihood for rearranging ^{18}O-containing isotopomers than ^{16}O-containing isotopomers. We consider this improbable, given the generally small effect of oxygen isotope substitutions on rate constants for common chemical reactions (on the order of one per cent). In addition, when this correction is applied to samples heated at 25°C and 50°C, a SP_{18} in excess of the thermodynamically-predicted value is produced even though SP measurements suggest that these samples have not reached equilibrium (Table 4). Therefore, we conclude that while the sample heated at 93°C may have reached (or at least closely approached) equilibrium in SP, it has not reached equilibrium in SP_{18}. This is plausible because we only performed detailed bracketing and time-series experiments at 200°C, so only at that temperature can we confidently make the interpretation that gases reached an equilibrium distribution in their isotopic composition. If there is a difference in kinetics between the SP and SP_{18} indices, it might be the result of slower rates for N-O bond reordering than for N-N bond reordering. In any event, we believe the temperature dependence of our exchange experiments does not produce a self-consistent and reasonable calibration of site-preference scrambling.

Instead, we assume that rate of rearrangement is the same for both SP and SP_{18}. In other words, we use $f = 0.77\pm0.011$ in equation 23 to adjust measured $\Delta(^{14}N^{15}N^{18}O)$ values. For the replicated and bracketed results at 200°C we then take the $\Delta(^{14}N^{15}N^{18}O)$ composition of the reference gas as the difference between that calculated quantity and the predicted value for 200°C. Then, using this result and the value for $\Delta(^{14}N^{15}N^{18}O+^{15}N^{14}N^{18}O)$ of the reference gas determined above, we solve for $\Delta(^{15}N^{14}N^{18}O)$ of the working gas (Table 5). As shown in Figure 10, samples heated to temperatures of 25°C and 50°C approach equilibrium

compositions in SP_{18}, but they do not obtain equilibrium; this result matches our expectation from SP measurements. Notably, we see that the most anomalous result is the SP_{18} value for the 93˚C equilibration experiment—reinforcing our suspicion that this measurement produced an implausible result.

Diffusion experiments

A second way we can validate our new measurements is to generate fractionations of known amplitudes and/or mass laws through experimental manipulations of analytes; and then to see whether measured changes in composition, after correction for known artifacts such as ion source scrambling, match independent constraints or theoretical predictions. We performed three experiments in which N_2O was diffused through a needle valve and diffused and residual gas were collected and measured. We do not know the size of the aperture through which the gas was diffused. Therefore we cannot be sure whether experiments were conducted in the Knudsen diffusion or gas-phase interdiffusion regime (and in each experiment it could be different). In every case, the measured fractionations between diffused and residual gas are between the predictions for these two end-member possibilities, suggesting that the experimental setup is in an intermediate regime with respect to the ratio of aperture diameter to gas mean free path (i.e., a Knudsen number near one). For this reason we do not have a prediction of the amplitude of the experimentally generated diffusive fractionation. However, since the mass laws for Knudsen and gas-phase interdiffusion are closely similar, we can predict the mass law of the fractionation. Then, we can use the observed difference between diffused and residual gases in values of $\delta^{18}O$ (a measurement

we have already established is measured accurately and precisely by our techniques) to calculate expected differences between diffused and residual gases for the values of $\delta^{15}N$, $\delta^{17}O$, site preference, $\Delta(^{14}N^{15}N^{18}O+^{15}N^{14}N^{18}O)$ and clumped isotope site preference. We compare these predictions to our measured results in Figure 11. Experiments 1 and 2 date from before the introduction of complete background corrections for $\delta(^{14}N^{15}N^{18}O)$ and $\delta(^{14}N^{15}N^{18}O+^{15}N^{14}N^{18}O)$ and therefore results are shown only for $\delta^{15}N$, $\delta^{18}O$, and $\delta^{15}N^{\alpha}$ measurements. Experiment 3 includes the appropriate background correction for CH_2F, CH_3OH, and other isobars on $^{15}N^{18}O$ at mass 33, and is the only one of the three made with sufficient control on the partial pressure of water in the ion source, which is important for achieving the best accuracy and precision for measurements of $\delta^{17}O$. We find the scrambling-corrected differences in composition between residual and diffused gas agree with the mass law of the kinetic theory of gases, within the nominal errors of each measured isotope ratio. However, it is important to note that since the final result is the difference between a diffused and residual gases, it is not sensitive to small variations in the scrambling coefficient. These results demonstrate the ability to measure all isotopologues, including those for which no standards exist, with accuracy.

Representative measurements of biogenic N_2O

In Table 6 we report the $\delta^{15}N$, $\delta^{18}O$, $\Delta^{17}O$, SP, SP_{18}, and $\Delta(^{14}N^{15}N^{18}O+^{15}N^{14}N^{18}O)$ values for nitrous oxide produced by the denitrifying bacterium *Pseudomonas aeruginosa* strain PA14 Δ*nosZ*. Because these bacteria lack the enzyme for nitrous oxide reduction, the isotopic composition of nitrous oxide that accumulates in their cultures does not reflect any N_2O

consumption reactions.[67] The measurements of $\Delta(^{14}N^{15}N^{18}O+^{15}N^{14}N^{18}O)$ and SP_{18} values from these samples provide the first determination of the clumped isotope fingerprint of a biogenic N_2O source.

The conventional site preference (SP) measurements for these samples, –3.67±0.25‰, match previous measurements of N_2O from bacterial denitrifiers (–0.5 to –5.7‰[28, 30]). While the values of $\Delta(^{14}N^{15}N^{18}O+^{15}N^{14}N^{18}O)$ for these gases are consistent with thermodynamic equilibrium near room temperature (0.4‰ at 20°C), the observed values of SP and SP_{18} are not consistent with homogeneous equilibrium at any temperature.[50] Therefore the full, 6-dimensional stable isotope 'fingerprint' demonstrates that at least one step in that synthesis is an irreversible reaction that expresses a kinetic isotope effect. Using prior understanding of the mechanisms of N_2O biosynthesis in denitrification, we may be able to reach more specific conclusions: values of SP and SP_{18} must be set at the point when the N_2O molecule is synthesized by a nitric oxide reductase enzyme. As these properties violate equilibrium, we should conclude that this particular forward reaction expresses a kinetic isotope effect. Our results present a target for fitting mechanistic models of this reaction step.

On the other hand, $\Delta(^{14}N^{15}N^{18}O+^{15}N^{14}N^{18}O)$, a property that approaches or equals equilibrium in these samples, is influenced by the abundance of ^{15}N-^{18}O bonds, and may record information set at any of several steps in N_2O synthesis where N-O bonds are formed or exchanged: from the nitrate provided as a substrate, or from any (or all) of the three reductive reactions from nitrate to nitrite to nitric oxide to nitrous oxide. If any of these reactions is highly reversible or involves equilibration with water, as is commonly observed in denitrification,[68] there is the possibility that the distribution of ^{15}N-^{18}O bonds achieves an

equilibrium composition in that step and that this equilibrium is not disturbed by the kinetic isotope effects controlling the final step of formation of N—N bonds, and is therefore recorded in the $\Delta(^{14}N^{15}N^{18}O+^{15}N^{14}N^{18}O)$ value.

Summary and Conclusions

We have described techniques to measure six distinct isotope ratios on a single sample of nitrous oxide, including the first measurements of the clumped isotopomers $^{14}N^{15}N^{18}O$ and $^{15}N^{14}N^{18}O$. We have documented the precision and reproducibility of this technique and have introduced the use of activated alumina as a catalyst for equilibration of N_2O to produce standards with elevated and predictable ^{15}N site preference and to calibrate the measurement of $\Delta(^{14}N^{15}N^{18}O+^{15}N^{14}N^{18}O)$ and SP_{18}. Measurements of N_2O produced by a denitrifying bacterium are consistent with a production pathway primarily of irreversible reactions, but with the possibility for some parameters to be set in reversible, equilibrium reactions. These measurements provide the first fingerprint of the composition of clumped isotopologues in a biogenic sample of N_2O. The addition of these isotopic constrains may provide new insights into the environmental sources and sinks of N_2O.

Acknowledgements

This work was supported by a grant from the Gordon and Betty Moore Foundation Marine Microbiology Initiative (Grant #3306) and by NSF-EAR. We thank Dianne Newman for providing the *P. aeruginosa* ΔnosZ mutant and for the use of her laboratory; Sebastian Kopf for aid in microbial culturing; Nami Kitchen for assistance in the laboratory; and Daniel Stolper, Alison Piasecki, and Matthieu Clog for helpful discussions. We thank Karen

Casciotti, Shuhei Ono, and Nathaniel Ostrom for providing calibrated reference samples and Sakae Toyoda and Naohiro Yoshida for measuring the isotopic composition of our reference gas. Finally, we thank Nathaniel Ostrom for helpful comments on an an earlier draft of this manuscript, as well as two anonymous reviewers for their comments.

References

[1] G. Myrhe, D. Shindell, F.-M. Bréon, W. Collins, J. Fuglestvedt, J. Huang, D. Koch, J.-F. Lamarque, D. Lee, B. Mendoza, T. Nakajima, A. Robock, G. Stephens, T. Takemura, H. Zhang. Anthropogenic and Natural Radiative Forcing. In *Climate Change 2013: The Physical Science Basis. Contribution of Working Group I to the Fifth Assessment Report of the Intergovernmental Panel on Climate Change* **2013**, pp. 1–82.

[2] A. R. Ravishankara, J. S. Daniel, R. W. Portmann. Nitrous Oxide (N_2O): The Dominant Ozone-Depleting Substance Emitted in the 21st Century. *Science* **2009**, *326*, 123.

[3] L. Y. Stein, Y. L. Yung. Production, Isotopic Composition, and Atmospheric Fate of Biologically Produced Nitrous Oxide. *Annu. Rev. Earth Planet. Sci.* **2003**, *31*, 329.

[4] W. G. Zumft. Cell Biology and Molecular Basis of Denitrification. *Microbiol. Molec. Biol. Rev.* **1997**, *61*, 533.

[5] T. J. Goreau, W. A. Kaplan, S. C. Wofsy, M. B. McElroy, F. A. Valois, S. W. Watson. Production of NO_2^- and N_2O by Nitrifying Bacteria at Reduced Concentrations of Oxygen. *Appl. Environ. Microbiol.* **1980**, *40*, 526.

[6] A. E. Santoro, C. Buchwald, M. R. McIlvin, K. L. Casciotti. Isotopic Signature of Marine Ammonia-Oxidizing Archaea. *Science* **2011,** *333*, 1282.

[7] C. R. Löscher, A. Kock, M. Könneke, J. LaRoche, H. W. Bange, R. A. Schmitz. Production of oceanic nitrous oxide by ammonia-oxidizing archaea. *Biogeosciences* **2012**, *9*, 2419.

[8] M. Stieglmeier, M. Mooshammer, B. Kitzler, W. Wanek, S. Zechmeister-Boltenstern, A. Richter, C. Schleper. Aerobic nitrous oxide production through N-nitrosating hybrid formation in ammonia-oxidizing archaea. *ISME J.* **2014,** *8*, 1135.

[9] W. Martens-Habbena, W. Qin, R. E. A. Horak, H. Urakawa, A. J. Schauer, J W. Moffett, E. V. Armbrust, A. E. Ingalls, A. H. Devol, D. A. Stahl. The production of nitric oxide by marine ammonia-oxidizing archaea and inhibition of archaeal ammonia oxidation by a nitric oxide scavenger. *Environ. Microbiol.* **2015,** *17*, 2261.

[10] J. A. Kozlowski, M. Stieglmeier, C. Schleper, M. G. Klotz, L. Y. Stein. Pathways and key intermediates required for obligate aerobic ammonia-dependent chemolithotrophy in bacteria and Thaumarchaeota. *ISME J.* **2016,** DOI:10.1038/ismej.2016.2

[11] L. Hink, G. W. Nichol, J. I. Prosser. Archaea produce lower yields of N_2O than bacteria during aerobic ammonia oxidation in soil. *Environ. Microbiol.* **2016,** DOI:10.1111/1462-2920.13282.

[12] N. Wrage, G. L. Veltholf, M. L. van Beusichem, O. Oenema. Role of nitrifier

denitrification in the production of nitrous oxide. *Soil Biol. Biochem.* **2001**, *33*, 1723.

[13] J. Heil, B. Wolf, N. Brüggemann, L. Emmenegger, B. Tuzson, H. Vereecken, J. Mohn. Site-specific ^{15}N isotopic signatures of abiotically produced N_2O. *Geochim. Cosmochim. Acta* **2014,** *139*, 72.

[14] W. F. Harper Jr., Y. Takeuchi, S. Riya., M. Hosomi, A. Terada. Novel abiotic reactions increase nitrous oxide production during partial nitrification: Modeling and experiments. *Chem. Engineer. J.* **2015,** *281,* 1017.

[15] X. Zhu-Barker, A. R. Cavazos, N. E. Ostrom, W. R. Horwath, J. B. Glass. The importance of abiotic reactions for nitrous oxide production. *Biogeochem.* **2015,** *126*, 251.

[16] C. Buchwald, K. Grabb, C. M. Hansel, S. D. Wankel. Constraining the role of iron in environmental nitrogen transformations: Dual stable isotope systematics of abiotic NO_2^- reduction by Fe(II) and its production of N_2O. *Geochim. Cosmochim. Acta* **2016,** *186*, 1.

[17] D. Fowler, K. Pilegaard, M. A. Sutton, P. Ambus, M. Raivonen, J. Duyzer, D. Simpson, H. Fagerli, S. Fuzzi, J. K. Schjoerring, C. Granier, A. Neftel, I. S. A. Isaksen, P. Laj, M. Maione, P. S. Monks, J. Burkhardt, U. Daemmgen, J. Neirynck, E. Personne, R. Wichink-Kruit, K. Butterbach-Bahl, C. Flechard, J. P. Tuovinen, M. Coyle, G. Gerosa, B. Loubet, N. Altimir, L. Gruenhage, C. Ammann, S. Cieslik., E. Paoletti, T. N. Mikkelsen, H. Ro-Poulsen, P. Cellier, J. N. Cape, L. Horváth, F. Loreto, Ü Niinemets, P. I. Palmer, J. Rinne, P. Misztal, E. Nemitz, D. Nilsson, S. Pryor, M. W. Gallagher, T. Vesala, U. Skiba, N. Brüggemann, S. Zechmeister-Boltenstern, J. Williams., C. O. Dowd, M. C. Facchini, G. de Leeuw, A. Flossman, N. Chaumerliac, J. W. Erisman. Atmospheric composition change: Ecosystems–Atmosphere interactions. *Atmos. Environ.* **2009**, *43*, 5193.

[18] N. Yoshida. ^{15}N-depleted N_2O as a product of nitrification. *Nature* **1988**, *335*, 528.

[19] K. Kim, H. Craig. Nitrogen-15 and Oxygen-18 Characteristics of Nitrous Oxide: A Global Perspective. *Science* **1993**, *262*, 1855.

[20] D. M. Snider, J. J. Venkiteswaran, S. L. Schiff, J. Spoelstra. Deciphering the oxygen isotopic composition of nitrous oxide produced by nitrification. *Global Change Biol.* **2012,** *18*, 356.

[21] D. M. Snider, J. J. Venkiteswaran, S. L. Schiff, J. Spoelstra. A new mechanistic model of $\delta^{18}O$-N_2O formation by denitrification. *Geochim. Cosmochim. Acta* **2013**, *112*, 102.

[22] L. Rohe, T.-H. Anderson, G. Braker, H. Flessa, A. Giesemann, N. Wrage-Mönnig, R. Well. Fungal oxygen exchange between denitrification intermediates and water. *Rapid Commun. Mass Spectrom.* **2013**, *28*, 377.

[23] S. S. Cliff, M. Thiemens. The $^{18}O/^{16}O$ and $^{17}O/^{16}O$ Ratios in Atmospheric Nitrous Oxide: A Mass-Independent Anomaly. *Science* **1997**, *278*, 1774.

[24] D. M. Snider, J. J. Venkiteswaran, S. L. Schiff, J. Spoelstra. From the Ground Up: Global Nitrous Oxide Sources are Constrained by Stable Isotope Values. *PLoS ONE* **2015,** DOI:10.1371/journal.pone.0118954.

[25] C. Brenninkmeijer, T. Röckmann. Mass spectrometry of the intramolecular nitrogen isotope distribution of environmental nitrous oxide using fragment-ion analysis. *Rapid Commun. Mass Spectrom.* **1999**, *13*, 2028.

[26] S. Toyoda, N. Yoshida. Determination of Nitrogen Isotopomers of Nitrous Oxide on a

Modified Isotope Ratio Mass Spectrometer. *Anal. Chem.* **1999**, *71*, 4711.

[27] R. Sutka, N. Ostrom, P. Ostrom, H. Gandhi, J. Breznak. Nitrogen isotopomer site preference of N_2O produced by Nitrosomonas europaea and Methylococcus capsulatus Bath. *Rapid Commun. Mass Spectrom.* **2003**, *17*, 738.

[28] R. Sutka, N. Ostrom, P. Ostrom, J. Breznak, H. Gandhi, A. Pitt, F. Li. Distinguishing nitrous oxide production from nitrification and denitrification on the basis of isotopomer abundances. *Appl. Environ. Microbiol.* **2006**, *72*, 638.

[29] C. Frame, K. L. Casciotti Biogeochemical controls and isotopic signatures of nitrous oxide production by a marine ammonia-oxidizing bacterium. *Biogeosciences* **2010**, *7*, 2695.

[30] N. E. Ostrom, R. L. Sutka, P. H. Ostrom, A. S. Grandy, K. M. Huizinga, H. Gandhi, J. C. von Fischer, G. P. Robertson. Isotopologue data reveal bacterial denitrification as the primary source of N_2O during a high flux event following cultivation of a native temperate grassland. *Soil Biol. Biochem.* **2010**, *42*, 499.

[31] R. L. Sutka, G. C. Adams, N. E. Ostrom, P. H. Ostrom. Isotopologue fractionation during N_2O production by fungal denitrification. *Rapid Commun. Mass Spectrom.* **2008**, *22*, 3989.

[32] T. Kato, S. Toyoda, N. Yoshida, Y. Tang, E. Wada. Isotopomer and isotopologue signatures of N_2O produced in alpine ecosystems on the Qinghai-Tibetan Plateau. *Rapid Commun. Mass Spectrom.* **2013**, *27*, 1517.

[33] S. Toyoda, N. Yoshida, K. Koba. Isotopocule Analysis of Biologically Produced Nitrous Oxide in Various Environments. *Mass Spectrom. Rev.* **2015,** DOI:10.1002/mas.21459.

[34] C. H. Frame, E. Deal, C. D. Nevison, K. L. Casciotti. N_2O production in the eastern South Atlantic: Analysis of N_2O stable isotopic and concentration data. *Global Biogeochem. Cycles* **2014,** *28*, 1262.

[35] N. Yoshida, S. Toyoda. Constraining the atmospheric N_2O budget from intramolecular site preference in N_2O isotopomers. *Nature* **2000**, *405*, 330.

[36] S. Park, R. Croteau, K. A. Boering, D. M. Etheridge, D. Ferretti, P. J. Fraser, K.-R. Kim, P. B. Krummel, R. L. Langenfelds, T. D. van Ommen, L. P. Steele, C. M. Trudinger. Trends and seasonal cycles in the isotopic composition of nitrous oxide since 1940. *Nat. Geosci.* **2012**, *5*, 261.

[37] J. M. Eiler. "Clumped-isotope" geochemistry—The study of naturally-occurring, multiply-substituted isotopologues. *Earth Planet. Sci. Lett.* **2007**, *62*, 309.

[38] J. M. Eiler. The Isotopic Anatomies of Molecules and Minerals. *Annu. Rev. Earth Planet. Sci.* **2013**, *41*, 411.

[39] J. M. Eiler, E. A. Schauble. $^{18}O^{13}C^{16}O$ in Earth's atmosphere. *Geochim. Cosmochim. Acta* **2004**, *68*, 4767.

[40] D. A. Stolper, A. L. Sessions, A. A. Ferreira, E. V. Santos Neto, A. Schimmelmann, S. S. Shusta, D. L. Valentine, J. M. Eiler. Combined ^{13}C–D and D–D clumping in methane: Methods and preliminary results. *Geochim. Cosmochim. Acta* **2014**, *126*, 169.

[41] L. Y. Yeung, E. D. Young, E. A. Schauble. Measurements of $^{18}O^{18}O$ and $^{17}O^{18}O$ in the atmosphere and the role of isotope-exchange reactions. *J. Geophys. Res.* **2012**, *117*, D18306.

[42] P. Ghosh, J. F. Adkins, H. P. Affek, B. Balta, W. Guo, E. A. Schauble, D. P. Schrag, J.

M. Eiler. ^{13}C-^{18}O bonds in carbonate minerals: A new kind of paleothermometer. *Geochim. Cosmochim. Acta* **2006**, *70*, 1439.

[43] D. A. Stolper, M. Lawson, C. L. Davis, A. A. Ferreira, E. V. Santos Neto, G. S. Ellis, M. D. Lewan, A. M. Martini, Y. Tang, M. Schoell, A. L. Sessions, J. M. Eiler. Formation temperatures of thermogenic and biogenic methane. *Science* **2014**, *344*, 1500.

[44] M. Daeron, W. Guo, J. Eiler, D. Genty, D. Blamart, R. Boch, R. Drysdale, R. Maire, K. Wainer, G. Zanchetta. $^{13}C^{18}O$ clumping in speleothems: Observations from natural caves and precipitation experiments. *Geochim. Cosmochim. Acta* **2011**, *75*, 3303.

[45] M. Clog M., A. Martini, M. Lawson, J. Eiler. Doubly ^{13}C-substituted ethane in shale gases, Goldschmidt Conference. *Mineralogical Magazine,* **2014**, Sacramento, CA, p. 435.

[46] L. Y. Yeung, J. L. Ash, E. D. Young. Biological signatures in clumped isotopes of O_2. *Science* **2015**, *348*, 431.

[47] D. T. Wang, D. S. Gruen, B. S. Lollar, K.-U. Hinrichs, L. C. Stewart, J. F. Holden, A. N. Hristov J. W. Pohlman, P.L. Morrill, M. Könneke, K. B. Delwiche, E. P. Reeves, C. N. Sutcliffe, D. J. Ritter, J. S. Seewald, J. C. McIntosh, H. F. Hemond, M. D. Kubo, D. Cardace, T. M. Hoeher, S. Ono. Nonequilibrium clumped isotope signals in microbial methane. *Science* **2015**, *348*, 428.

[48] J. Kaiser, T. Röckmann, C. A. M. Brenninkmeijer. Assessment of $^{15}N^{15}N^{16}O$ as a tracer of stratospheric processes. *Geophys. Res. Lett.* **2003**, *30*, 1046.

[49] J. M. Eiler, M. Clog, P. Magyar, A. Piasecki, A. Sessions, D. Stolper, M. Deerberg, H.-J. Schlueter, J. Schwieters. A high-resolution gas-source isotope ratio mass spectrometer. *Int. J. Mass Spectrom.* **2013**, *35*, 45.

[50] Z. Wang, E. A. Schauble, J. M. Eiler. Equilibrium thermodynamics of multiply substituted isotopologues of molecular gases. *Geochim. Cosmochim. Acta* **2004**, *68*, 4779.

[51] M. A.Webb, T. F. Miller. Position-specific and clumped stable isotope studies: comparison of the urey and path-integral approaches for carbon dioxide, nitrous oxide, methane, and propane. *J. Phys. Chem. A* **2014**, *118*, 467.

[52] J. Bigeleisen, L. Friedman. The Infra-Red Spectra of $N^{15}N^{14}O^{16}$ and $N^{14}N^{15}O^{16}$. Some Thermodynamic Properties of the Isotopic N_2O Molecules. *J. Chem. Phys.* **1950**, *18*, 1656.

[53] J. Bigeleisen, M. Mayer. Calculation of equilibrium constants for isotopic exchange reactions. *J. Chem. Phys.* **1947**, *15*, 261.

[54] H. C. Urey. The thermodynamic properties of isotopic substances. *J. Chem. Soc.* **1947**, 562.

[55] L. Y. Yeung, J. L. Ash, E. D. Young. Rapid photochemical equilibration of isotope bond ordering in O_2. *J. Geophys Res. Atmos.* **2014**, *119,* 10522.

[56] K. J. Dennis, H. P. Affek, B. H. Passey, D. P. Schrag, J. M. Eiler. Defining an absolute reference frame for 'clumped' isotope studies of CO_2. *Geochim. Cosmochim. Acta* **2011**, *75*, 7117.

[57] D. A. Stolper, A. M. Martini, M. Clog, P. M. Douglas, S. S. Shusta, D. L. Valentine, A. L. Sessions, J. M. Eiler. Distinguishing and understanding thermogenic and biogenic sources of methane using multiply substituted isotopologues. *Geochim. Cosmochim. Acta* **2015**, *161*, 219.

[58] E. R. S. Winter. The Decomposition of N_2O on Oxide Catalysts III. The Effect of O_2. *J. Catal.* **1974**, *34*, 431.
[59] E. R. S. Winter. The Decomposition of Nitrous Oxide on Metallic Oxides. *J. Catal.* **1970**, *19*, 32.
[60] H. Craig. The geochemistry of the stable carbon isotopes. *Geochim. Cosmochim. Acta* **1953**, *3*, 53.
[61] T. E. Cerling, D. K. Solomon, J. Quade, J. R. Bowman. On the isotopic composition of carbon in soil carbon dioxide. *Geochim. Cosmochim. Acta* **1991**, *55*, 3403.
[62] L. Friedman, J. Bigeleisen. Oxygen and Nitrogen Isotope Effects in the Decomposition of Ammonium Nitrate. *J. Chem. Phys.* **1950**, *18*, 1325.
[63] M. Westley, B. Popp, T. Rust. The calibration of the intramolecular nitrogen isotope distribution in nitrous oxide measured by isotope ratio mass spectrometry. *Rapid Commun. Mass Spectrom.* **2007**, *21*, 391.
[64] S. Park, E. L. Atlas, K. A. Boering. Measurement of N_2O isotopologues in the stratosphere: Influence of transport on the apparent enrichment factors and the isotopologue fluxes to the troposphere. *J. Geophys. Res.* **2004**, *109*, D01305, DOI:10.1029/2003JD003731.
[65] E. Harris, D. D. Nelson, W. Olszewski, M. Zahniser, K. E. Potter, B. J. McManus, A. Whitehill, R. G. Prinn, S. Ono. Development of a Spectroscopic Technique for Continuous Online Monitoring of Oxygen and Site-Specific Nitrogen Isotopic Composition of Atmospheric Nitrous Oxide. *Anal. Chem.* **2014,** *86*, 1726.
[66] J. Mohn, B. Wolf, S. Toyoda S., C.-T. Lin, M. C. Liang, N. Brüggemann, H. Wissel, A. E. Steiker, J. Dyckmans, L. Szwec, N. E. Ostrom, K. L. Casciotti, M. Forbes, A. Giesemann, R. Well, R. R. Doucett, C. T. Yarnes, A. R. Ridley, J. Kaiser, N. Yoshida. Interlaboratory assessment of nitrous oxide isotopomer analysis by isotope ratio mass spectrometry and laser spectroscopy: current status and perspectives. *Rapid Commun. Mass Spectrom.* **2014**, *28*, 1995.
[67] N. E. Ostrom, A. Pitt, R. Sutka, P. H. Ostrom, A. S. Grandy, K. M. Huizinga, G. P. Robertson. Isotopologue effects during N_2O reduction in soils and in pure cultures of denitrifiers. *J.Geophys. Res.* **2007**, *112*, G02005, DOI:10.1029/2006JG000287.
[68] D. M. Kool, N. Wrage, O. Oenema, D. Harris, J. W. Van Groenigen. The ^{18}O signature of biogenic nitrous oxide is determined by O exchange with water. *Rapid Commun. Mass Spectrom.* **2009**, *23*, 104.

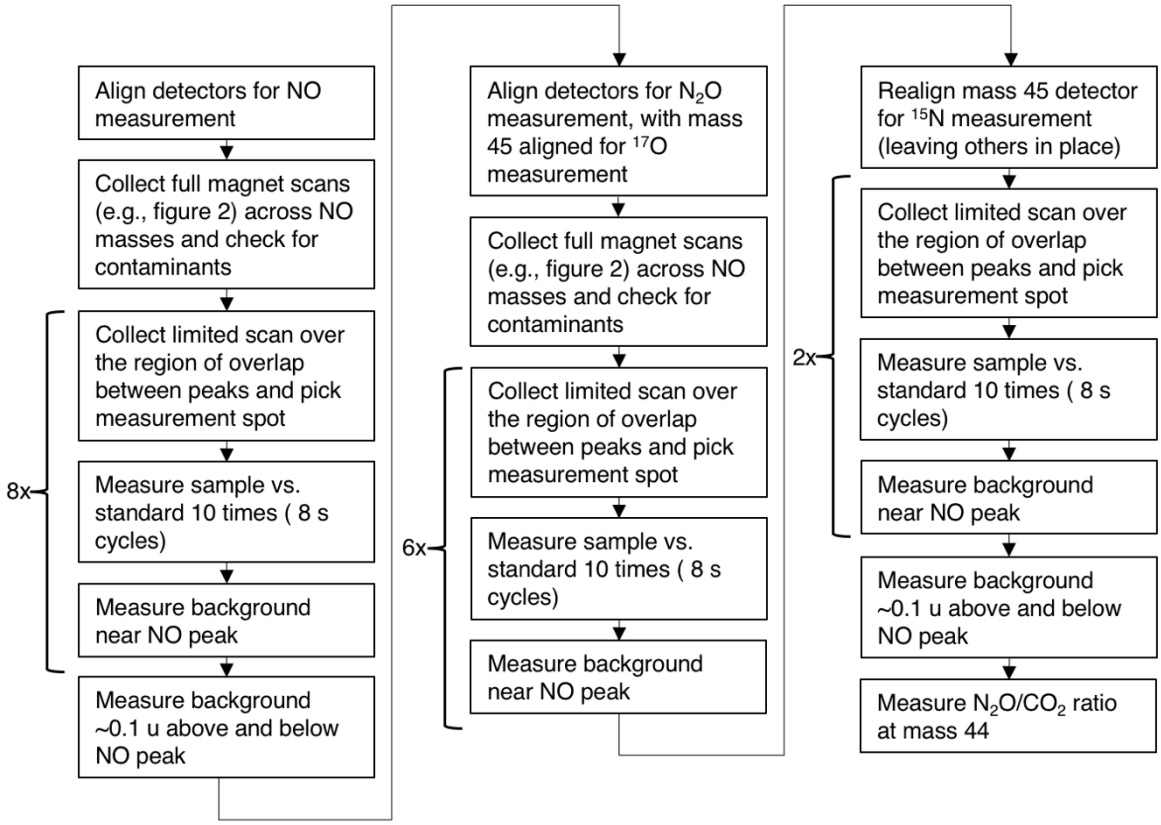

Figure 1. A flow chart of the steps required for the measurement of a sample.

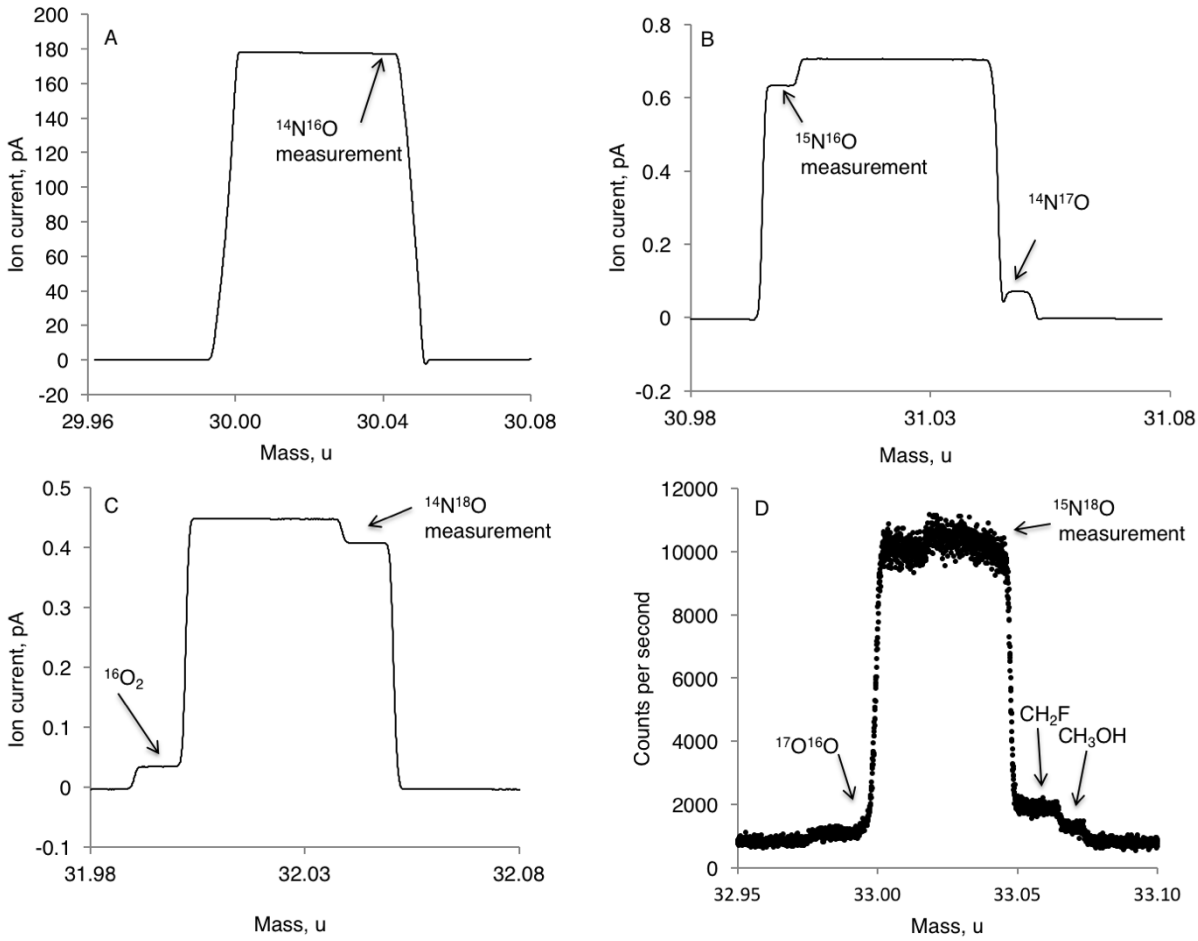

Figure 2. Mass spectra of the NO fragment of N_2O, collected by varying the magnet setting of the mass spectrometer. On each spectrum the position of measurement is indicated, as are other isotopologues of NO and contaminating species. (A) Mass 30. (B) Mass 31. (C) Mass 32. (D) Mass 33.

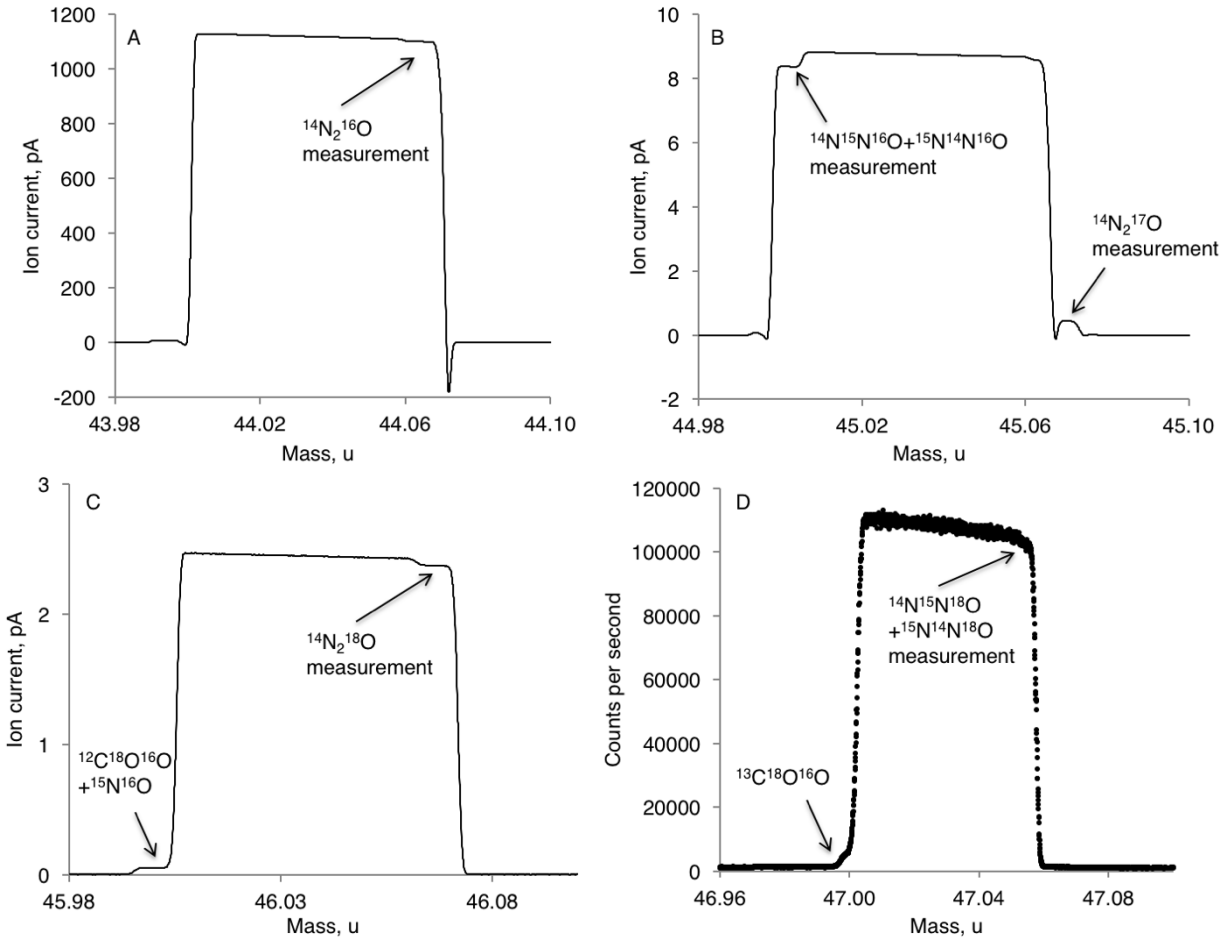

Figure 3. Mass spectra of of N_2O. On each spectrum the position of measurement is indicated, as are other isotopologues of N_2O and contaminating species. (A) Mass 44. (B) Mass 45. (C) Mass 46. (D) Mass 47.

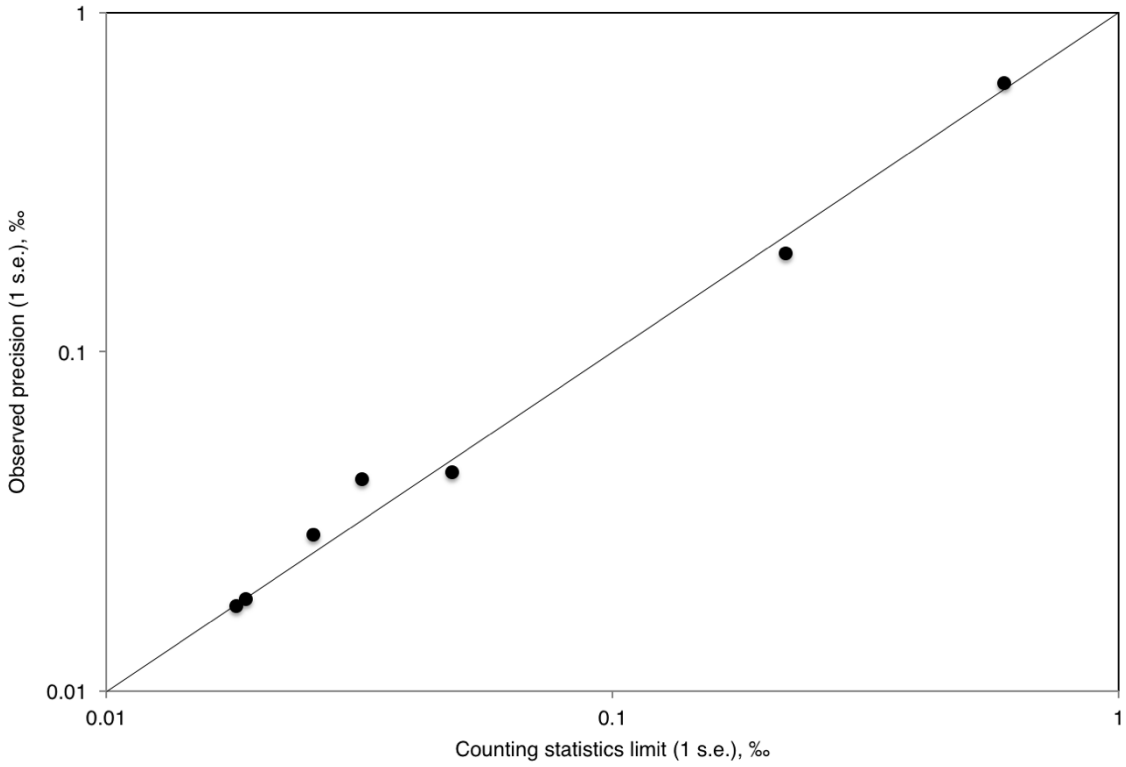

Figure 4. Comparison of observed internal precision and the counting statistics limit. Each point represents the standard error for one complete measurement of a single isotopic ratio in a typical sample. As is expected from counting statistics, more abundant isotopologues are observed with greater precision.

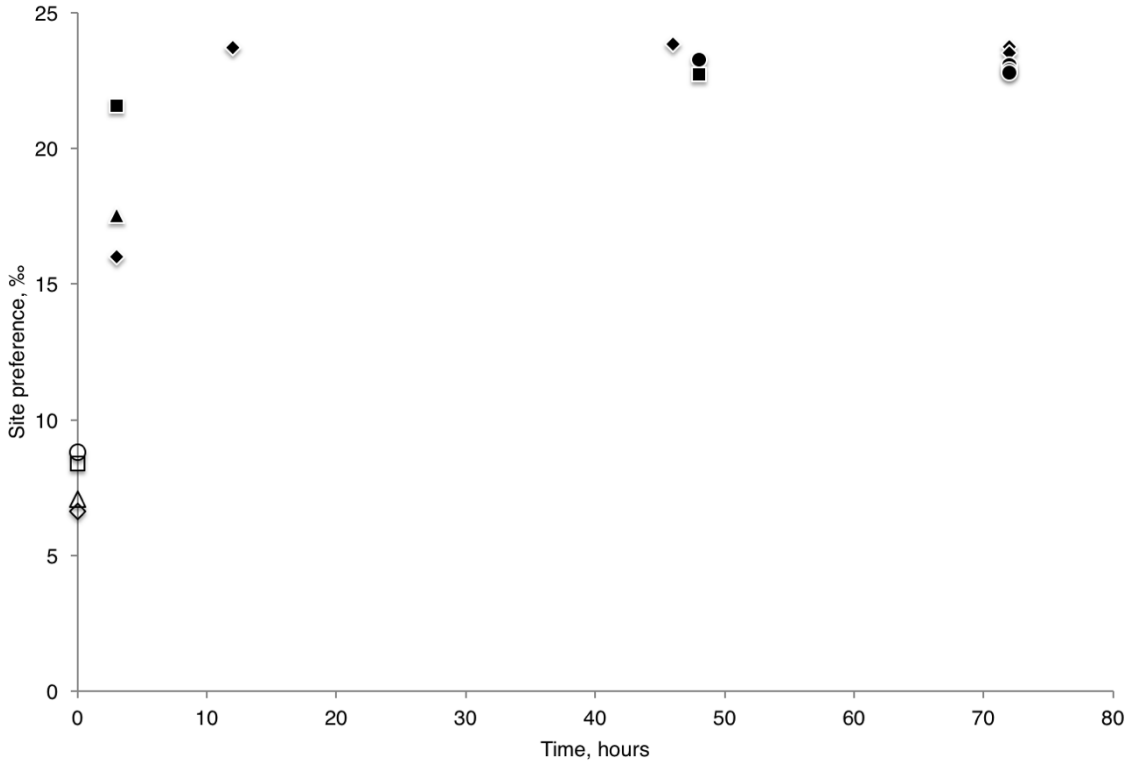

Figure 5. Behavior of SP upon heating at 200°C in the presence of a catalyst. Hollow symbols represent starting compositions; filled symbols represent the composition of equivalent samples after heating at 200°C in the presence of a catalyst for 3-72 h, as marked. All samples use the reference gas calibration and correction for scrambling that is described in the main text. All samples heated for >12 hours have reached a common, time-invariant composition. 1 s.e. mass spectrometric error bars are smaller than each point.

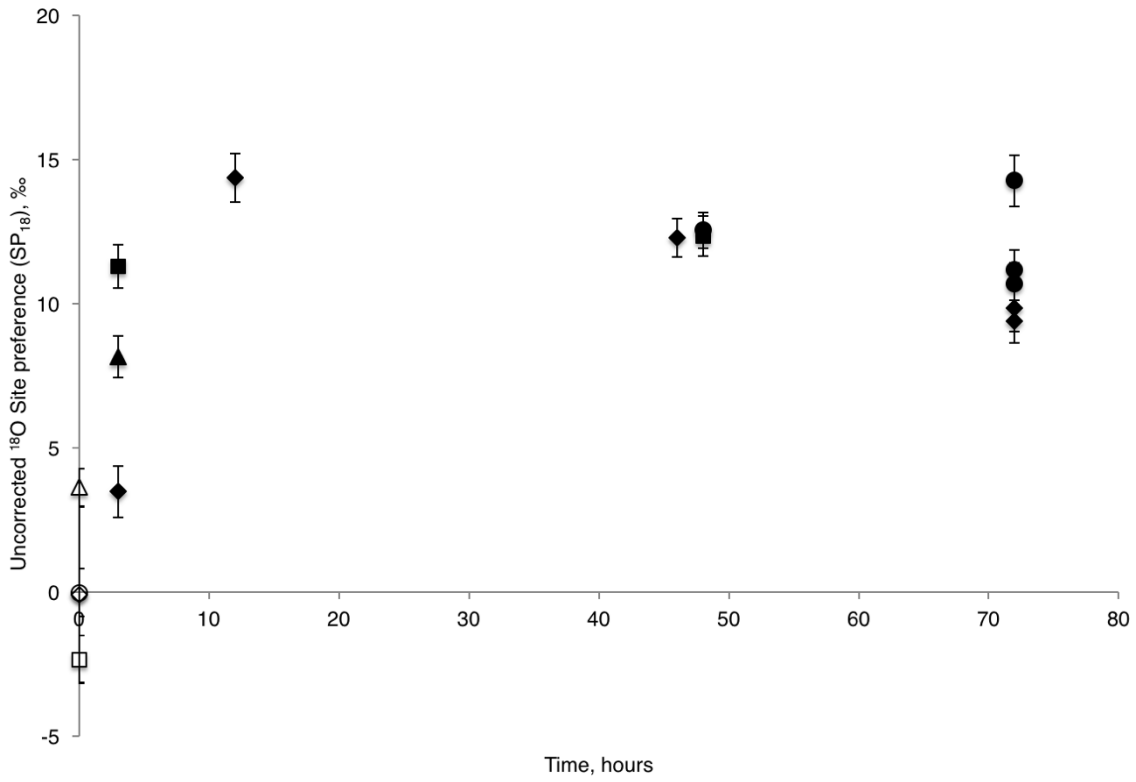

Figure 6. Behavior of SP_{18} upon heating at 200°C in the presence of a catalyst. Symbols are the same as in Fig. 4. Samples are reported relative to the internal working N_2O standard. Again, all samples that have been heated in the presence of a catalyst have reached a common, time-invariant composition. These results are used to determine the rearrangement correction and reference gas composition for $^{14}N^{15}N^{18}O$ and $^{15}N^{14}N^{18}O$, as described in the main text. Error bars represent 1 s.e. mass spectrometric error.

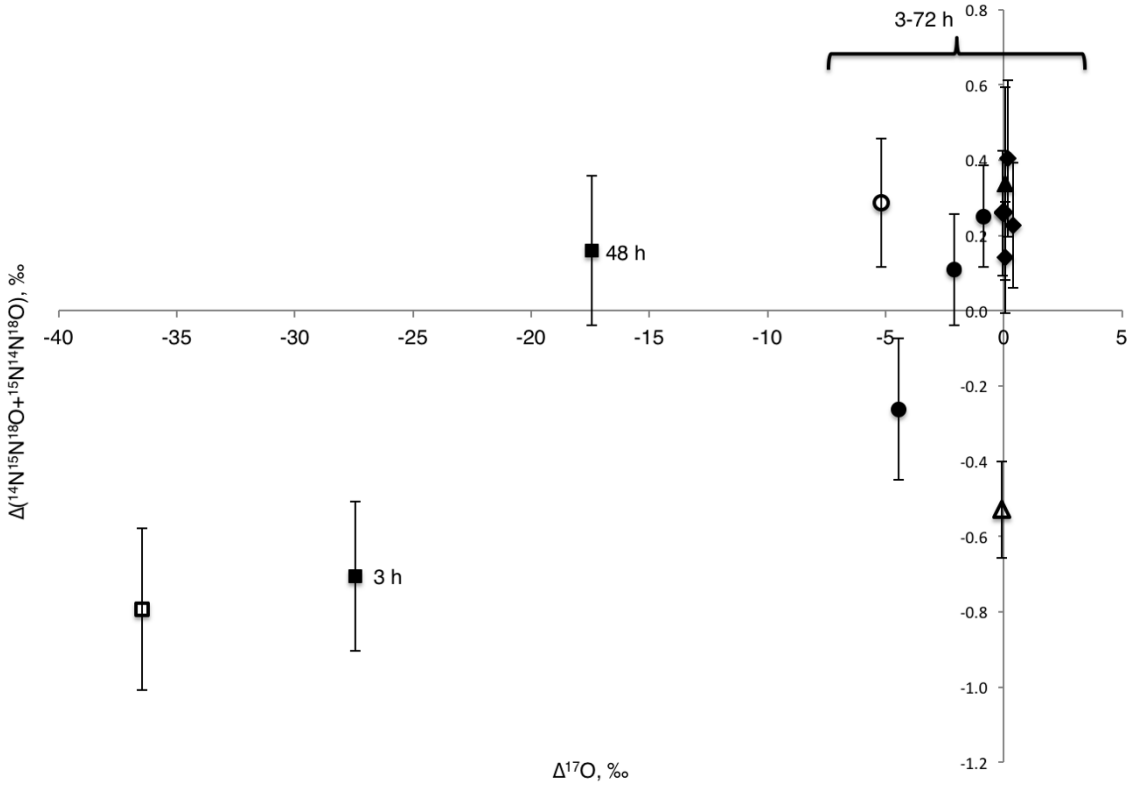

Figure 7. Behavior of $\Delta^{17}O$ and $\Delta(^{14}N^{15}N^{18}O+^{15}N^{14}N^{18}O)$ upon heating at 200°C. Symbols are the same as in Fig. 4. Gases of all starting compositions converge at a common value of $\Delta(^{14}N^{15}N^{18}O+^{15}N^{14}N^{18}O)$. Samples that begin at $\Delta^{17}O > 0$ approach but do not reach $\Delta^{17}O = 0$, suggesting that position-specific and clumped isotopologues can be fully equilibrated even without all O atoms experiencing exchange. Error bars represent 1 s.e. mass spectrometric error.

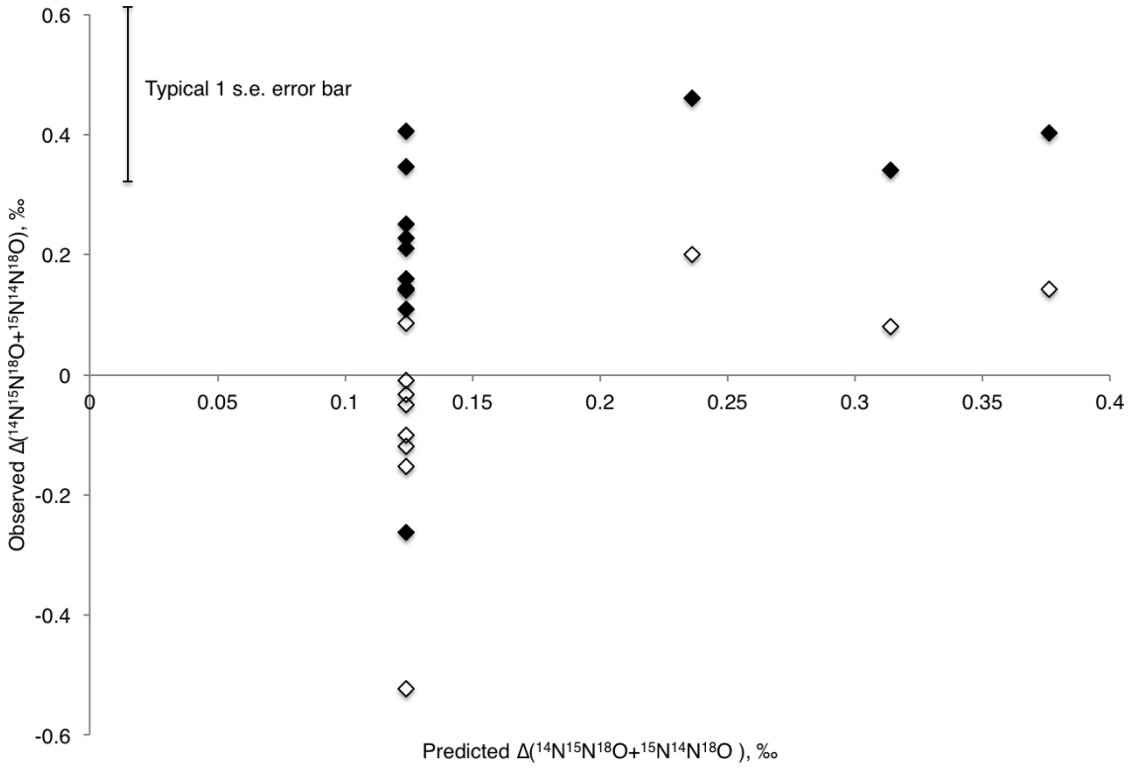

Figure 8. Measured $\Delta(^{14}N^{15}N^{18}O+^{15}N^{14}N^{18}O)$ compared to statistical mechanical predictions. Samples were heated at 200°C, 93°C, 50°C, and 25°C, which each decrease in temperature leading to an increase in the predicted $\Delta(^{14}N^{15}N^{18}O+^{15}N^{14}N^{18}O)$, but with no significant change in the observed property. Hollow symbols are reported against the internal reference gas; filled symbols have been corrected for the composition of the reference N_2O, as described in the main text. For clarity, the typical 1 s.e. error envelope of ±0.15‰ is shown.

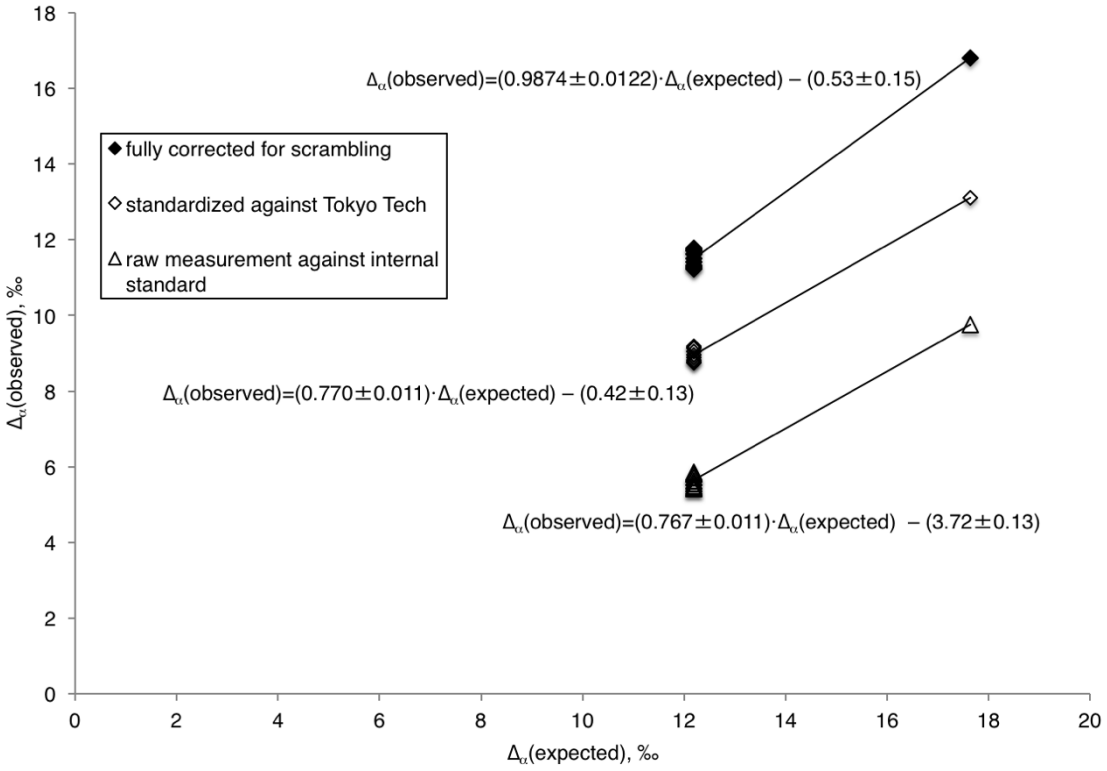

Figure 9. Measured Δ_α compared to statistical mechanical predictions. Samples are the same as those in Fig. 7 (heated to 200°C and 93°C), as described in the text; with decreasing temperature both observed and predicted values of Δ_α increase. Hollow triangles represent uncorrected measurements reported against internal standard. Hollow diamonds have been adjusted to the scale of $\delta^{15}N$ vs. N_2 in air through calibration of the internal standard by S. Toyoda and N. Yoshida, Tokyo Tech. Filled diamonds have been corrected for scrambling by the additional measurement of a secondary standard provided by S. Ono, MIT, as described in the main text. All corrections are independent of the results of the equilibration experiments reported here.

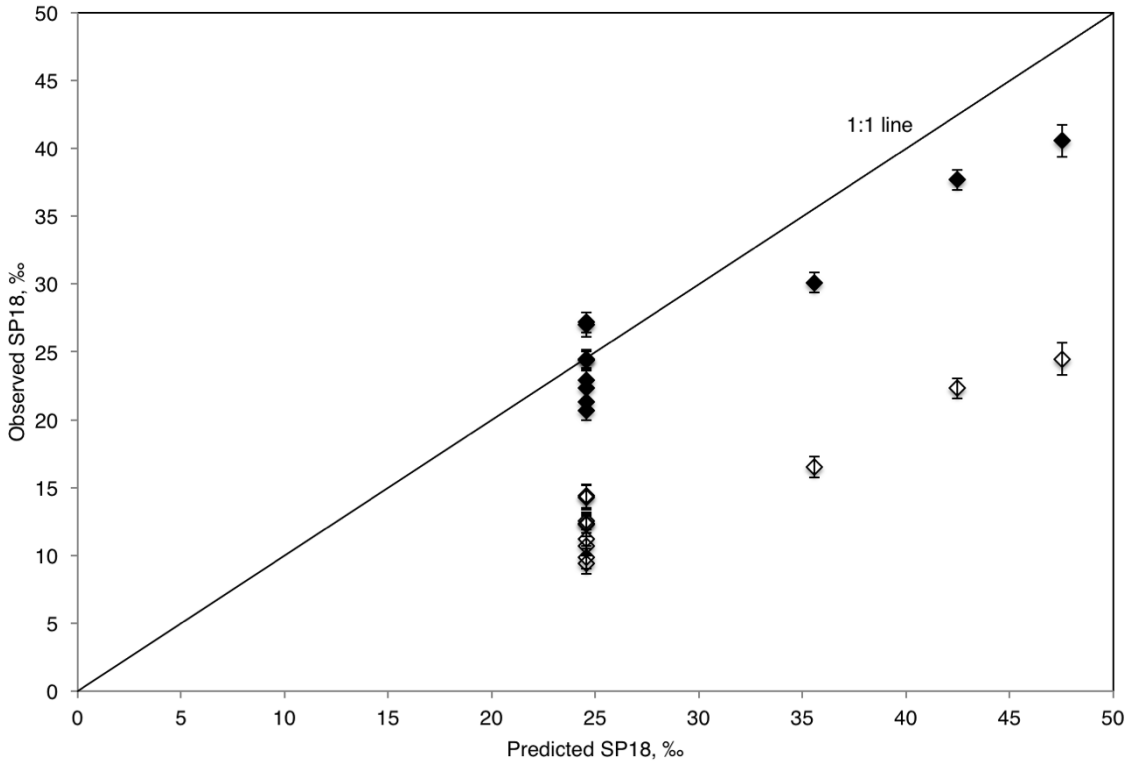

Figure 10. Measured SP_{18} compared to statistical mechanical predictions. Samples were heated at 200°C, 93°C, 50°C, and 25°C, as described in the text; with decreasing temperature both observed and predicted values of $\Delta(^{14}N^{15}N^{18}O)$ increase. Hollow symbols represent uncorrected measurements, reported against the internal reference gas. The corrected results (filled symbols) are adjusted using a value *f* of 0.77 and an SP_{18} of the reference gas chosen to make the average value measured at 200°C match the statistical mechanical prediction (see Table 5). These results suggest that the quantity SP_{18} has approached but not reached equilibrium for experiments at 25°C-93°C. 1 s.e. error bars are shown for each point.

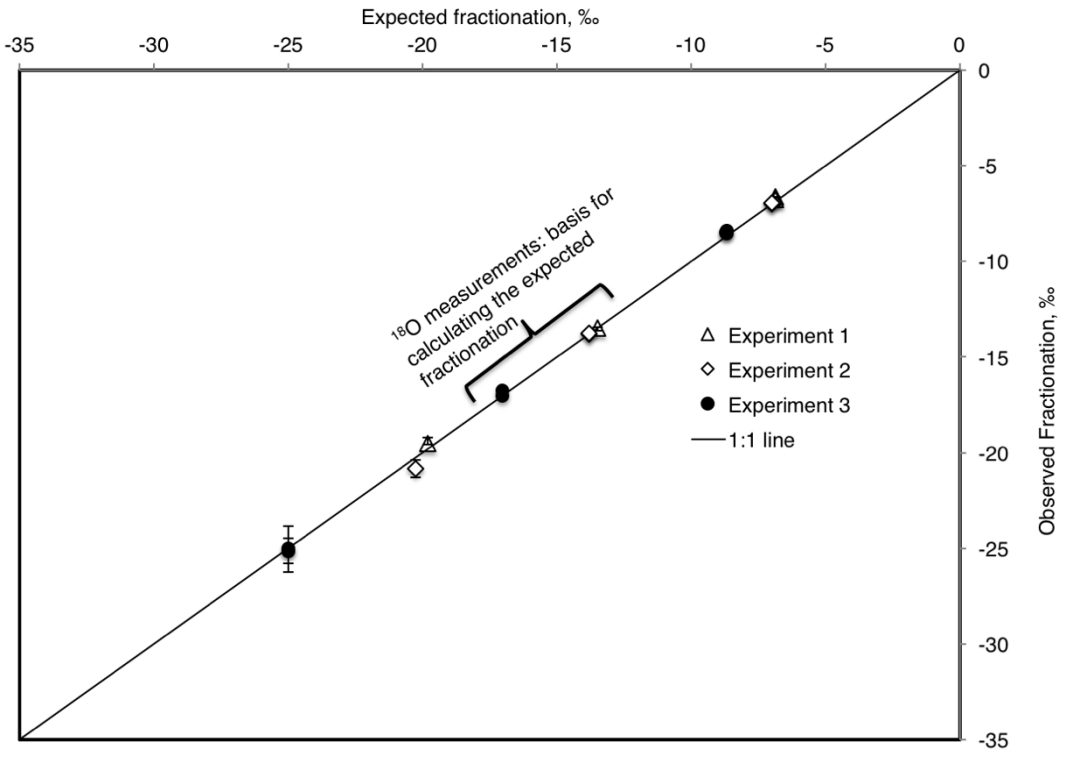

Figure 11. Comparison of the observed and expected fractionation for diffused N_2O. Experiments 1 and 2 were conducted before establishment of complete background and cleaning procedures for eliminating or correcting for isobaric interferences to $^{14}N_2{}^{17}O$ and $^{14}N^{15}N^{18}O$. Observed fractionations are interpreted to differ from experiment to experiment because of varying contributions from gas-phase interdiffusion and Knudsen diffusion

Cardinal Mass	Isotopic Variant	Mass (u)	Proportional abundance[a]
44	$^{14}N_2{}^{16}O$	44.0011	9.90×10^{-1}
45	$^{14}N^{15}N^{16}O$	44.9981	3.64×10^{-3}
	$^{15}N^{14}N^{16}O$	44.9981	3.64×10^{-3}
	$^{14}N_2{}^{17}O$	45.0053	3.83×10^{-4}
46	$^{15}N^{15}N^{16}O$	45.9951	1.34×10^{-5}
	$^{14}N^{15}N^{17}O$	46.0023	1.41×10^{-6}
	$^{15}N^{14}N^{17}O$	46.0023	1.41×10^{-6}
	$^{14}N_2{}^{18}O$	46.0053	1.99×10^{-3}
47	$^{15}N^{15}N^{17}O$	46.9993	5.17×10^{-8}
	$^{14}N^{15}N^{18}O$	47.0023	7.30×10^{-6}
	$^{15}N^{14}N^{18}O$	47.0023	7.30×10^{-6}
48	$^{15}N^{15}N^{18}O$	47.9994	2.68×10^{-8}

Table 1
Masses and abundances of the isotopic variants of N_2O.
[a]Calculated for a sample of N_2O with a random distribution of rare isotopes and with $\delta^{15}N$=0‰ relative to Air-N_2 and $\delta^{17}O$ and $\delta^{18}O$=0‰ relative to VSMOW.

	$\delta^{15}N$, ‰			$\delta^{18}O$, ‰			$\delta^{15}N^{\alpha}$, ‰		
Sample	Meas.	+/-	Reported	Meas.	+/-	Reported	Meas.	+/-	Reported
MSU (n=4)	-0.86	0.15	-0.9	38.67	0.22	38.5	0.23	0.20	0.7
MIT (n=4)	0.00	0.25	-0.24	40.76	0.40	40.43	-0.07	0.17	-0.78
Stanford (n=1)	0.27		0.31	40.59		40.85	0.76		-0.31

Table 2
Isotopic composition of standard gases, as measured versus Caltech internal reference gas and referenced to international standards (N_2 in air for $\delta^{15}N$ and VSMOW for $\delta^{18}O$ as described in the main text. Uncertainties are calculated as 1 standard deviation for the analysis of replicate samples. Reported values are the composition of each standard gas as determined by Tokyo Tech.

	Average (n=4)	+/- (1 s.d.)
$\Delta(^{14}N^{15}N^{18}O+^{15}N^{14}N^{18}O)$	0.44	0.26
$\Delta(^{14}N^{15}N^{18}O)$	2.50	0.30
SP_{18}	3.61	0.86

Table 3
Average of repeated measurements of MSU reference gas between July 2012 and August 2014, corrected and standardized as described in the Reproducibility and Standardization section of the main text.

			^{15}N site preference, ‰			Difference between SP at given T and 200°C	
T,°C	Time, h		Measured	+/- (1 s.d.)	Predicted[a]	Measured	Predicted
200	12-72	n = 8	23.28	0.43	24.37	—	—
93	143	n = 1	34.19		35.28	10.66	10.65
50	146	n = 1	37.26		42.09	13.66	17.28
25	1225	n = 1	39.42		47.12	15.77	22.20

Table 4
Comparison of SP for heated N_2O samples and theoretical predictions.
[a]Based on Wang et al.;[50] anharmonic partition functions are chosen to best match Webb and Miller.[51]

	Δ_i(reference), ‰	±, ‰
$^{14}N^{15}N^{18}O$	4.67	1.08
$^{15}N^{14}N^{18}O$	-4.15	1.09
$^{14}N^{15}N^{18}O$+$^{15}N^{14}N^{18}O$	0.26	0.19

Table 5
Reference gas compositions for clumped isotopic measurements of N_2O, based on equilibration experiments. Uncertainties are ±1 standard deviation.

Replicate	$\delta^{15}N$, ‰	+/-	$\delta^{17}O$, ‰	+/-	$\delta^{18}O$, ‰	+/-	SP, ‰	+/-	SP_{18}, ‰	+/-	$\Delta(^{14}N^{15}N^{18}O + {}^{15}N^{14}N^{18}O)$, ‰	+/-
1	-5.61	0.02	25.16	0.05	47.80	0.04	-3.91	0.04	2.6	0.8	-0.06	0.36
2	-5.32	0.02	24.91	0.07	47.86	0.03	-3.70	0.04	2.8	0.8	0.57	0.25
3	-5.32	0.02	25.09	0.04	48.05	0.02	-3.41	0.05	-3.8	0.9	0.67	0.20
average	**-5.42**	**0.17**	**25.05**	**0.13**	**47.90**	**0.13**	**-3.67**	**0.25**	**-0.5**	**3.8**	**0.39**	**0.40**

Table 6
Isotopic composition of N_2O produced by replicate cultures of *Pseudomonas aeruginosa,* strain PA14, Δ*nosZ* mutant.

C h a p t e r 2

^{15}N SITE PREFERENCE IN N_2O SUPPORTS A *TRANS* MECHANISM FOR BACTERIAL NITRIC OXIDE REDUCTASE

Introduction

The bacterial nitric oxide reductase (NOR) enzyme represents the point of synthesis for a large proportion of the nitrous oxide (N_2O) produced by biological processes and released into the atmosphere (Schreiber et al., 2012). Bacterial NOR enzymes synthesize a molecule of N_2O from two molecules of nitric oxide (NO) (Zumft, 1997). The most commonly studied bacterial NOR is termed cNOR; this enzyme is responsible for N_2O generation for all isotopic results in this paper. The catalytic site of cNOR consists of two adjacent iron atoms, one in a heme ('Fe_{heme}'; also coordinated by histidine), the other ('Fe_B') coordinated by 3 histidines and a glutamine (Hino et al., 2010). There are two main classes of hypothesized mechanisms for how bacterial NOR enzymes produce N_2O, which are described as *cis* and *trans*. In the *'trans'* mechanism, one NO binds to one of these iron atoms, after which an N-N bond is formed and an N-O bond is broken in a series of reductive steps, with trans-hyponitrite ($^{-}ONNO^{-}$) as an intermediate species bridging the two iron centers (Shiro et al., 2012). In this mechanism, it has been suggested that the α nitrogen and the oxygen comes from NO bonded to Fe_{heme} and that the β nitrogen comes from NO bonded to Fe_B. Alternatively, in the '*cis'* mechanisms, one NO molecule binds to one or the other iron center. Then, the second NO binds directly to the first and N_2O is released (M. R. A. Blomberg and Siegbahn, 2012). Which of these mechanisms is true remains the subject of debate; experimental studies generally favor a *trans* mechanism (Hino et al., 2010; Shiro et

al., 2012; Matsumura et al., 2014), while studies using computational approaches favor a *cis* mechanism (L. M. Blomberg et al., 2006; M. R. A. Blomberg and Siegbahn, 2012; Berto et al., 2014).

Stable isotope measurements of nitrous oxide can be used to reveal information about the reactions that generate it. Because nitrous oxide is an asymmetric molecule, it has two distinct nitrogen sites: a central site, denoted α, and an outer site, denoted β. Each of these sites has distinct chemical properties and may incorporate ^{15}N relative to ^{14}N differently. Such a difference in $^{15}N/^{14}N$ is referred to as the ^{15}N site preference (SP), which we define as[2]

$$\mathrm{SP} = \left(\frac{{}^{15}\mathrm{R}^{\alpha}_{\mathrm{SA}}}{{}^{15}\mathrm{R}^{\beta}_{\mathrm{SA}}} - 1 \right) = \left(\frac{\delta^{15}\mathrm{N}^{\alpha} + 1}{\delta^{15}\mathrm{N}^{\beta} + 1} - 1 \right) \cong \delta^{15}\mathrm{N}^{\alpha} - \delta^{15}\mathrm{N}^{\beta} . \quad (1)$$

The ^{15}N site preference is measureable by mass spectrometric (Toyoda and Yoshida, 1999; Magyar et al., 2016) and spectroscopic techniques (Mohn et al., 2012). Other isotopic parameters of relevance to N_2O are the bulk isotopic constraints of $\delta^{15}N$ and $\delta^{18}O$ and the clumped isotopic parameters $\Delta(^{14}N^{15}N^{18}O+^{15}N^{14}N^{18}O)$ and SP_{18} (Magyar et al., 2016).

Measurements of the ^{15}N site preference are thought to be sensitive to the particular reaction in which N_2O is formed. In particular, a number of studies have found that the ^{15}N site preference for pure cultures of bacterial denitrifiers (Toyoda et al., 2005; Sutka et al., 2006; Frame and Casciotti, 2010; Toyoda et al., 2015; Magyar et al., 2016), as well as purified cNOR protein (Yamazaki et al., 2014) is between –10‰ and 0‰ (see Table 1). The observation that this result is typically near 0‰ has been used as evidence for a cNOR

[2] $\delta = (R/R_{ref} - 1)$, where $R=^{15}N/^{14}N$, $^{17}O/^{16}O$, or $^{18}O/^{16}O$, and R_{ref} refers to N_2 in air for $\delta^{15}N$ and VSMOW for $\delta^{17}O$ and $\delta^{18}O$.

reaction mechanism in which equivalent isotope effects are observed at each position; in other words, consistent with the *trans* mechanism

(Stein and Yung, 2003; Yamazaki et al., 2014; Toyoda et al., 2015). On the other hand, this simplification accounts neither for the fact that the two iron sites are not exactly identical, and so binding to each site might be expected to subtly different isotope effects; nor for the observation, described above, that SP for N_2O produced by bacterial denitrifiers and specifically by bacterial cNOR proteins typically extends below 0‰.

We hypothesize that the position specific and clumped isotope effects in N_2O are set at the catalytic center of a nitric oxide reductase (NOR), where the N-N bond first appears and one of two N-O bonds is selectively broken. We develop a quantitative model for isotopologue fractionation by the bacterial nitric oxide reductase enzyme cNOR, based on spectroscopic constraints and a *trans* mechanism. We test this model by comparing its results to experimentally determined isotopic fractionation factors and ^{15}N site preference values for N_2O generated by denitrifying bacteria and by the cNOR enzyme. Finally, as a proxy for what isotopologue results might be expected for a *cis* mechanism, we use observed isotopologue effects from fungal denitrifiers, which have a P450 nitric oxide reductase that contains just one iron center; as well as modelled and measured results for the abiotic dimerization of HNO through a *cis* mechanism.

The Model

Here we refine the predictions of the isotope effects imparted by the cNOR enzyme by developing a statistical mechanical model based on the vibrational properties of NO bound to the Fe centers in cNOR, which we base on spectroscopic measurements of cNOR and analogous Fe centers in proteins. The vibrational motions of Fe, N, and O are described

by three vibrational modes: an N-O stretch ('$\nu_{N\text{-}O}$'), the motion of Fe relative to NO ('$\nu_{Fe\text{-}NO}$') and an Fe-N-O bending motion ($\delta_{Fe\text{-}N\text{-}O}$). Our description of the vibrational energetics of this complex is simplified because the iron atoms in question are bound to an entire enzyme rather than being bound to NO alone; a more complete description would require consideration of vibrational modes that involve the concerted motion of the N-O unit relative to each atom in the enzyme. Nevertheless, we expect that these three modes will be the most important and will capture the first-order features of any isotopic fractionation.

We base our model on the stepwise *trans* mechanism described in Shiro et al. (Shiro et al., 2012), in which the binding of 2 NO atoms to the two irons in cNOR is followed by formation of the N–N bond to make *trans* hyponitrite. One possible way to describe this process is as a fast, reversible binding of NO to Fe as a pre-equilibrium step, followed by the slow, irreversible formation of the N-N bond. In this case, any isotope effects will be set by the pre-equilibrium step (i.e., because all NO ultimately forms N-N bonds, thus there is no branching effect at or after this point) which can be described quantitatively by partition function ratios of the relevant reactant and product species (Bigeleisen and Mayer, 1947; Urey, 1947; Bigeleisen and Wolfsberg, 1958). For instance, for SP, we can calculate equilibrium constants for each Fe-NO binding reaction:

$$—Fe\text{-}^{14}NO + {}^{15}NO \rightleftharpoons —Fe\text{-}^{15}NO + {}^{14}NO$$

If the catalytic sites in cNOR are truly identical, α_{15} for binding Fe_{heme} and Fe_B will also be identical and the observed site preference will be 0‰. While this is true in an approximate sense, in both previous studies (Toyoda et al., 2015) and this work (Fig. 3), we instead typically observe a site preference slightly less than zero (here, –2.7 to –6.1‰). Viewed in

the context of the *trans* mechanism hypothesis, this slight negative preference must reflect the fact that the equilibrium constant is slightly larger for binding Fe_B (β N) than for binding Fe_{heme} (α N), or in other words, substitution of ^{15}N for ^{14}N is favored slightly more for Fe_{heme} than for Fe_B.

We combine the Urey-Bigeleisen theory for the partition function with a structural descriptions of cNOR to quantitatively predict values of the isotope effect, α_i, associated with cNOR for the isotopologues reported in this study. To determine all these kinetic isotope effects, we need to define the vibrational properties of $^{14}N^{16}O$, $^{15}N^{16}O$, $^{14}N^{17}O$, $^{14}N^{18}O$, and $^{15}N^{18}O$ bound to Fe_{heme} and of $^{14}N^{16}O$, $^{15}N^{16}O$, $^{14}N^{17}O$, and $^{14}N^{18}O$ bound to Fe_B.

To choose fundamental frequencies for the vibrational modes we consider, we rely on spectroscopic characterizations of NO bound in a chemical environment similar to the cNOR catalytic center. We choose from among available spectroscopic measurements for natural isotope abundance NO (i.e., dominantly ^{14}N-^{16}O) to best match the isotopic results reported here, in the hope that chosen vibrational frequencies yield mechanistic insights. The first-order control on these frequencies is iron oxidation state. We find that choosing frequencies associated with Fe^{2+} for both Fe_{heme} and Fe_B provides the best match to observed SP results. The frequencies for the modes we consider are listed in Table 2. We calculate corresponding vibrational frequencies for isotopically-substituted Fe-N-O complexes using reduced masses and the expression,

$$\frac{\nu_1}{\nu_2} = \sqrt{\frac{\mu_2}{\mu_1}},$$

where ν_1 and ν_2 denote vibrational frequencies for unsubstituted and substituted isotopologues, respectively, and μ is the reduced mass (Bigeleisen and Wolfsberg, 1958). For Fe_{heme} we choose the measurements of (Hu, 1993) for Fe^{2+} in myoglobin, where the Fe heme-bound iron atom is also coordinated by an additional histidine, as in cNOR. For Fe_B we choose a value from the study of (Matsumura et al., 2014)for an engineered Fe_B mimic. The results of these calculations are shown in Table 3. For SP, the predicted value of –7.4‰ is close to the minimum observed values for SP (Table 1). This result supports the conclusion that N_2O is generated in cNOR by a version of the *trans* mechanism that includes an equilibrium between bound and unbound NO, and that the Fe_{heme} and Fe_B atoms have the same oxidation state at the time of NO binding. If the individual binding isotope effects described here for Fe_B and Fe_{heme} are each subject to a Rayleigh fractionation law, we find that the predicted SP varies from its minimum of –7.4‰ to a maximum of 0‰, for the case in which a pool of NO atoms is completely consumed. In an actual enzymatic system we expect that the conditions for Rayleigh fractionation will rarely be satisfied and that there will instead be a steady state supply of NO atoms to the cNOR catalytic center, where they bind and are reduced. We hypothesize that under conditions of faster growth the SP approaches 0‰, as an equilibrium between bound and unbound NO will not be established, so any distinction between the 2 iron sites imparted by binding will be erased; the samples of Sutka et al. (2006) where SP for denitrifiers is ~0‰ were generated by concentrated cell suspensions. On the other hand, the lowest reported SP values are for ammonia oxidizers conducting nitrifier denitrification (Frame and Casciotti, 2010), which grow relatively slowly and produce N_2O from only a fraction of the NO_2^- they produce.

As discussed above, the principal kinetic isotope effect observed for $^{18}O/^{16}O$ is the branching isotope effect, $^{18}\varepsilon_{branching}$; even for the complete conversion of all NO molecules to N_2O, only half the oxygen atoms end up in the final product. Based on the structural model of cNOR, we can state that the oxygen atom that ends up in N_2O comes from NO bound to Fe_{heme} and that the NO bond that is cleaved is in NO bound to Fe_B. Therefore, $^{18}\varepsilon_{branching}$ arises from the relative preference for $^{14}N^{18}O$ to bind to Fe_B. The calculated value for $^{18}\varepsilon_{branching}$ for cNOR is –10.4‰, which is consistent with both the results reported here and past estimates for the overall NO_2^--N_2O branching isotope effect.

The measured (Magyar et al., 2016) and calculated results for SP_{18} and $\Delta(^{14}N^{15}N^{18}O+^{15}N^{14}N^{18}O)$ match less well than those for SP. As described above, these clumped isotopic parameters reflect not only the N-N bond-making reaction but also potentially preceding reactions dating back to the formation of the ^{15}N-^{18}O bond. Therefore, one possible explanation for any mismatch is that it reflects this inherited component of the clumped isotopic signature. Or, an equilibrium state for the pre-equilibration of bound versus unbound NO may be reached in for one set of isotopologues but not for another. Alternatively, the use of reduced masses to calculate vibrational modes for the clumped isotopologues may not adequately describe their properties.

With these results we cannot conclusively rule out the *cis* mechanism, but several lines of isotopic evidence lead us to conclude that it is unlikely. First, the fungal P450nor contains only one iron center and necessarily reduces NO to N_2O by a mechanism analogous, though not identical, to the *cis* mechanisms proposed for bacterial cNOR (Riplinger and Neese, 2011; McQuarters et al., 2014). The typicall ^{15}N site preference of N_2O generated from

fungal denitrification is 33‰ to 37‰ (Sutka et al., 2008; Rohe et al., 2014); these elevated values for 15N site preference are what we would expect for the *cis* mechanism. As a second line of evidence for what result we would expect from a *cis* mechanism, we consider N_2O generated by a range of abiotic reactions all thought to proceed through *cis*-hyponitrite as an intermediate (Fehling and Friedrichs, 2011), which also exhibit elevated SP values, 34.5±0.6‰ (Heil et al., 2014). Finally, a first principles prediction of SP for N_2O generation through the *cis*-hyponitrite intermediate also predicts an elevated SP (Fehling, 2012). Therefore, we expect that if N_2O generation in bacterial cNOR proceeded through a *cis*-hyponitrite intermediate, it would also have a SP of 30-40‰, not the values of –10‰ to 0‰ that are observed.

Conclusions

By comparing measurements of the ^{15}N site preference for N_2O generated by bacterial denitrification to a model based spectroscopic descriptions of the behavior of NO bound to the two iron centers in such an enzyme, we conclude that the isotopic results support a *trans* mechanism for the cNOR enzyme, in which a NO molecule reversibly binds to each iron center before N_2O is synthesized. Since this model assumes that this binding step is reversible, we hypothesize that at higher rates of NO supply to cNOR, the ^{15}N site preferences approaches 0‰. We also use ^{15}N site preference results from fungal denitrifiers to predict that a *cis* mechanism in bacterial cNOR would produce a ^{15}N site preference of >30‰.

References

Berto T. C., Xu N., Lee S. R., McNeil A. J., Alp E. E., Zhao J., Richter-Addo G. B. and Lehnert N. (2014) Characterization of the Bridged Hyponitrite Complex {[Fe(OEP)] 2(μ-N 2O 2)}: Reactivity of Hyponitrite Complexes and Biological Relevance. *Inor. Chem.* **53**, 6398–6414.

Bigeleisen J. and Mayer M. (1947) Calculation of equilibrium constants for isotopic exchange reactions. *J. Chem. Phys.* **15**, 261.

Bigeleisen J. and Wolfsberg M. (1958) Theoretical and experimental aspects of isotope effects in chemical kinetics. *Adv. Chem. Phys.*, 15–76.

Blomberg L. M., Blomberg M. R. A. and Siegbahn P. E. M. (2006) Reduction of nitric oxide in bacterial nitric oxide reductase—a theoretical model study. *Biochim. Biophys. Acta* **1757**, 240–252.

Blomberg M. R. A. and Siegbahn P. E. M. (2012) Mechanism for N_2O Generation in Bacterial Nitric Oxide Reductase: A Quantum Chemical Study. *Biochem.* **51**, 5173–5186.

Fehling C. (2012) Mechanistic Insights from the ^{15}N-Site Preference of Nitrous Oxide utilizing High Resolution Near-Infrared *cw* Cavity Ringdown Spectroscopy and Density Functional Theory Calculations. Kiel University.

Fehling C. and Friedrichs G. (2011) Dimerization of HNO in Aqueous Solution: An Interplay of Solvation Effects, Fast Acid-Base Equilibria, and Intramolecular Hydrogen Bonding? *J. Am. Chem. Soc.* **133**, 17912–17922.

Frame C. and Casciotti K. L. (2010) Biogeochemical controls and isotopic signatures of nitrous oxide production by a marine ammonia-oxidizing bacterium. *Biogeosci.* **7**, 2695–2709.

Heil J., Wolf B., Brüggemann N., Emmenegger L., Tuzson B., Vereecken H. and Mohn J. (2014) Site-specific ^{15}N isotopic signatures of abiotically produced N_2O. *Geochim. Cosmochim. Acta* **139**, 72–82.

Hino T., Matsumoto Y., Nagano S., Sugimoto H., Fukumori Y., Murata T., Iwata S. and Shiro Y. (2010) Structural Basis of Biological N_2O Generation by Bacterial Nitric Oxide Reductase. *Science* **330**, 1666–1670.

Hu S. (1993) Resonance Raman-Spectroscopic Studies of the Nitric-Oxide Adducts of Cobaltous-Reconstituted Myoglobin and Hemoglobin. *Inor. Chem.* **32**, 1081–1085.

Magyar P. M., Orphan V. J. and Eiler J. M. (2016) Measurement of rare isotopologues of nitrous oxide by high-resolution multi-collector mass spectrometry. *Rapid Commun. Mass Spectrom.* **30**, 1923–1940.

Matsumura H., Hayashi T., Chakraborty S., Lu Y. and Moënne-Loccoz P. (2014) The Production of Nitrous Oxide by the Heme/Nonheme Diiron Center of Engineered Myoglobins (Fe_BMbs) Proceeds through a *trans*-Iron-Nitrosyl Dimer. *J. Am. Chem. Soc.* **136**, 2420–2431.

McQuarters A. B., Wirgau N. E. and Lehnert N. (2014) Model complexes of key intermediates in fungal cytochrome P450 nitric oxide reductase (P450nor). *Curr. Opin. Chem. Biol.* **19**, 82–89.

Mohn J., Tuzson B., Manninen A., Yoshida N., Toyoda S., Brand W. A. and Emmenegger L. (2012) Site selective real-time measurements of atmospheric N_2O isotopomers by laser spectroscopy. *Atmos. Meas. Tech.* **5**, 1601–1609.

Riplinger C. and Neese F. (2011) The Reaction Mechanism of Cytochrome P450 NO Reductase: A Detailed Quantum Mechanics/Molecular Mechanics Study. *ChemPhysChem* **12**, 3192–3203.

Rohe L., Anderson T.-H., Braker G., Flessa H., Giesemann A., Lewicka-Szczebak D., Wrage-Mönnig N. and Well R. (2014) Dual isotope and isotopomer signatures of nitrous oxide from fungal denitrification - a pure culture study. *Rapid Commun. Mass Spectrom.* **28**, 1893–1903.

Schreiber F., Wunderlin P., Udert K. M. and Wells G. F. (2012) Nitric oxide and nitrous oxide turnover in natural and engineered microbial communities: biological pathways, chemical reactions, and novel technologies. *Front. Microbiol.* **3**.

Shiro Y., Sugimoto H., Tosha T., Nagano S. and Hino T. (2012) Structural basis for nitrous oxide generation by bacterial nitric oxide reductases. *Philosophical Transactions of the Royal Society B: Biological Sciences* **367**, 1195–1203.

Stein L. Y. and Yung Y. (2003) Production, Isotopic Composition, and Atmospheric Fate of Biologically Produced Nitrous Oxide. *Annu. Rev. Earth Planet. Sci.* **31**, 329–356.

Sutka R. L., Adams G. C., Ostrom N. E. and Ostrom P. H. (2008) Isotopologue fractionation during N_2O production by fungal denitrification. *Rapid Commun. Mass Spectrom.* **22**, 3989–3996.

Sutka R., Ostrom N., Ostrom P., Breznak J., Gandhi H., Pitt A. and Li F. (2006) Distinguishing nitrous oxide production from nitrification and denitrification on the basis of isotopomer abundances. *Appl. Environ. Microbiol.* **72**, 638.

Toyoda S. and Yoshida N. (1999) Determination of Nitrogen Isotopomers of Nitrous Oxide on a Modified Isotope Ratio Mass Spectrometer. *Anal. Chem.* **71**, 4711–4718.

Toyoda S., Mutobe H., Yamagishi H., Yoshida N. and Tanji Y. (2005) Fractionation of N_2O isotopomers during production by denitrifier. *Soil Biol. Biochem.* **37**, 1535–1545.

Toyoda S., Yoshida N. and Koba K. (2015) Isotopocule analysis of biologically produced nitrous oxide in various environments. *Mass Spectrom. Rev.*

Urey H. (1947) The thermodynamic properties of isotopic substances. *J. Chem. Soc.*, 562.

Yamazaki T., Hozuki T., Arai K., Toyoda S., Koba K., Fujiwara T. and Yoshida N. (2014) Isotopomeric characterization of nitrous oxide produced by reaction of enzymes extracted from nitrifying and denitrifying bacteria. *Biogeosci.* **11**, 2679–2689.

Zumft W. G. (1997) Cell biology and molecular basis of denitrification. *Microbiology and Molecular Biology Reviews* **61**, 533–616.

Species	^{15}N site preference (‰)	Study
Pseudomonas aureofaciens	–5.1±1.8	Toyoda et al., 2005
Pseudomonas chloroaphis	–0.5±0.6	Sutka et al., 2006
Pseudomonas aureofaciens	–0.5±1.9	Sutka et al., 2006
Nitrosomonas multiformis	0.1±1.7	Sutka et al., 2006
Nitrosomonas marina C-113a	–10.7±2.9	Frame and Casciotti, 2010
Pseudomonas aeruginosa	–3.7±0.3	Magyar et al., 2016
cNOR from *Paracoccus denitrificans*	–5.9±2.1	Yamazaki et al., 2014

Table 1. Published ^{15}N site preference measurements associated with bacterial denitrification.

mode (cm^{-1})	Fe_{heme}	Fe_B
ν(N-O)	1624	1755
ν(Fe-NO)	449	445
δ(Fe-N-O)	554	577

Table 2. Vibrational modes used in the statistical mechanical model for cNOR active site.

	Isotopologue effect
SP	–7.4‰
SP_{18}	–18.9‰
$\Delta(^{14}N^{15}N^{18}O+^{15}N^{14}N^{18}O)$	4.4‰
$^{15}\varepsilon$	10.3‰
$^{18}\varepsilon_{branching}$	–10.4‰
$^{17}\varepsilon_{branching}$	–5.2‰
$\lambda^{17/18}$	0.497
$\Delta(^{15}N^{15}N^{16}O)$	–0.01‰
$\Delta(^{14}N^{15}N^{17}O+^{15}N^{14}N^{17}O)$	2.2‰

Table 3. Results of statistical mechanical model for the cNOR active site.

C h a p t e r 3

INSIGHTS INTO NITROUS OXIDE GENERATION BY DENITRIFIERS FROM MULTI-ISOTOPOLOGUE MEASUREMENTS

1. Introduction

Denitrification is a central process in the biological nitrogen cycle in which microbes respire N oxides, thereby converting oxidized species to more reduced species, moving from the left to the right in the following chain:

$NO_3^- \rightarrow NO_2^- \rightarrow NO \rightarrow N_2O \rightarrow N_2$,

It may act on any of three starting substrates—nitrate (NO_3^-), nitrite (NO_2^-), or N_2O—and end with any of three more reduced products—NO_2^-, N_2O, or N_2 (Zumft, 1997). Denitrifiers release N_2O both as a leakage product on the way to N_2 or, for those that lack a nitrous oxide reductase, as the final product; denitrification is thought to be the major anaerobic source of N_2O to the atmosphere. But in any given environmental setting it can be unclear whether denitrification or the aerobic processes of ammonia oxidation are responsible for N_2O generation (Stein and Yung, 2003). The ability to identify which processes are responsible for N_2O generation, and an understanding of the molecular mechanisms of those processes are essential for making predictions of how N_2O emissions respond to human activities and other environmental variables.

Measurements of the abundances of rare stable isotopes (^{15}N, ^{17}O, and ^{18}O) in N_2O can provide clues into its metabolic origins. Because of its asymmetric structure, nitrous oxide records a surprisingly large number of isotopic constraints for a molecule of its size. Measurement techniques have been described for six isotopic parameters in N_2O: $\delta^{15}N$, $\delta^{17}O$,

$\delta^{18}O$, ^{15}N site preference (SP), ^{15}N-^{18}O site preference (SP_{18}), and the overall abundance of ^{15}N+^{18}O-containing clumped isotopologues, $\Delta(^{14}N^{15}N^{18}O+^{15}N^{14}N^{18}O)$ (Kim and Craig, 1993; Toyoda and Yoshida, 1999; Magyar et al., 2016)[3]. Each of these parameters records different aspects of the processes that lead to N_2O production in denitrification, including the successive cleavage of N—O bonds by nitrate, nitrite, and nitric oxide reductase enzymes, the formation of a N—N bond by the NO reductase (NOR), the movement of substrates and products to and from enzyme catalytic sites, and isotope exchange reactions between the various N oxides and water. The bulk isotopic constraint of $\delta^{15}N$ is also subject to the constraints of mass balance; e.g., in the limiting case of complete conversion of NO_3^- to N_2O, the $\delta^{15}N$ of the product must equal that of the substrate (Mariotti et al., 1981; Hayes, 2001). However, the clumped and position specific parameters—SP, $\Delta(^{14}N^{15}N^{18}O+^{15}N^{14}N^{18}O)$, and SP_{18}—will generally preserve a record of isotope effects that are controlled by the various mechanisms of making and breaking bonds in the chain of reactions from substrate to product.

The SP variable—or ^{15}N site preference in ^{16}O bearing isotopologues—describes the difference in ^{15}N abundance between the central (α) and outer (β) positions in N_2O[4]. Measurement of SP has already proven useful for describing N_2O biosynthesis pathways (Yoshida and Toyoda, 2000; Toyoda et al., 2015). Previous studies have demonstrated that

---

[3] $\delta = (R/R_{ref} - 1)x1000$, where $R=^{15}N/^{14}N$, $^{17}O/^{16}O$, or $^{18}O/^{16}O$, and R_{ref} refers to N_2 in air for $\delta^{15}N$ and VSMOW for $\delta^{17}O$ and $\delta^{18}O$.

[4] The ^{15}N site preference is conventionally defined as $SP = \delta^{15}N^{\alpha} - \delta^{15}N^{P}$; here it is defined instead as

$$SP = \left(\frac{^{15}R^{\alpha}_{SA}}{^{15}R^{\beta}_{SA}} - 1\right)\cdot 1000 = \left(\frac{\frac{\delta^{15}N^{\alpha}}{1000}+1}{\frac{\delta^{15}N^{\beta}}{1000}+1} - 1\right)\cdot 1000$$

These definitions are only subtly different for most results reported here.

N_2O generated by bacterial denitrification in pure cultures (Toyoda et al., 2005; Sutka et al., 2003; 2004; Frame and Casciotti, 2010; Magyar et al., 2016), cell suspensions (Sutka et al., 2006), and by purified nitric oxide reductase enzyme (Yamazaki et al., 2014) have a ^{15}N site preference between -10.7‰ and 0.1‰, which is distinct from N_2O generated by other natural sources (Toyoda et al., 2015). N_2O produced by pure cultures of fungal denitrifiers has typically been found to have a SP between 34‰ and 37‰, though lower values have also been observed (Sutka et al., 2008; Rohe et al., 2014; Yang et al., 2014); these values are similar to those observed for hydroxylamine oxidation by ammonia oxidizers (Sutka et al., 2003; 2004; 2006; Frame and Casciotti, 2010; Yamazaki et al., 2014). Here, we build on this prior work by adding new constraints on this problem by measuring the abundances of multiply substituted ('clumped') isotopologues of N_2O produced by various denitrifiers.

Clumped isotopologues have been used to study carbon dioxide (Affek and Eiler, 2006), carbonate minerals (Ghosh et al., 2006; Eiler, 2007, 2011 and references therein), methane (Stolper et al., 2014; 2015; Wang et al., 2015), and oxygen (Yeung et al., 2015). Most recently, we have demonstrated mass spectrometric techniques for clumped isotope analysis of nitrous oxide (Magyar et al., 2016). The clumped isotopologues are of interest to the study of biochemical products in particular because they provide new constraints on the mechanisms of biochemical reactions, and thus can help solve problems that are underconstrained by measurements of singly substituted isotopologues alone. The first studies of CO_2 revealed that human and microbial respiration are characterized by small deficits in $^{13}C^{18}O^{16}O$ compared to equilibrium (Affek and Eiler, 2006). The physical causes of these anomalies have not been explored in detail. Several biological influences on the clumped isotope compositions of biogenic carbonates are known or suspected, including

strong excesses in $^{13}C^{18}O^{16}O_2^{-2}$ in some deep-sea and surface corals (Thiagarajan et al., 2011; Saenger et al., 2012)—suspected to reflect kinetic isotope effects associated with irreversible CO_2 hydration/hydroxylation reactions. In the case of biogenic methane, the Δ_{18} value — a measure of the enrichment of (mostly) $^{13}CH_3D$ and (a trace of) $^{12}CH_2D_2$ — is thought to reflect the variable reversibility of the methane synthesis pathway, with values that equal or closely approach those expected for equilibrium at the temperature of methanogenesis when the reaction is relatively reversible, and values that are controlled by an as-yet only loosely understood kinetic isotope effect when the reaction is irreversible (Stolper et al., 2014; 2015; Wang et al., 2015). In the case of O_2, the Δ_{36} value (a measure of $^{18}O_2$ enrichment) is thought to be controlled by the sampling statistics of assembling two rare isotopes that pass through different biosynthetic pathways and thus differ in $\delta^{18}O$ together into one molecule (Yeung et al., 2015). A goal of this study is to establish whether the clumped isotopologues of N_2O have the potential to record specific mechanisms of its biosynthesis.

As described in Magyar et al. (2016) it is possible to describe the abundances of the two isotopologues $^{14}N^{15}N^{18}O$ and $^{15}N^{14}N^{18}O$ with two parameters, SP_{18} and $\Delta(^{14}N^{15}N^{18}O+^{15}N^{14}N^{18}O)$. SP_{18} is defined analogously to SP as

$$SP_{18} = \left(\frac{R_{^{14}N^{15}N^{18}O}}{R_{^{15}N^{14}N^{18}O}} - 1 \right) \cdot 1000.$$

where $R_i = = [i]/[^{14}N_2{}^{16}O]$. SP_{18} can be thought of as a measure of the selectivity for or against a ^{15}N-^{18}O bond as opposed to the case where both ^{15}N and ^{18}O are co-located in the same molecule but are not bonded to each other. The value, $\Delta(^{14}N^{15}N^{18}O+^{15}N^{14}N^{18}O)$, provides a

measure of the total abundance of $^{15}N + ^{18}O$-containing isotopologues, relative to a random distribution of rare isotopes among all isotopologues; it is defined as

$$\Delta_{^{14}N^{15}N^{18}O+^{15}N^{14}N^{18}O} = \left(\frac{R_{^{14}N^{15}N^{18}O+^{15}N^{14}N^{18}O}}{R^{*}_{^{14}N^{15}N^{18}O+^{15}N^{14}N^{18}O}} - 1 \right) \cdot 1000.$$

Here we explore the isotopic composition, including both singly and doubly substituted species, of N_2O generated by denitrification by analyzing nitrous oxide produced by two species of denitrifying bacteria, *Pseudomonas aeruginosa* strain PA14 (Δ*nosZ* mutant), and *Pseudomonas chlororaphis* subsp. *aureofaciens*. Each of these organisms lacks nosZ, the gene for N_2O reduction (*P. aeruginosa* through a genetic mutation, *P. aureofaciens* naturally), meaning N_2O is the terminal product, with no reduction of N_2O to N_2. Because our study examines proportions of seven isotopic species ($^{15}N^{14}N^{16}O$, $^{14}N^{15}N^{16}O$, $^{14}N_2{}^{18}O$, $^{14}N_2{}^{17}O$, $^{15}N^{14}N^{18}O$, $^{14}N^{15}N^{18}O$, all ratiod to $^{14}N_2{}^{16}O$), we are able to recognize and quantify relative rates of several equilibrium and kinetic isotope effects associated with N_2O synthesis.

2. Methods

Nitrous oxide was generated by and collected from two species of bacteria, *Pseudomonas aeruginosa* strain PA14, ΔnosZ, and *Pseudomonas aureofaciens* (ATCC #13985) and from the nitric oxide reductase of the fungus *Histoplasma capsulatum*.

Pseudomonas aeruginosa strain PA14, Δ*nosZ*, was provided by D. K. Newman and cultivated as described in Magyar et al. (2016). Briefly, cultures were grown at 37°C in 150 mL autoclaved Luria-Bertani (LB) medium (in one liter: 25 g LB mix, Difco; 0.78 g KH_2PO_4; 2.50 g K_2HPO_4) with either sodium nitrate (20 mM; 1.72 g/L) or sodium nitrite (10 mM;

0.69 g/L) provided for respiration. Two replicate experiments were conducted with nitrate. The results for experiment 1 were presented in Magyar et al. (2016) and were conducted with nitrate #1 (Sigma-Aldrich), which has (±1 s.d.) $\delta^{15}N$ = -6.9±0.7‰, $\delta^{18}O$ = 23.0±1.5‰, and $\Delta^{17}O$ = -0.1±1.8‰. Experiment #2 was conducted with nitrate #2, which has $\delta^{15}N$ = 0.9±0.2‰, $\delta^{18}O$ = 61.2±0.6‰, and $\Delta^{17}O$ = 19.5±0.8‰. Isotopic compositions of nitrate were measured at the University of Washington by the denitrifier method (Casciotti et al., 2002; Kaiser et al., 2007).

Pseudomonas chlororaphis ssp. *aureofaciens* (ATCC #13985), was obtained from the U.S. Department of Agriculture Research Service Culture Collection. Importantly, as described in Casciotti et al. (2002), *Pseudomonas chlororaphis* and *P. chlororaphis* ssp. *aureofaciens* have quite different biochemical properties; the first has a heme nitrite reductase (NirS), while the second has a copper nitrite reductase (NirK). For clarity, we will refer to it here as *Pseudomonas aureofaciens*. It has also been observed that concentrated cell suspensions of *Pseudomonas aureofaciens* exhibited exceptionally low ^{18}O exchange with water (Casciotti et al. 2002). It naturally lacks the gene for N_2O reduction, so all nitrate provided for growth will be converted to nitrous oxide (Casciotti et al., 2002). Methods for its cultivation were adapted from Casciotti et al. (2002) and McIlvin and Casciotti (2011). Cultures were grown at room temperature (~20°C) in autoclaved tryptic soy broth (TSB) medium (in 1 liter: 30 g TSB mix; 0.42 g NH_4Cl; 4.9 g KH_2PO_4). After autoclaving, the optical density of the medium at 500 nm was checked to ensure that it was close to the value of 0.335 recommended by McIlvin and Casciotti (2011). Starter cultures were cultivated aerobically in capped tubes containing ~10 milliliters of medium, which were used to

inoculate anaerobic cultures. The anaerobic cultures used for the collection of nitrous oxide were grown in 150 mL of TSB medium amended with 10 mM sodium nitrate (0.85 g/L; nitrate #1).

All bacterial cultures were cultivated in custom 200 mL bottles designed for headspace sampling. Growth of cultures was monitored by optical density and by measurement of NO_2^- production and consumption. When growth plateaued and cultures were thought likely to have converted all the nitrate or nitrite provided in N_2O, the headspace was sampled by expanding it into an evacuated glass sampling volume connected to the bottle and separated from both the bottle and a vacuum line by Teflon vacuum valves. This gas was then expanded to a glass vacuum line and cleaned cryogenically as described below.

Fungal nitric oxide reductase N_2O samples were produced at Michigan State University by purified samples of the nitric oxide reductase ('P450NOR') from *Histoplasma capsulatum*, as described in Yang et al. (2014). The isolated enzyme was exposed to NO ($\delta^{15}N = -36.7‰$, $\delta^{18}O = 19.7‰$) and NADH, permitting N_2O to be generated by the reaction

$$2NO + NADH + H^+ \rightarrow N_2O + NAD^+ + H_2O.$$

The reaction was allowed to proceed until ~65% of the supplied NO was converted to N_2O at which point all the accumulated N_2O was collected.

All samples were cryogenically and chemically purified on a glass vacuum line after collection and before analysis to remove N_2, O_2, water, CO_2, and organic contaminants. Samples were frozen into a glass trap immersed in liquid nitrogen and exposed to vacuum to remove N_2, O_2, and other noncondensible gases. Water was removed by passage over a trap immersed in a slurry of dry ice and ethanol. CO_2 was removed by repeated passage over

Ascarite (Ascarite-II, Thomas Scientific) while collecting evolved water in a dry ice/ethanol trap. Organic contaminants, including methanol and ethanol, were removed by passage over a trap immersed in a slurry of liquid nitrogen and ethanol, monitored to ensure its temperature remained below -100ºC. Purified samples were frozen into a glass tube sealed with a flame. Isotopic measurements of N_2O were made on the Thermo MAT 253 Ultra (Eiler et al., 2013) following the procedure described in Magyar et al. (2016).

3. Results and Discussion

Measurements of $\delta^{15}N$, $\delta^{18}O$, and SP in the two species of denitrifying bacteria examined in this study (*Pseudomonas aeruginosa* and *Pseudomonas chlororaphis)* are consistent with the expectations based on past measurements of N_2O generated by denitrifiers. In particular, for bacteria grown on nitrate, $\delta^{15}N$ reflects near-complete conversion of substrate into N_2O; using a value of $^{15}\varepsilon$ of 27‰ (Peters et al., 2014; Brandes et al., 1998) and a Rayleigh fractionation model we find that the observed $\delta^{15}N$ values for all samples correspond to between 91% and 103% conversion of nitrate to N_2O (Figure 1). Measurements of SP range from –2.7‰ to –6.1‰, which overlaps with the range observed in previous experiments with pure cultures and cell suspensions (Toyoda et al., 2005; Sutka et al., 2003; 2004; 2006; Frame and Casciotti, 2010). The oxygen isotope composition ($\delta^{18}O$ and $\Delta^{17}O$) can be explained by varying proportions of exchange between nitrogen oxides and water, accompanied by branching kinetic isotope effects associated with the successive cleavages of N–O bonds (Casciotti et al., 2007), which will be described in detail in a subsequent section.

3.1. Oxygen isotopic composition is set by exchange with water and branching isotope effects

It is imaginable that oxygen isotope exchange between H_2O and NO_3^-, NO_2^-, NO, and/or N_2O takes place during N_2O synthesis, and if that exchange is reversible it may closely approach or reach an equilibrium fractionation. Of these, only exchange with N_2O can be ruled out conclusively: Oxygen isotope exchange at ambient pressures and temperatures between H_2O and N_2O has never been observed (Bonner and Bigeleisen, 1952; Cliff and Thiemens, 1997). On the other hand, exchange between water and the oxides NO_3^-, NO_2^-, and NO has been reported, either as inorganic exchange reactions or associated with protein catalysis of N oxide reduction reactions (Kool et al., 2007). The exchange reaction that seems likely to occur most readily is the exchange between water and nitrite:

$N^{16}O_2^- + H_2{}^{18}O \rightleftharpoons N^{16}O^{18}O^- + H_2{}^{16}O$.

In the case that nitrite and water have reached oxygen isotope exchange equilibrium, the $\delta^{18}O$ of nitrite is controlled by temperature and $\delta^{18}O$ of the water (for $\delta^{18}O_{H2O}$ = -7‰, $\delta^{18}O_{NO2}$ = 6.5‰ at 20°C and 4.5‰ at 37°C; Buchwald and Casciotti, 2013). Any branching reactions that may affect nitrite subsequent to its equilibration with water may be associated with a kinetic isotope effect and therefore be noticed as a disturbance of this nitrite-water equilibrium fractionation.

By growing *P. aeruginosa* on nitrate with two distinct $\Delta^{17}O$ values, but under otherwise identical conditions, we were able to distinguish between the branching kinetic isotope effect for oxygen isotopes and the exchange of oxygen between metabolic intermediates and water. This process is illustrated in Figure 2. The paths in this figure from

the compositions of starting nitrate to the compositions of the product N_2O project to a common point, which we interpret as the composition that would be observed if the oxygen in N_2O underwent complete exchange with the water in which the culture was incubated (which would erase the $\Delta^{17}O$ imparted by nitrate #2), added to the composition-space vector associated with the branching isotope effects subsequent to that equilibration. Thus, for each sample, the net vector connecting the composition of the nitrate and the N_2O and directed toward this point of intersection can be decomposed into two component vectors: One, with a slope of ~0.518 (the mass law expected of kinetic isotope effects), and a length of ~38‰ (Casciotti et al., 2007), describes the branching kinetic isotope effect; the other is directed at the expected composition for a particular N oxide in equilibrium with water (i.e., whatever species undergoes O isotope exchange with water prior to further reaction to make N_2O; Buchwald and Casciotti, 2010; Kaneko and Poulson, 2013). For each experiment, we calculate the fraction of O atoms in product N_2O that come from exchange of an N oxide with water by dividing the distance traveled between nitrous oxide and the nitrate from which it was produced by the distance between that nitrate and the intersection between the trends for the two experiments. The average result for our two experiments is 52±5% (1 s.d.). We have no direct evidence for the specific N oxide species that undergoes exchange but can consider the relative plausibility of several options: First, even if we did not accept prior arguments against exchange between N_2O and water, as discussed above, our own results rule this out, as in this case the intersection between the two experiments would occur at the predicted value for the N_2O-H_2O equilibrium, which is 20.3‰ at 37°C (Bigeleisen and Friedman, 1950; Richet, 1977), with no possibility for branching isotope effects to modify this composition thereafter. If we assume nitrate equilibrates with water and accept prior

constraints on that equilibrium (Böhlke et al., 2003), our results are explained by a branching isotope effect of –32±3‰ superimposed on that equilibrium. If instead exchange occurs between nitrite and water, we would instead need to invoke a branching isotope effect of –37±3‰. For comparison, Casciotti et al. (2007) described the total branching isotope effect for NO_3^- to N_2O as –38±5‰, but for NO_2^- to N_2O as –11±5‰. Therefore, our results are most readily reconciled with this prior work if exchange occurs between nitrate and water, perhaps accompanied by with a lesser fraction of later exchange between nitrite and nitric oxide leading to the difference between the observed branching isotope effect of –32‰ and the expected value of –38‰.

This result would be consistent with the conclusion of Kool et al., (2011) that exchange equilibria play a role in setting the oxygen isotope signature of NO_3^- in soil incubations. But it is also quite surprising, since exchange between NO_3^- and water is expected to be extremely slow except at pH values approaching 0; e.g., Kaneko and Poulson (2013) suggest a $t_{1/2}$ for nitrate-water exchange of 10^9 years at 25°C and pH 7 (Kaneko and Poulson, 2013). On the other hand, exchange of ^{18}O between nitrite and water occurs readily at acidic pH. One possibility is that the nitrate-water ^{18}O exchange reaction is catalyzed by the nitrate reductase enzyme, or that this enzyme is at least partially reversible. However, past characterizations of nitrate reduction in bacteria have observed no evidence for reversibility (Granger et al., 2008).

We can evaluate some of these conclusions by analyzing samples of N_2O generated by *P. aeruginosa* grown on nitrite instead of nitrate. The nitrite remained in solution in the culturing bottles at a pH ~ 7 and temperature of 37°C for > 24 h before growth was observed, so based on the calibration of Buchwald and Casciotti (2013) it is likely that it had fully

equilibrated with water and so its $\delta^{18}O$ was 6.5‰. Therefore the $\delta^{18}O$ of N_2O of 18.9±0.4‰ corresponds to $^{18}\varepsilon_{branching}$ of –13.4±0.4‰., which closely approaches the value of –11‰ for reduction of nitrite to N_2O reported in Casciotti et al. (2007), and larger than the $^{18}\varepsilon$ of –6±3‰ reported for the iron-containing nitrite reductase, NirS, by Martin and Casciotti (2016). That the complete expected kinetic isotope effect for the reduction of nitrite to N_2O is preserved supports the conclusion that much of the ^{18}O exchange observed in the previous experiments is derived from exchange between nitrate and water.

Finally, by measuring the isotopic composition of N_2O generated by *Pseudomonas aureofaciens* we test the effect of varying physiology as well as the role of the nitrite reductase enzyme. Unlike *P. aeruginosa,* which contains the iron nitrite reductase NirS, *P. aureofaciens* contains the copper nitrite reductase NirK. NirK is often associated with lower rates of oxygen exchange and is though to catalyze exchange less readily than NirS (Casciotti et al., 2002; Martin and Casciotti, 2016). In our experiments, the oxygen isotopic composition of product N_2O is lower than the composition of the starting nitrate. These results can be explained by ~100% exchange between water and NO_3^-, followed by little to no branching isotope effect, or by exchange between water and nitrite, which, if complete, is accompanied by a branching isotope effect for nitrite and NO reductase of –7.2±1.0‰. This result is consistent with the results of Martin and Casciotti (2016) that the NirK has a branching isotope effect of –2±2‰. Even though it is expected that for NirK there is little enzyme-catalyzed exchange of ^{18}O between water and nitrite (Casciotti et al., 2002), the elapsed time between inoculation and growth of these culture permits exchange to proceed entirely inorganically with no enzyme catalysis.

Any equilibrium reactions that partially or fully reset the oxygen isotope composition of the intermediate oxides that are eventually converted to N_2O are also expected to reset at least some of the clumped isotope species (i.e., the abundance of ^{15}N-^{18}O bonds of those intermediates should be shifted to the equilibrium composition at a given temperature, though there is no prediction regarding the ^{15}N-^{15}N-^{x}O bearing species). In this case, the predicted equilibrium abundance of $^{15}N^{14}N^{18}O$ and $^{14}N^{15}N^{18}O$ will then be reflected in the SP_{18} and $\Delta(^{14}N^{15}N^{18}O+^{15}N^{14}N^{18}O)$ values of N_2O, mediated by any kinetic isotope effects of the subsequent branching reactions.

3.2 Clumped and position-specific measurements

The results for clumped and position specific measurements of N_2O from bacterial denitrifiers are consistent with the preliminary results described in Magyar et al. (2016) and support an irreversible mechanism for the synthesis of N_2O at the step involving NO reductase, but also suggest a role for reversible reactions at other points in the biosynthetic pathway from NO_3^- to N_2O. SP, SP_{18}, and $\Delta(^{14}N^{15}N^{18}O+^{15}N^{14}N^{18}O)$ are all potentially influenced by both reversible and irreversible reactions, but SP will only record processes during or after the synthesis of the N-N bond. In contrast, SP_{18} and $\Delta(^{14}N^{15}N^{18}O+^{15}N^{14}N^{18}O)$ will record processes starting at the time that the $^{15}N^{18}O$ bond is first made, including initial synthesis of nitrate (i.e., prior to any reaction that occurs in our experiments), equilibrium exchange reactions between N oxides and water, and the selective N-O bond-breaking reactions in the reduction of nitrate and nitrite.

In these results we observe compelling relationships between SP and both time and $\delta^{18}O$ (Figures 3, 4). Both these correlations are somewhat surprising, as there are so many possible confounding variables. The correlation between SP and time has a p-value of 0.016. As time increases, ^{15}N site preference approaches the modelled ^{15}N site preference for the nitric oxide reductase enzyme that is described in Chapter 2 of this thesis; as time approaches 0, the ^{15}N site preferences approaches 0‰. Since the enzyme binding model is based on an equilibrium between bound and unbound NO molecules, it fits that if allowed more time, the result is the closest to this equilibrium result, while when the reaction proceeds more quickly, the discrimination between the two iron sites in the cNOR enzyme disappears. A similar correlation is observed between $\Delta(^{14}N^{15}N^{18}O+^{15}N^{14}N^{18}O)$ and time (Figure 5), albeit with a p-value of 0.06. This trend does not make a close approach to the result of the cNOR model, and its closest approach is at the shortest times, which is the opposite of the result observed for SP.

The most compelling relationship observed in these results is the relationship between SP_{18} and $\Delta(^{14}N^{15}N^{18}O+^{15}N^{14}N^{18}O)$, which is shown in Figure 6. As noted above, both these parameters provide records of all processes as far back as there has been an N–O bond in the molecule. Here that means that they bear the imprint of the ^{15}N-^{18}O content of the nitrate or nitrite that was provided as a substrate, and then of the processes of nitrate and nitrite reduction that preceded NO reduction. It is also noteworthy that neither SP_{18} (Figure 7) nor $\Delta(^{14}N^{15}N^{18}O+^{15}N^{14}N^{18}O)$ exhibit a statistically significant correlation with SP (p-values of 0.13 and 0.12). Since SP only records events at or after the formation of the N–O bond, this lack of correlation suggests that whatever gives rise to the covariance between

SP_{18} and $\Delta(^{14}N^{15}N^{18}O+^{15}N^{14}N^{18}O)$ occurs before the NO reduction step. This relationship includes samples generated from both nitrate and nitrite, and from species with distinct nitrite reductase enzymes, which suggest that whatever sets this trend is independent of the isotopic composition of the substrate, occurs after nitrate reduction but before nitric oxide reduction, and does not depend on the specific identity of the nitrite reductase enzyme.

Looking at the end members of this trend in more detail, one extreme of this trend has a value of $\Delta(^{14}N^{15}N^{18}O+^{15}N^{14}N^{18}O)$ between 0 and 1 ‰, which is in the range of low temperature equilibrium for N oxides (Wang et al., 2004; Schauble et al., 2006) and plausibly could be controlled by exchange between an N oxide intermediate and water. The other extreme of this trend is characterized by negative values in $\Delta(^{14}N^{15}N^{18}O+^{15}N^{14}N^{18}O)$, meaning the overall abundance of species containing both a ^{15}N and an ^{18}O is less than random probability. It is less obvious how such a signature could be made (the 'selection rule' effects hypothesized by Yeung (2016) do not apply here because the clumping index in question involves two different elements and non-equivalent sites).

3.3 Isotopologue signature of fungal P450nor

The clumped and position specific composition of N_2O generated by the fungal NO reductase, P450nor, is distinct from that generated by bacterial denitrifiers (Figures 2-3). Its ^{15}N site preference (36.8±0.7‰) is quite similar to nearly all previous results measured for N_2O from pure cultures of fungal denitrifiers (Sutka et al., 2008; Rohe et al., 2014). Its combined SP, SP_{18}, and $\Delta(^{14}N^{15}N^{18}O+^{15}N^{14}N^{18}O)$ signature could be interpreted as a single coherent temperature of 80˚C (i.e., all three indices are consistent with mutual equilibrium at that temperature). However, the samples were produced at room temperature; the self-

consistency of these three parameters must be a coincidence. Its ^{15}N site preference is also quite similar to N_2O generated from hydroxylamine oxidation by ammonia oxidizers or by abiotic reactions (Toyoda et al., 2015), which suggest possible mechanistic similarities to these processes. Also, these samples were generated by a purified enzyme, not by the complete process of fungal denitrification; the parameters SP_{18} and $\Delta(^{14}N^{15}N^{18}O+^{15}N^{14}N^{18}O)$ may be expected to be quite different for the complete fungal denitrification process.

5. Conclusion

Measurement of six isotopic constraints N_2O from bacterial denitrifiers and a fungal P450nor enzyme support the conclusion that the N_2O synthesis reaction at both bacterial cNOR and fungal P450nor nitric oxide reductase enzymes is irreversible and the ^{15}N site preference recorded in natural samples generated by denitrifiers reflects the kinetics of this reaction. But both oxygen and clumped isotopic measurements suggest a role for reversible reaction in earlier steps of denitrification.

References

Affek H. P. and Eiler J. M. (2006) Abundance of mass 47 CO_2 in urban air, car exhaust, and human breath. *Geochim. Cosmochim. Acta* **70,** 1–12.

Bigeleisen J. (1949) The Relative Reaction Velocities of Isotopic Molecules. *J. Chem Phys.* **17,** 675–678.

Bigeleisen J. and Mayer M. G. (1947) Calculation of Equilibrium Constants for Isotope Exchange Reactions. *J. Chem. Phys.* **15,** 261–267.

Bigeleisen J. and Wolfsberg M. (1958) Theoretical and Experimental Aspects of Isotope Effects in Chemical Kinetics. *Adv. Chem. Phys.* **1,** 15–76.

Blomberg M. R. A. and Siegbahn P. E. M. (2012) Mechanism for N_2O Generation in Bacterial Nitric Oxide Reductase: A Quantum Chemical Study. *Biochemistry* **51,** 5173–5186.

Bonner F. and Bigeleisen J. (1952) Non-exchange of Oxygen between Water and Some Compounds of Nitrogen. *J. Am. Chem. Soc.* **74,** 4944–4945.

Brandes J. A., Devol A. H., Yoshinari T., Jayakumar D. A. and Naqvi S. W. A. (1998) Isotopic composition of nitrate in the central Arabian Sea and eastern tropical North Pacific: A tracer for mixing and nitrogen cycles. *Limnol. Oceanogr.* **43,** 1680–1689.

Buchwald C. and Casciotti K. L. (2013) Isotopic ratios of nitrite as tracers of the sources and age of oceanic nitrite. *Nat. Geosci.* **6,** 308–313.

Casciotti K. L. (2009) Inverse kinetic isotope fractionation during bacterial nitrite oxidation. *Geochim. Cosmochim. Acta* **73,** 2061–2076.

Casciotti K. L., Böhlke J. K., McIlvin M. R., Mroczkowski S. J. and Hannon J. E. (2007) Oxygen Isotopes in Nitrite: Analysis, Calibration, and Equilibration. *Anal. Chem.* **79,** 2427–2436.

Casciotti K. L., Sigman D. M., Hastings M. G., Böhlke J. and Hilkert A. (2002) Measurement of the oxygen isotopic composition of nitrate in seawater and freshwater using the denitrifier method. *Anal. Chem.* **74**, 4905–4912.

Cliff S. S. and Thiemens M. H. (1997) The $^{18}O/^{16}O$ and $^{17}O/^{16}O$ Ratios in Atmospheric Nitrous Oxide: A Mass-Independent Anomaly. *Science* **278,** 1774–1776.

Clog M., Martini A., Lawson M. and Eiler J. (2014) Doubly ^{13}C-substituted ethane in shale gases, Goldschmidt Conference. *Mineralogical Magazine,* Sacramento, CA, p. 435.

Eiler J. M., Clog M., Magyar P., Piasecki A., Sessions A., Stolper D., Deerberg M., Schueter H.-J. and Schwieters J. (2013) A high-resolution gas-source isotope ratio mass spectrometer. *Int. J. Mass Spectrom.* **335,** 45–56.

Eiler J. M., Bergquist B., Bourg I., Cartigny P., Farquhar J., Gagnon A., Guo W., Halevy I., Hofmann A., Larson T. E., Levin N., Schauble E. A. and Stolper D. (2014) Frontiers of stable isotope geoscience. *Chem. Geol.* **372,** 119–143.

Fehling C. (2012) Mechanistic Insights from the ^{15}N-Site Preference of Nitrous Oxide utilizing High Resolution Near-Infrared *cw* Cavity Ringdown Spectroscopy and Density Functional Theory Calculations. Ph. D. thesis, Kiel Univ.

Fehling C. and Friedrichs G. (2011) Dimerization of HNO in Aqueous Solution: An Interplay of Solvation Effects, Fast Acid–Base Equilibria, and Intramolecular Hydrogen Bonding? *J. Am. Chem. Soc.* **133,** 17912–17922.

Frame C. H. and Casciotti K. L. (2010) Biogeochemical controls and isotopic signature of nitrous oxide production by a marine ammonia-oxidizing bacterium. *Biogeosciences* **7,** 2695–2709.

Granger J., Sigman D. M., Lehmann M. F. and Tortell P. D. (2008) Nitrogen and oxygen fractionation during dissimilatory nitrate reduction by denitrifying bacteria. *Limnol. Oceanogr.* **53,** 2533–2545.

Hayes, J. M. (2001) Fractionation of carbon and hydrogen isotopes in biosynthetic processes. *Rev. Mineral. Geochem.* **43,** 193–200.

Heil J., Wolf B., Brüggemann N., Emmenegger L., Tuzson B., Vereecken H. and Mohn J. (2014) Site-specific ^{15}N signatures of abiotically produced N_2O. *Geochim. Cosmochim. Acta* **139,** 72–82.

Hino T., Matsumoto Y., Nagano S., Sugimoto H., Fukumori Y., Murata T., Iwata S. and Shiro Y. (2010) Structural Basis of Biological N_2O Generation by Bacterial Nitric Oxide Reductase. *Science* **330**, 1666–1670.

Hu S. (1993) Resonance Raman Spectroscopic Studies of the Nitric Oxide Adducts of Cobaltous-Reconstituted Myoglobin and Hemoglobin. *Inorg. Chem.* **32,** 1081–1085.

Kaiser J., Hastings M. G., Houlton B. Z., Röckmann T. and Sigman D. M. (2007) Triple Oxygen Isotope Analysis of Nitrate Using the Denitrifer Method and Thermal Decomposition of N_2O. *Anal. Chem.* **79,** 599–607.

Kim K.-R. and Craig H. (1993) Nitrogen-15 and Oxygen-18 Characteristics of Nitrous Oxide: A Global Perspective. *Science* **262,** 1855–1857.

Kaneko M. and Poulson S. R. The oxygen isotope exchange between nitrate and water. *Geochim. Cosmochim. Acta* **118,** 148–156.

Kool D. M., Wrage N., Oenema O., Dolfing J., Van Groenigen J. W. (2007) Oxygen exchange between (de)nitrification intermediates and H_2O and its implications for source determination of NO_3^- and N_2O: a review. *Rapid Commun. Mass Spectrom.* **21,** 3569–3578.

Kool D. M., Wrage N., Oenema O., Van Kessel C., Van Groenigen J. W. (2011) Oxygen exchange with water alters the oxygen isotopic signature of nitrate in soil ecosystems. *Soil Biol. Biochem.* **43,** 1180–1185.

Magyar P. M., Orphan, V. J. and Eiler, J. M. (2016) Measurement of rare isotopologues of nitrous oxide by high-resolution multi-collector mass spectrometry. *Rapid Commun. Mass Spectrom.* **30,** 1923–1940.

Martin T. S. and Casciotti K. L. (2016) Nitrogen and oxygen isotopic fractionation during microbial nitrite reduction. *Limnol. Oceanogr.* **61,** 1134–1143.

Mariotti A., Germon J. C., Hubert P., Kaiser P., Letolle R., Tardieux A. and Tardieux P. (1981) Experimental Determination of Nitrogen Kinetic Isotope Fractionation: Some

Principles; Illustration for the Denitrification and Nitrification Processes. *Plant and Soil* **62,** 413–430.

Matsumura H., Hayashi T., Chakraborty S., Lu Y. and Moënne-Loccoz P. (2014) The Production of Nitrous Oxide by the Heme/Nonheme Diiron Center of Engineered Myoglobins (Fe_BMbs) Proceeds through a *trans*-Iron-Nitrosyl Dimer. *J. Am. Chem. Soc.* **136,** 2420–2431.

McIlvin M. R. and Casciotti K. L. (2011) Technical Updates to the Bacterial Method for Nitrate Isotopic Analyses. *Anal. Chem.* **83**, 1850–1856.

McQuarters A. B., Wirgau N. E. and Lehnert N. (2014) Model complexes of key intermediates in fungal cytochrome P450 nitric oxide reductase (P450nor). *Curr. Opin. Chem. Biol.* **19,** 82–89.

Richet P., Bottinga Y. and Javoy M. (1977) A Review of Hydrogen, Carbon, Nitrogen, Oxygen, Sulphur, and Chlorine Stable Isotope Fractionation among Gaseous Molecules. *Annu. Rev. Earth Planet Sci.* **5,** 65–110.

Riplinger C. and Neese F. (2011) The Reaction Mechanism of Cytochrome P450 NO Reductase: A Detailed Quantum Mechanics/Molecular Mechanics Study. *ChemPhysChem* **12,** 3192–3203.

Rohe L., Anderson T.-H., Braker G., Flessa H., Giesemann A., Lewicka-Szczebak D., Wrange-Mönnig N. and Well R. (2014) Dual isotope and isotopomers signatures of nitrous oxide from fungal denitrification – a pure culture study. *Rapid Commun. Mass Spectrom.* **28,** 1893–1903.

Saenger C., Affek H. P., Felis T., Thiagarajan N., Lough J. M. and Holcomb M. (2012) Carbonate clumped isotope variability in shallow water corals: Temperature dependence and growth-related vital effects. *Geochim. Cosmochim. Acta* **99,** 224–242.

Schauble E. A., Ghosh P. and Eiler J. M. (2006) Preferential formation of ^{13}C-^{18}O bonds in carbonate minerals, estimated using first-principles lattice dynamics. *Geochim. Cosmochim. Acta* **70,** 2510–2529.

Shiro Y., Sugumoto H., Tosha T., Nagano S. and Hino T. (2010) Structural basis for nitrous oxide generation by bacterial nitric oxide reductases. *Phil. Trans. Roy. Soc. B* **367,** 1195–1203.

Stein L. Y. and Yung Y. L. (2003) Production, Isotopic Composition, and Atmospheric Fate of Biologically Produced Nitrous Oxide. *Annu. Rev. Earth Planet Sci.* **31,** 329–356.

Stolper D. A., Lawson M., Davis C. L., Ferreira A. A., Santos Netos E. V., Ellis G. S., Lewan M. D., Martini A. M., Tang Y., Schoell M., Sessions A. L. and Eiler J. M. (2014) Formation temperatures of thermogenic and biogenic methane. *Science* **344,** 1500–1503.

Stolper D. A., Martini A. M., Clog M., Douglas P. M., Shusta S. S., Valentine D. L., Sessions A. L. and Eiler J. M. (2015) Distinguishing and understanding thermogenic and biogenic sources of methane using multiply substituted isotopologues. *Geochim. Cosmochim. Acta* **161,** 219–247.

Sutka R. L., Ostrom N. E., Ostrom P. H., Gandhi H. and Breznak J. A. (2003) Nitrogen isotopomer site preference of N_2O produced by *Nitrosomonas europaea* and *Methylococcus capulatus* Bath. *Rapid Commun. Mass Spectrom.* **17,** 738–745.

Sutka R. L., Ostrom N. E., Ostrom P. H., Gandhi H. and Breznak J. A. (2004) Erratum: Nitrogen isotopomer site preference of N_2O produced by *Nitrosomonas europaea* and *Methylococcus capulatus* Bath. *Rapid Commun. Mass Spectrom.* **18,** 1411–1412.

Sutka R. L., Adams G. C., Ostrom N. E. and Ostrom P. H. (2008) Isotopologue fractionation during N_2O production by fungal denitrification. *Rapid Commun. Mass Spectrom.* **22,** 3989–3996.

Thiagarajan N., Adkins J. and Eiler J. (2011) Carbonate clumped isotope thermometry of deep-sea corals and implications for vital effects. *Geochim. Cosmochim. Acta* **75,** 4416–4425.

Toyoda S., Mutobe H., Yamagishi H., Yoshida N. and Tanji Y. (2005) Fractionation of N_2O isotopomers during production by denitrifier. *Soil Biol. Biochem.* **37,** 1535–1545.

Toyoda S., Yoshida Y. and Koba K. (2015) Isotopocule analysis of biologically produced nitrous oxide in various environments. Mass Spectrom. Rev. doi:10.1002/mas.21459, 1–26.

Urey H. C. (1947) The Thermodynamic Properties of Isotopic Substances. J. Chem. Soc., 562–581

Wang Z., Schauble E. A. and Eiler J. M. (2004) Equilibrium thermodynamics of multiply substituted isotopologues of molecular gases. *Geochim. Cosmochim. Acta* **68,** 4779–4797.

Wang D. T., Gruen D. S., Lollar B. S., Hinrichs K.-U., Stewart L. C., Holden J. F., Hristov A. N., Pohlman J. W., Morrill P. L., Könneke M., Delwiche K. B., Reeves E. P., Sutcliffe C. N., Ritter D. J., Seewald J. S., McIntosh J. C., Hemond H. F., Kubo M. D., Cardace D., Hoehler T. M. and Ono S. (2015) Nonequilibrium clumped isotope signatures in microbial methane. *Science* **348,** 428–431.

Yang H., Gandhi H., Ostrom N. E. and Hegg E. L. (2014) Isotopic Fractionation by a Fungal P450 Nitric Oxide Reductase during Production of N_2O. *Environ. Sci. Technol.* **48,** 10707–10715.

Yamazaki T., Hozuki T., Arai K., Toyoda S., Koba K., Fujiwara T. and Yoshida N. (2014)

Isotopomeric characterization of nitrous oxide produced by reaction of enzymes extracted from nitrifying and denitrifying bacteria. *Biogeosciences* **11,** 2679–2689.

Yeung L. Y. (2016) Combinatorial effects on clumped isotopes and their significance in biogeochemistry. *Geochim. Cosmochim. Acta* **172,** 22–38.

Yeung L. Y., Ash J. L. and Young E. D. (2015) Biological signatures in clumped isotopes of O_2. *Science* **348,** 431–434.

Zumft W. G. (1997) Cell biology and molecular basis of denitrification. *Microbiology and Molecular Biology Reviews* **61**, 533–616.

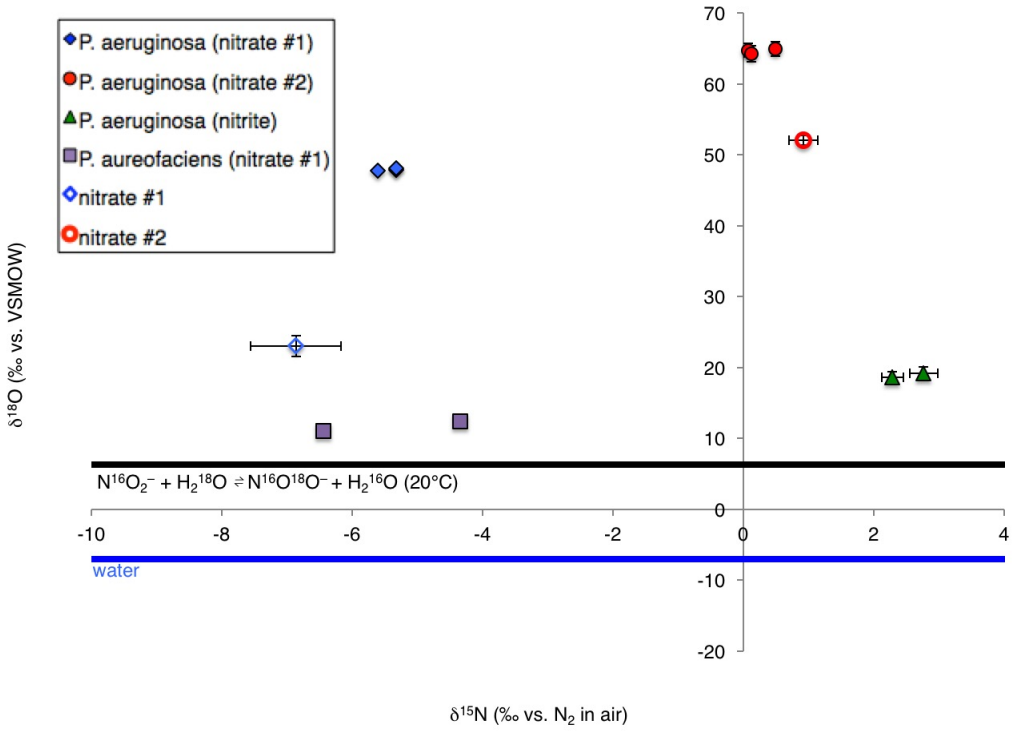

Fig. 1. $\delta^{15}N$-$\delta^{18}O$ for N_2O from bacterial denitrifiers. For cultures grown on nitrate, $\delta^{15}N$ measurements suggest nearly complete conversion of that nitrate to N_2O. The range in oxygen isotope composition is due to the combination of kinetic and equilibrium effects as illustrated in Fig. 2.

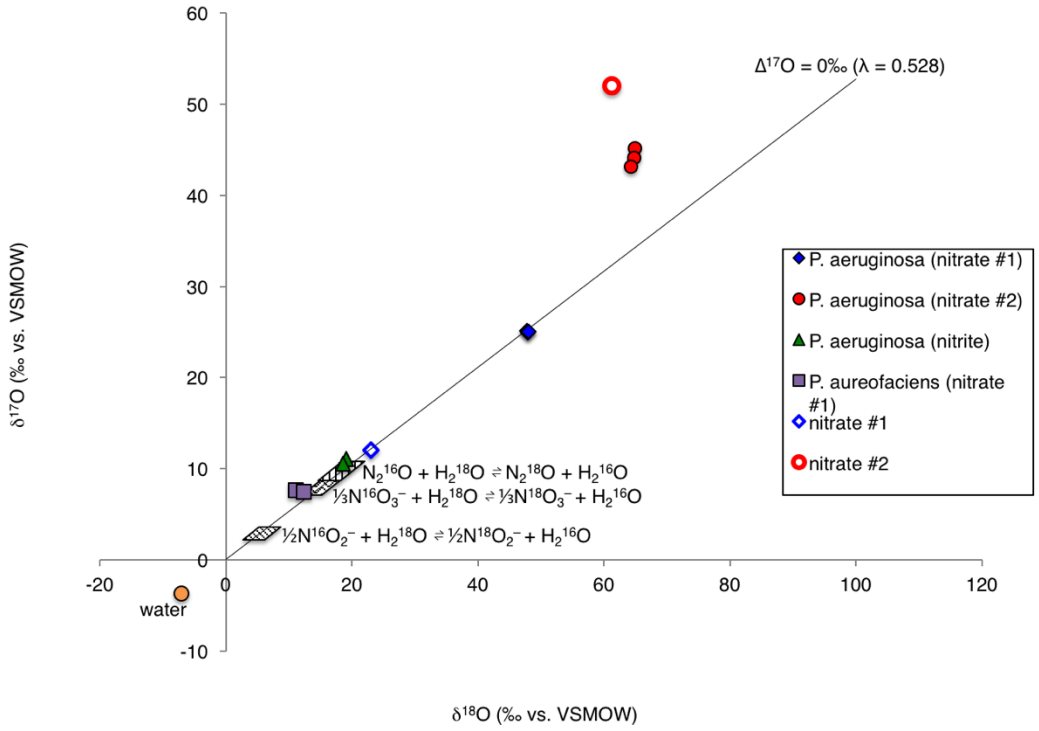

Fig. 2. $\delta^{17}O$-$\delta^{18}O$ for N_2O from bacterial denitrifiers. The oxygen isotope composition of N_2O samples is controlled by varying contributions from the composition of sources (hollow symbols), branching isotope effects, and equilibrium with water (shaded boxes), which can be quantitatively apportioned as described in the main text.

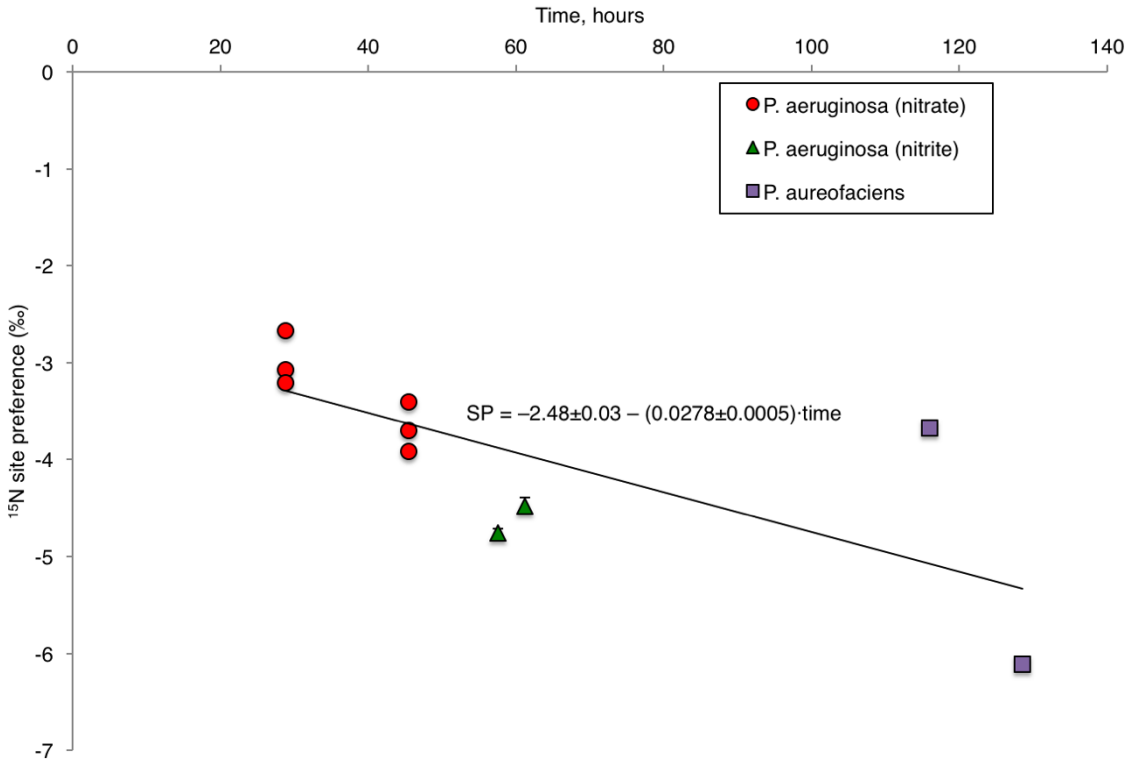

Fig. 3. Variation of SP with time. This relationship holds across samples produced by two different species, as well as those grown with both nitrate and nitrite as a starting substrate. It makes its closest approach to the predicted steady-state SP for cNOR (–7.4‰; chapter 2, this thesis) at the longest times and approaches 0‰ as time approaches 0, consistent with the hypothesis that the reversible binding effect described in chapter 2 is washed out when denitrification is happening at a faster rate.

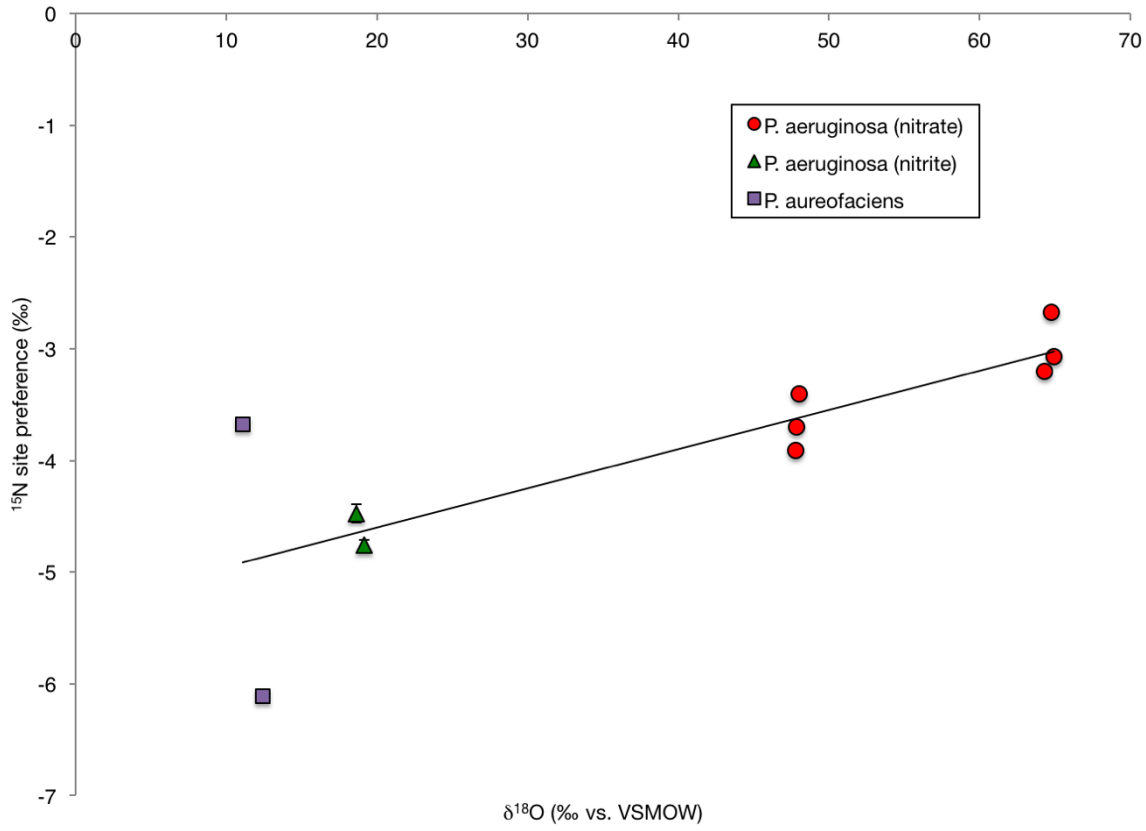

Fig. 4. Variation of SP with $\delta^{18}O$.

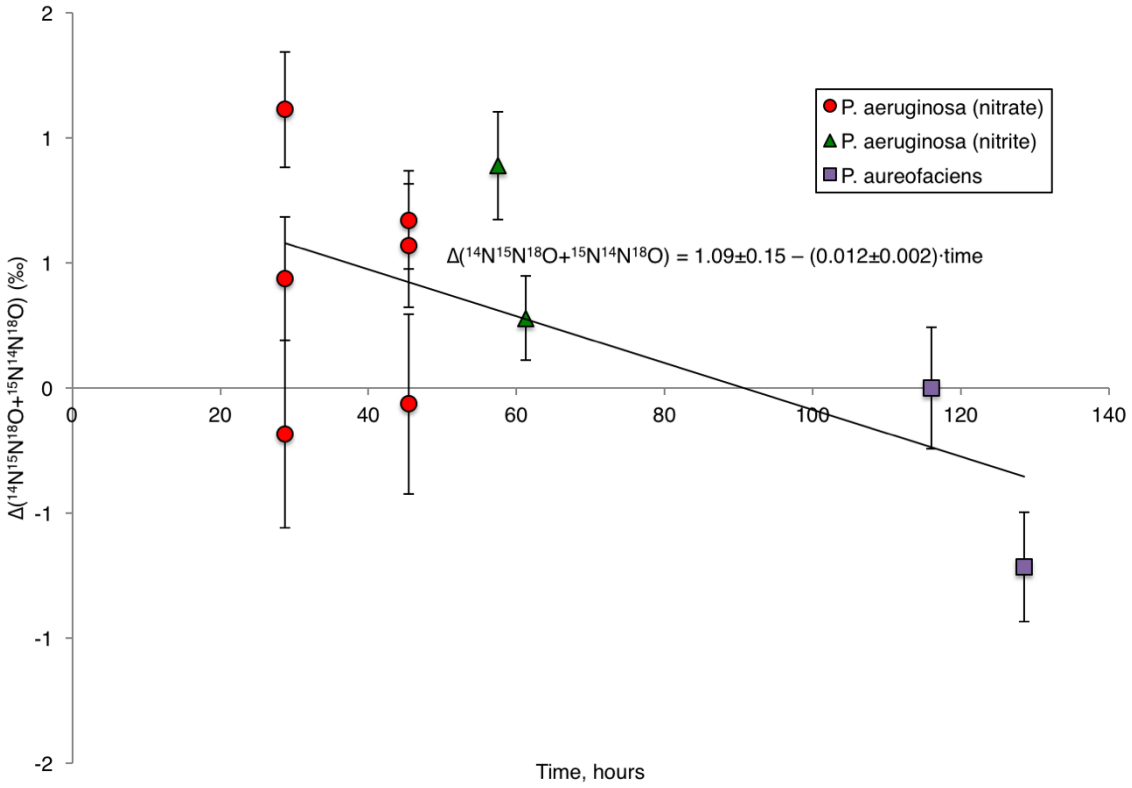

Fig. 5. Variation of $\Delta(^{14}N^{15}N^{18}O+^{15}N^{14}N^{18}O)$ with time.

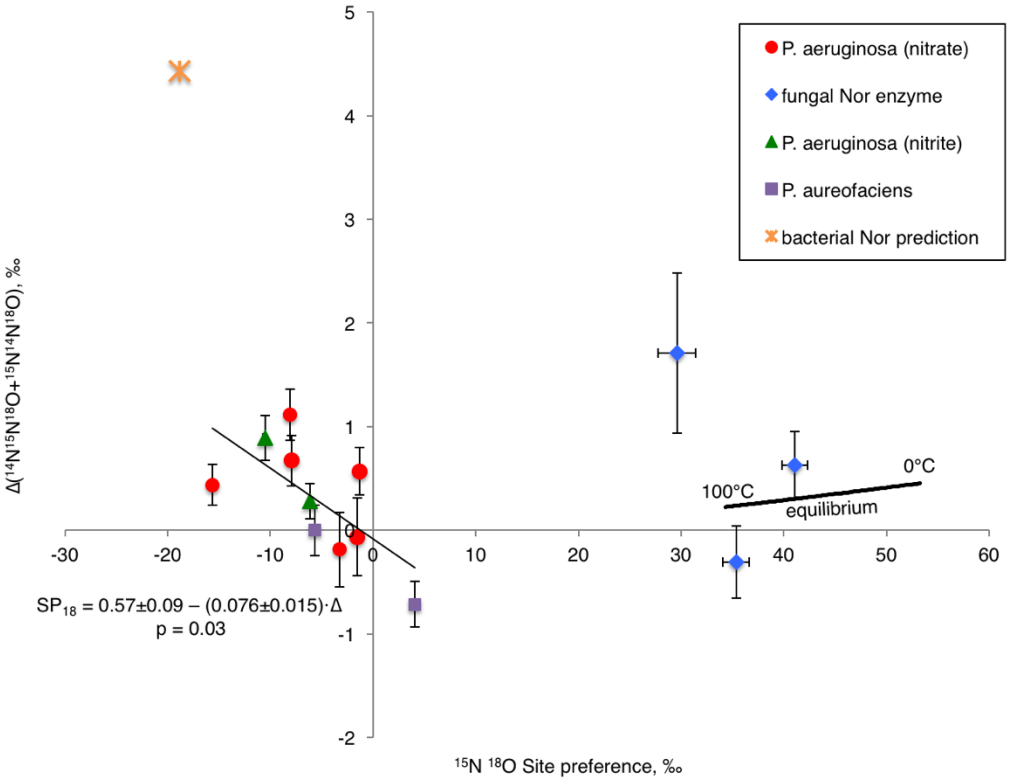

Fig. 6. The clumped isotopic composition of N_2O. The predominant feature of recorded by the two clumped isotopic parameters SP_{18} and $\Delta(^{14}N^{15}N^{18}O+^{15}N^{14}N^{18}O)$ is likely the processing of nitrate, nitrite, and nitric oxide in the earlier steps of denitrification properties, but the N-N bond forming reaction, is also likely to be recorded.

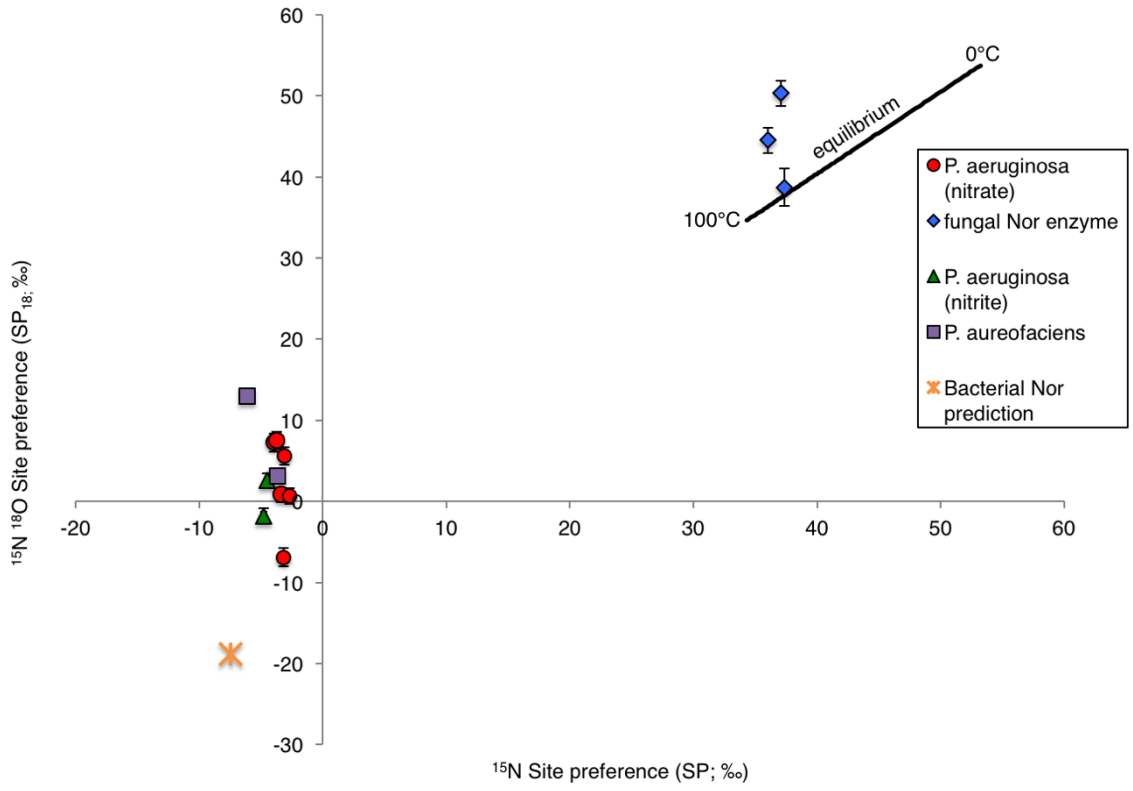

Fig. 7. Position specific composition of N_2O. The two position-specific parameters SP and SP_{18} both reflect that irreversible reactions control the final composition of N_2O generated by both bacterial denitrifiers and a fungal NO reductase enzyme (P450nor). SP_{18} may also record information about the history of $^{15}N^{18}O$ bonds that are incorporated into N_2O but have been formed and processed in earlier reactions.

Chapter 4

CLUMPED ISOTOPE MEASUREMENTS OF NITROUS OXIDE FROM AMMONIA OXIDIZING BACTERIA REVEAL THREE DISTINCT MECHANISMS OF N_2O GENERATION

Introduction

Ammonia oxidizing bacteria (AOB) have long been known to produce nitrous oxide (N_2O) (Falcone et al., 1963), which is a greenhouse gas (Yung et al., 1976; Myrhe et al., 2013), a major depleter of tropospheric ozone (Ravishankara et al., 2009), and a principal fingerprint of the anthropogenic disruption of the nitrogen cycle (Canfield et al., 2010). The AOB have been shown to be responsible for N_2O production in both terrestrial and marine settings, and to be stimulated by anthropogenic nitrogen addition (Freing et al., 2012; Zhu et al., 2013).

The ammonia oxidizing bacteria grow by chemoautotrophic oxidation of ammonia (NH_3) to nitrite (NO_2^-) by oxygen (O_2), with hydroxylamine (NH_2OH) as an intermediate. These steps are performed by the enzymes ammonia monooxygenase (Amo) and hydroxylamine oxidase (Hao), respectively. Nitrous oxide is not involved in energy conservation for the metabolism; any N_2O generation is the result of either a detoxification mechanism or accidental leakage. But there are (at least) three possible mechanisms for N_2O generation by the AOB; N_2O can be produced from hydroxylamine, nitrite, or nitric oxide. Further the possible mechanisms may mix variously under stresses, including low O_2, high or low pH, or build-up of intermediates including nitrite and hydroxylamine. Therefore it remains unclear what mechanisms are most important in environmental settings.

The best characterized N_2O generating mechanism in the AOB is nitrifier denitrification. In this pathway, the nitrite generated by ammonia oxidation is converted to N_2O via the enzymes nitrite reductase (NIR) and nitric oxide reductase (NOR) from the heterotrophic denitrification pathway. This mechanism is not thought to be used for metabolism, but is instead likely a way to deplete toxic accumulations of nitrite (Wrage et al., 2001). Nitrifier denitrification has been shown to be a significant source of N_2O in both terrestrial and marine environments, especially in fertilized soils (Wrage et al., 2001; Kool et al., 2011; Zhu et al., 2013).

A second set of mechanisms focuses on hydroxylamine (NH_2OH), which is the product of the oxidation of ammonia by oxygen at the ammonia mono-oxygenase (Amo) enzyme. In turn it is reduced by the hydroxylamine oxidase (Hao) enzyme, with nitrite as the final product of the process. N_2O generation associated with this process has long been observed (Hooper and Terry, 1979) (Kozlowski et al., 2016). Hydroxylamine addition to pure cultures of AOB has been shown to stimulate N_2O production (Kozlowski et al., 2016), and the Hao enzyme has also been shown to catalyze the generation of N_2O from NH_2OH (Hooper and Terry, 1979; Yamazaki et al., 2014). Furthermore, NH_2OH can also be oxidized to N_2O abiotically by various metals (Heil et al., 2014). Finally, recent work has shown that a cytochrome (cyt) P460 oxidase present in some AOB generates N_2O from hydroxylamine under both aerobic and anaerobic conditions, with N_2O the exclusive product under anaerobic conditions (Caranto et al., 2016). There is also a growing body of work that supports the generation of nitrous oxide via abiotic reactions involving nitrite (Kopf et al., 2013; Jones et al., 2015; Zhu-Barker et al., 2015; Buchwald et al., 2016; Grabb et al., 2017).

These reactions can be catalyzed by mineral surfaces or organic ligands; it is also imaginable that in a living cell they can be catalyzed by any number of proteins.

Stable isotope measurements of N_2O provide useful constraints on its sources. There are now abundant measurements of three parameters related to ammonia oxidizing bacteria: $\delta^{15}N$, $\delta^{18}O$, and ^{15}N site preference[5]. The $\delta^{15}N$ has been shown to be quite depleted no matter the mechanism of N_2O generation, mostly reflecting a large isotopic fractionation imparted by the oxidation of NH_3 (Yoshida, 1988; Casciotti et al., 2010; Frame and Casciotti, 2010). The $\delta^{18}O$ appears to vary with mechanism, making it possible to draw a distinction between O atoms derived from water and O_2 (Casciotti et al., 2010; Frame and Casciotti, 2010). The ^{15}N site preference is quite useful for distinguishing among mechanisms of N_2O generation, with samples derived from nitrifier denitrification falling into the same –10‰ to –0‰ range as bacterial denitrifiers, while samples derived from hydroxylamine are generally between 35‰ and 40‰ (Sutka et al., 2003; Sutka et al., 2004; Sutka et al., 2006; Frame and Casciotti, 2010; Yamazaki et al., 2014). Many natural samples fall between these two end-member compositions and may are typically attributable to a mixture between these two classes of processes.

In this study we use high resolution mass spectrometry to add three additional isotopic constraints: $\delta^{17}O$, and the clumped isotopic parameters $\Delta(^{14}N^{15}N^{18}O+^{15}N^{14}N^{18}O)$ and SP_{18}. These clumped isotopic parameters are are defined as

[5] $\delta = (R/R_{ref} - 1)x1000$, where $R=^{15}N/^{14}N$, $^{17}O/^{16}O$, or $^{18}O/^{16}O$, and R_{ref} refers to N_2 in air for $\delta^{15}N$ and VSMOW for $\delta^{17}O$ and $\delta^{18}O$. The ^{15}N site preference has conventionally been defined as $SP = \delta^{15}N^{\alpha} - \delta^{15}N^{\beta}$; here it is defined instead as $SP = (^{15}R^{\alpha}/^{15}R^{\beta} - 1)\bullet 1000$

$$\Delta_{^{14}N^{15}N^{18}O+^{15}N^{14}N^{18}O} = \left(\frac{R_{^{14}N^{15}N^{18}O+^{15}N^{14}N^{18}O}}{R^{*}_{^{14}N^{15}N^{18}O+^{15}N^{14}N^{18}O}} - 1 \right) \cdot 1000.$$

$$SP_{18} = \left(\frac{R_{^{14}N^{15}N^{18}O}}{R_{^{15}N^{14}N^{18}O}} - 1 \right) \cdot 1000.$$

Together these two parameters completely describe the abundance of the two isotopologues $^{14}N^{15}N^{18}O$ and $^{15}N^{14}N^{18}O$ (Magyar et al., 2016). One way of describing the comparative utility of these various isotopic parameters is that the bulk isotopic composition ($\delta^{15}N$ and $\delta^{18}O$) tracks the progress of atoms through various chemical and physical processes, while the clumped and position-specific parameters of SP, SP_{18}, and $\Delta(^{14}N^{15}N^{18}O+^{15}N^{14}N^{18}O)$ track bonds. SP starts 'recording' when the asymmetry that makes for distinct central and outer N positions is introduced, while SP_{18} and $\Delta(^{14}N^{15}N^{18}O+^{15}N^{14}N^{18}O)$ start recording at the formation of the N–O bond that ends up N_2O and continue recording through the synthesis of the N_2O molecule. All three parameters will also reflect processes by which N_2O is consumed. Another distinction between the bulk isotopic measurements and the position specific and clumped measurements is that the latter can be set by homogeneous equilibrium reactions—if a sample of N_2O is allowed to reach isotopic equilibrium with itself, the composition of all three of these parameters can predicted solely based on the temperature of equilibration (Bigeleisen and Friedman, 1950; Wang et al., 2004; Webb and Miller, 2014; Magyar et al., 2016).

We applied clumped isotope analysis of N_2O as a new tool for distinguishing amongst N_2O generation mechanisms in the ammonia oxidizing bacteria. By applying the methods described by Magyar et al. (2016) we were able to a bulk, position-specific, and clumped-

isotopic composition for each sample studied. To better distinguish among the various processes that the AOB are capable of we worked with three different AOB species that have been shown to have different assortments of the enzymes associated with N_2O generation. Specifically, *Nitrosospira communis* lacks a nitrite reductase and appears incapable of performing nitrifier denitrification, while *Nitrosomonas multiformis* lacks the cyt P460 proposed as a direct pathway from NH_2OH to N_2O (Kozlowski et al., 2016). The third species, *Nitrosomonas europaea*, has the full complement of N_2O-associated enzymes (Kozlowski et al., 2014; Kozlowski et al., 2016). For comparison to the N_2O generated by the AOB, we also measured samples generated by abiotic reduction of nitrite with iron and from the oxidation of NH_2OH by a purified cyt P460 enzyme. Finally, we compare these experimental results, as well as those reported in Magyar et al. (2016) and in chapter 3 of this thesis, to N_2O generated by incubations of worm castings to attempt to use this stable isotope approach to assign the N_2O source in those simple environmental systems.

Methods

Cultivation of ammonia oxidizing bacteria

We grew three species of ammonia oxidizing bacteria, *Nitrosomonas europaea*, *Nitrosomonas communis*, and *Nitrosospira multiformis*. Culture stocks were provided by J. A. Kozlowski and L. Y. Stein of the University of Alberta. *Nitrosomonas europaea* was grown in ATCC medium 2265. To prepare this medium, three separate solutions were prepared and then filter sterilized and collected in a common 1 L bottle. Solution 1 contained, in 800 mL Nanopure water 3.30 g $(NH_4)_2SO_4$, 0.41 g KH_2PO_4, 0.18 g $MgSO_4 \cdot 7H_2O$, 27 mg $CaCl_2 \cdot 2H_2O$, 0.13 mg $CuSO_4 \cdot 5H_2O$, and 330 μL of 30 mM $FeSO_4$ stock solution in 50 mM

EDTA. Solution 2 contained, in 200 mL Nanopure water, 5.47 g KH_2PO_4 and 0.47 g NaH_2PO_4, and was adjusted to a pH of 8.0 by addition of NaOH. Solution 3, in 8 mL, contained 0.40 g Na_2CO_3. *Nitrosomonas communis* and *Nitrosospira multiformis* were cultivated in HK medium (15 mM HEPES, 5 mM $(NH_4)_2SO_4$, 1 mM $CaCl_2 \cdot 2H_2O$, 1 mM KCl, 0.2 mM $MgSO_4 \cdot 7H_2O$, 0.4 mM KH_2PO_4, 1 mL of a AOB trace elements solution (Verhagen and Laanbroek, 1991), and 2 mL of a 0.02% w/v phenol red solution). To prepare 1 L of this medium, these constituents were dissolved in 800 mL of nanopure water, the pH was adjusted in 7 by addition of 1M NaOH, after which the final 200 mL of Nanopure water was added. The medium was stirred ~30 minutes before filter sterilization.

Importantly, as noted above, *N. europaea* was grown in 50 mM ammonium sulfate, while *N. communis* and *N. multiformis* were grown in 5 mM ammonium sulfate. Cultures were maintained in the dark in a 28°C incubator, shaking at 60 rpm, in open capped bottles that allow free exchange of oxygen. For N_2O generation experiments, cultures were grown in either 1 L or 2 L Pyrex bottles containing 500 mL to 1 L of medium. These large cultures were inoculated by addition of 10% by volume of a growing culture. The bottles were sealed with a rubber stopper, with atmospheric air as their headspace. Each bottle included a magnetic stir-bar and was slowly stirred to permit the oxygen in the headspace to mix into the liquid culture. Bottles were maintained at room temperature on the benchtop and were wrapped in foil to exclude light. Periodically, 10% w/w $NaHCO_3$ was added to these cultures to maintain a pH of ~7 to 8; the pH was monitored by test strips and by phenol red dye, which turned yellow when the pH became acidic.

Growth of these cultures was monitored by measurement of OD_{600}. In later experiments, these measurements also included a spectrometric determination of nitrite

concentrations. Measurements of the headspace gas composition by GC-TCD in the Environmental Analysis Center at Caltech provided the N_2O concentration and the N_2/O_2 ratio.

Sample harvest and cleaning

Samples were harvested from these AOB cultures using a custom headspace purging apparatus. A needle made from 1/8" steel tubing was used to puncture the rubber septum of the culture. This needle delivered a stream of helium at ~10 mL/min into the bottle. A second needle collected the outflow from the headspace, which was passed across dryerite and Ascarite to remove water and CO_2, respectively. Then the gas stream was passed through two glass traps submerged in liquid nitrogen, in which N_2O, plus any remaining water, CO_2, and condensable contaminants, was collected. Typical samples were harvested for 3 hours; the harvest was only concluded when a GC-TCD measurement of the headspace showed that all appreciable N_2O had been collected. The gases collected in the traps were concentrated on a vacuum line and cleaned as described below.

Iron experiments

Ferrous iron and nitrite were reacted in a chemostat to produce nitrous oxide. The chemostat was filled to a reaction volume of about 500 mL with a continuously refreshed medium that contained 5 mM ferrous ammonium sulfate hexahydrate ($Fe(NH_4)_2(SO_4)_2 \bullet 6H_2O$), 50 mM Na-PIPES as a pH buffer and 10 mM sodium citrate as a ligand (Kopf et al., 2013); the pH of this medium was adjusted to 7 by addition of NaOH. To this medium was added sodium nitrate from a 25 mM stock solution. The steady-state concentration of iron and nitrite was estimated to be 3.3 mM and 2.8 mM, respectively, at 25°C. The

headspace of this bottle was continually flushed with helium at a rate of ~20 mL/min. After allowing the reactor to reach steady state the gaseous outflow was passed through glass traps immersed in liquid nitrogen to cryogenically collect nitrous oxide, CO_2, water, and other volatile species condensable at –196°C; in each experiment gases were collected for ~4 hours. This experiment was performed at 10°C, 25°C, and 40°C, but only the 40°C condition yielded enough nitrous oxide for analysis. After collection, gases were transferred to a glass vacuum line for cleaning as described below.

Nitrous oxide was also generated from ferrous iron and nitrite in a series of three batch incubations in 160 mL bottles. These experiments were performed in a sterile buffer solution containing 30 mM Na-PIPES and 10 mM NaCl, set to a pH of 8.0 by addition of NaOH; these conditions were modified from those used by Jones et al. (Jones et al., 2015). To each bottle, 10 mM ferrous chloride tetrahydrate and 2 mM sodium nitrite was added. In addition, to some bottles, 10 mM sodium citrate was added. Bottles were split between 28°C and 37°C shaking incubators. After ~16 hours, GC-TCD showed nearly complete conversion of nitrite to nitrous oxide, which was collected by gastight syringe or sparging line as described above and cleaned as described below.

Cytochrome P460 Samples

Cytochrome (cyt) P460 samples were provided by J. Caranto and K. Lancaster of Cornell University. They were prepared in 5 mL septum-capped bottles of anaerobic 250 mM phosphate buffer by incubating 10 μM purified cyt p460, 10 mM NH_2OH, and 10-15 mM DCPIP at a pH of 8.0 and at room temperature. N_2O was collected from these incubation

bottles at Caltech by repeatedly expanding their headspace into a locking 5 mL syringe and then injecting the collected gases into a vacuum line, where they were cleaned as described below.

Sample preparation

Before analysis, all samples were cleaned on a vacuum line by repeated passage over Ascarite and a slurry of dry ice and ethanol, thereby removing CO_2, water, and various organic contaminants. Samples were also frozen into liquid nitrogen and exposed to vacuum, thereby removing He, N_2, O_2, and other contaminants that do not condense at –196°C. Samples were flame-sealed into glass tubes for storage and later introduction to the mass spectrometer.

Mass spectrometry measurements

The six-parameter isotopic composition of all samples was measured on the Thermo MAT253 Ultra, as described in Magyar et al. (Magyar et al., 2016). A brief summary of those methods follows. After collection and cleaning, purified N_2O is introduced into the bellows of the mass spectrometer. For each sample, a series of scans across the ion beams for NO (masses 30 to 33) and N_2O was collected to evaluate the presence of various contaminant ions. The measurement included eight acquisitions each for NO and N_2O, each with 10 cycles between sample and standard (which were each integrated 10 s per cycle). After each acquisition, background scans were collected near the measurement position of the peak of interest to remove the contributions of contaminants that underlie the measured ion beam. Finally, a measurement of the N_2O/CO_2 ratio was made at mass 44 to evaluate the potential for contributions from $^{13}C^{16}O_2$ to the $\delta^{15}N$ measurement at mass 45.

Results and Discussion

For all measured AOB samples, the $\delta^{15}N$ was strongly negative, falling between –28‰ and –60‰. This result is typical of N_2O generated by the AOB and is suggestive of the large isotope effect imparted during ammonia oxidation by the Amo enzyme (Yoshida, 1988; Casciotti et al., 2010; Frame and Casciotti, 2010). The $\delta^{18}O$ compositions ranges from 6‰ to 28‰, consistent with oxygen either derived from nitrite that is in equilibrium with water or from atmospheric oxygen (Casciotti et al., 2010; Frame and Casciotti, 2010; Buchwald and Casciotti, 2013). And the ^{15}N site preference also varies from –8.5‰, a typical value for nitrifier denitrification, to 37.6‰, a typical value for N_2O derived from hydroxylamine (Frame and Casciotti, 2010).

The results from the the position-specific and clumped parameters are most interesting when compared to bulk isotopic parameters. As seen in Figure 1, AOB samples have co-varying $\delta^{18}O$ and SP values. The low values of both parameters match N_2O that is generated from nitrifier denitrification in which the nitrite has fully exchanged its oxygen isotopes with water; the upper right end of the trend agrees with the expectation for N_2O that has been generated from NH_2OH, with the O atoms derived from O_2 from air. The particular AOB species at each endmember also conform with our expectations: *N. communis*, which seems to lacks the ability to perform nitrifier denitrification (Kozlowski et al., 2016), has a SP-$\delta^{18}O$ composition indicative of NH_2OH oxidation, while *N. multiformis*, which has a complete nitrifier denitrification pathway, but does not have cyt P460 (Kozlowski et al., 2016), the proposed direct pathway from hydroxylamine to N_2O (Caranto et al., 2016),

produced N_2O that matches nitrifier denitrification. Then the *N. europaea* measurements are dispersed between these two endmembers; *N. europaea* has the full complement of N_2O generating pathways. Based on this plot alone we can interpret these results as a simple mixture between two processes.

But expanding our view to the clumped isotope dimensions complicates this interpretation. As shown in Figure 2, when SP_{18} is plotted against $\delta^{18}O$ the single trend for AOB samples observed in SP vs. $\delta^{18}O$ splits into two branches. The left branch, with predominately negative SP_{18}, values extends from the result for *N. communis* that is attributed to hydroxylamine oxidation to the results for *N. multiformis* associated with nitrifier denitrification. The right branch extends from the *N. multiformis* to positive SP_{18} values. Also along this branch is the N_2O generated by abiotic reduction of iron and nitrite at steady state in a chemostat. Notably, the N_2O from this experiment also falls into a similar range as biogenic samples in the plot of SP vs. $\delta^{18}O$ (Figure 1), as do results from previously published experiments (Jones et al., 2015; Buchwald et al., 2016; Grabb et al., 2017). We hypothesize that a similar abiotic process (likely mediated by cellular materials) is responsible for the N_2O produced by *N. europaea* that lies along this branch. The elevated $\delta^{18}O$ may reflect a kinetic isotope effect for ^{18}O in this abiotic process. We also note that N_2O generated from the reaction of iron and nitrite in batch experiments has a much lower SP than observed in the chemostat experiment or in similar studies published previously(Jones et al., 2015; Buchwald et al., 2016); this likely reflects the isotopic signature of very fast N_2O generation by this mechanism. Finally, the SP signature of N_2O generated by cyt P460 is consistent with the biological samples associated with NH_2OH oxidiation; the

SP_{18} and $\Delta(^{14}N^{15}N^{18}O+^{15}N^{14}N^{18}O)$ do not match the culture results, likely because these parameters are set at other points in the N_2O biosynthesis pathway. This situation is analogous to the case of the fungal P450NOR N_2O discussed in chapter 3.

Further support to the idea of three N_2O generating pathways is provided by plotting $\delta^{15}N$ against SP (Figure 3) and SP_{18} (Figure 4). In each of these spaces, AOB samples match the expectation for N_2O derived from ≥3 process. In particular, Figure 3 shows a two branched pattern similar to Figure 2, but with samples from *N. multiformis* and *N. communis* having the heaviest $\delta^{15}N$ values and *N. europaea* samples that are likely to be associated with direct nitrite reduction having the most depleted $\delta^{15}N$ values.

Conclusions and Future Prospects

The combination of bulk, position-specific, and clumped isotopic analyses of N_2O generated by the AOB reveals three pathways of N_2O generation in these samples. By combining these isotopic results with genetic information and with the results of abiotic experiments, we propose that these three pathways are nitrifier denitrification, direct hydroxylamine oxidation to N_2O, and the non-enzymatic reduction of nitrite. The identification of three sources of N_2O generation even in a relatively simple set of culture experiments highlight the difficulty of identifying N_2O generation pathways in complex natural settings. The isotopic tools used in this work have a high prospect of utility in identifying N_2O generated by different pathways in these settings

References

Bigeleisen J. and Friedman L. (1950) The Infra-Red Spectra of $N^{15}N^{14}O^{16}$ and $N^{14}N^{15}O^{16}$. Some Thermodynamic Properties of the Isotopic N_2O Molecules. *J. Chem. Phys.* **18**, 1656–1659.

Buchwald C. and Casciotti K. L. (2013) Isotopic ratios of nitrite as tracers of the sources and age of oceanic nitrite. *Nat. Geosci.* **6**, 308–313.

Buchwald C., Grabb K., Hansel C. M. and Wankel S. D. (2016) Constraining the role of iron in environmental nitrogen transformations: Dual stable isotope systematics of abiotic NO^{2-} reduction by Fe(II) and its production of N_2O. *Geochim. Cosmochim. Acta* **186**, 1–12.

Canfield D. E., Glazer A. N. and Falkowski P. G. (2010) The Evolution and Future of Earth's Nitrogen Cycle. *Science*.

Caranto J. D., Vilbert A. C. and Lancaster K. M. (2016) Nitrosomonas europaea cytochrome P460 is a direct link between nitrification and nitrous oxide emission. *Proc Natl Acad Sci USA* **113**, 14704–14709.

Casciotti K. L., Buchwald C., Santoro A. E. and Frame C. (2010) Chapter Eleven - Assessment of Nitrogen and Oxygen Isotopic Fractionation During Nitrification and Its Expression in the Marine Environment. *Methods in Enzymology: Research on Nitrification and Related Processes, Part A* **486**, 253–280.

Falcone A. B., Shug A. L. and Nicholas D. (1963) Some properties of a hydroxylamine oxidase from *Nitrosomonas europaea*. *Biochim. Biophys. Acta*.

Frame C. and Casciotti K. L. (2010) Biogeochemical controls and isotopic signatures of nitrous oxide production by a marine ammonia-oxidizing bacterium. *Biogeosci.* **7**, 2695–2709.

Freing A., Wallace D. W. R. and Bange H. W. (2012) Global oceanic production of nitrous oxide. *Philosophical Transactions of the Royal Society B: Biological Sciences* **367**, 1245–1255.

Grabb K. C., Buchwald C., Hansel C. M. and Wankel S. D. (2017) A dual nitrite isotopic investigation of chemodenitrification by mineral-associated Fe(II) and its production of nitrous oxide. *Geochim. Cosmochim. Acta* **196**, 388–402.

Heil J., Wolf B., Brüggemann N., Emmenegger L., Tuzson B., Vereecken H. and Mohn J. (2014) Site-specific ^{15}N isotopic signatures of abiotically produced N_2O. *Geochim. Cosmochim. Acta* **139**, 72–82.

Hooper A. B. and Terry K. R. (1979) Hydroxylamine oxidoreductase of Nitrosomonas: Production of nitric oxide from hydroxylamine. *Biochimica et Biophysica Acta (BBA)-Enzymology*.

Jones L. C., Peters B., Lezama Pacheco J. S., Casciotti K. L. and Fendorf S. (2015) Stable Isotopes and Iron Oxide Mineral Products as Markers of Chemodenitrification. *Environ. Sci. Technol.* **49**, 3444–3452.

Kool D. M., Dolfing J., Wrage N. and Groenigen J. W. V. (2011) Nitrifier denitrification as a distinct and significant source of nitrous oxide from soil. *Soil Biol. Biochem.* **43**, 174–178.

Kopf S. H., Henny C. and Newman D. K. (2013) Ligand-Enhanced Abiotic Iron Oxidation and the Effects of Chemical versus Biological Iron Cycling in Anoxic Environments. *Environ. Sci. Technol.* **47**, 2602–2611.

Kozlowski J. A., Kits K. D. and Stein L. Y. (2016) Comparison of Nitrogen Oxide Metabolism among Diverse Ammonia-Oxidizing Bacteria. *Front. Microbiol.* **7**, 1090–1090.

Kozlowski J. A., Price J. and Stein L. Y. (2014) Revision of N2O-Producing Pathways in the Ammonia-Oxidizing Bacterium *Nitrosomonas europaea* ATCC 19718. *Appl. Environ. Microbiol.* **80**, 4930–4935.

Magyar P. M., Orphan V. J. and Eiler J. M. (2016) Measurement of rare isotopologues of nitrous oxide by high-resolution multi-collector mass spectrometry. *Rapid Commun. Mass Spectrom.* **30**, 1923–1940.

Myrhe G., Shindell D., Bréon F.-M., Collins W., Fuglestvedt J., Huang J., Koch D., Lamarque J.-F., Lee D., Mendoza B., Nakajima T., Robock A., Stephens G., Takemura T. and Zhang H. (2013) Anthropogenic and Natural Radiative Forcing. In *Climate Change 2013: The Physical Science Basis. Contribution of Working Group I to the Fifth Assessment Report of the Intergovernmental Panel on Climate Change* pp. 1–82.

Ravishankara A. R., Daniel J. S. and Portmann R. W. (2009) Nitrous Oxide (N2O): The Dominant Ozone-Depleting Substance Emitted in the 21st Century. *Science* **326**, 123–125.

Sutka R. L., Ostrom N. E., Ostrom P. H., Gandhi H. and Breznak J. A. (2004) Erratum: Nitrogen isotopomer site preference of N2O produced by Nitrosomonas europaea andMethylococcus capsulatus Bath. *Rapid Commun. Mass Spectrom.* **18**, 1411–1412.

Sutka R., Ostrom N., Ostrom P., Breznak J., Gandhi H., Pitt A. and Li F. (2006) Distinguishing nitrous oxide production from nitrification and denitrification on the basis of isotopomer abundances. *Appl. Environ. Microbiol.* **72**, 638.

Sutka R., Ostrom N., Ostrom P., Gandhi H. and Breznak J. (2003) Nitrogen isotopomer site preference of N2O produced by Nitrosomonas europaea and Methylococcus capsulatus Bath. *Rapid Commun. Mass Spectrom.* **17**, 738–745.

Verhagen F. J. and Laanbroek H. J. (1991) Competition for Ammonium between Nitrifying and Heterotrophic Bacteria in Dual Energy-Limited Chemostats. *Appl. Environ. Microbiol.* **57**, 3255–3263.

Wang Z., Schauble E. A. and Eiler J. M. (2004) Equilibrium thermodynamics of multiply substituted isotopologues of molecular gases. *Geochim. Cosmochim. Acta* **68**, 4779–4797.

Webb M. A. and Miller T. F. (2014) Position-specific and clumped stable isotope studies: comparison of the urey and path-integral approaches for carbon dioxide, nitrous oxide, methane, and propane. *J Phys Chem A* **118**, 467–474.

Wrage N., Velthof G. L., van Beusichem M. L. and Oenema O. (2001) Role of nitrifier denitrification in the production of nitrous oxide. *Soil Biol. Biochem.* **33**, 1723–1732.

Yamazaki T., Hozuki T., Arai K., Toyoda S., Koba K., Fujiwara T. and Yoshida N. (2014) Isotopomeric characterization of nitrous oxide produced by reaction of enzymes extracted from nitrifying and denitrifying bacteria. *Biogeosci.* **11**, 2679–2689.

Yoshida N. (1988) ^{15}N-depleted N_2O as a product of nitrification. *Nature* **335**, 528–529.

Yung Y. L., Wang W. C. and Lacis A. A. (1976) Greenhouse effect due to atmospheric nitrous oxide. *Geophys. Res. Lett.* **3**, 619–621.

Zhu X., Burger M., Doane T. A. and Horwath W. R. (2013) Ammonia oxidation pathways and nitrifier denitrification are significant sources of N_2O and NO under low oxygen availability. *Proc. Nat. Acad. Sci.* **110**, 6328–6333.

Zhu-Barker X., Cavazos A. R., Ostrom N. E., Horwath W. R. and Glass J. B. (2015) The importance of abiotic reactions for nitrous oxide production. *Biogeochem.* **126**, 251–267.

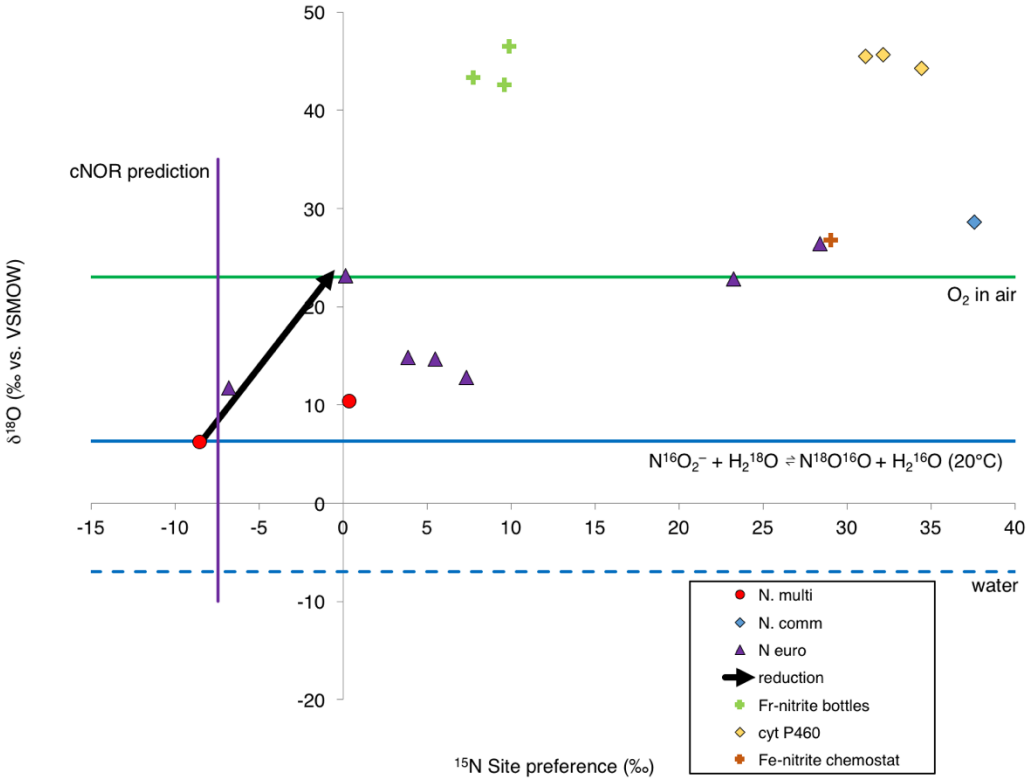

Figure 1. $\delta^{18}O$ vs. SP

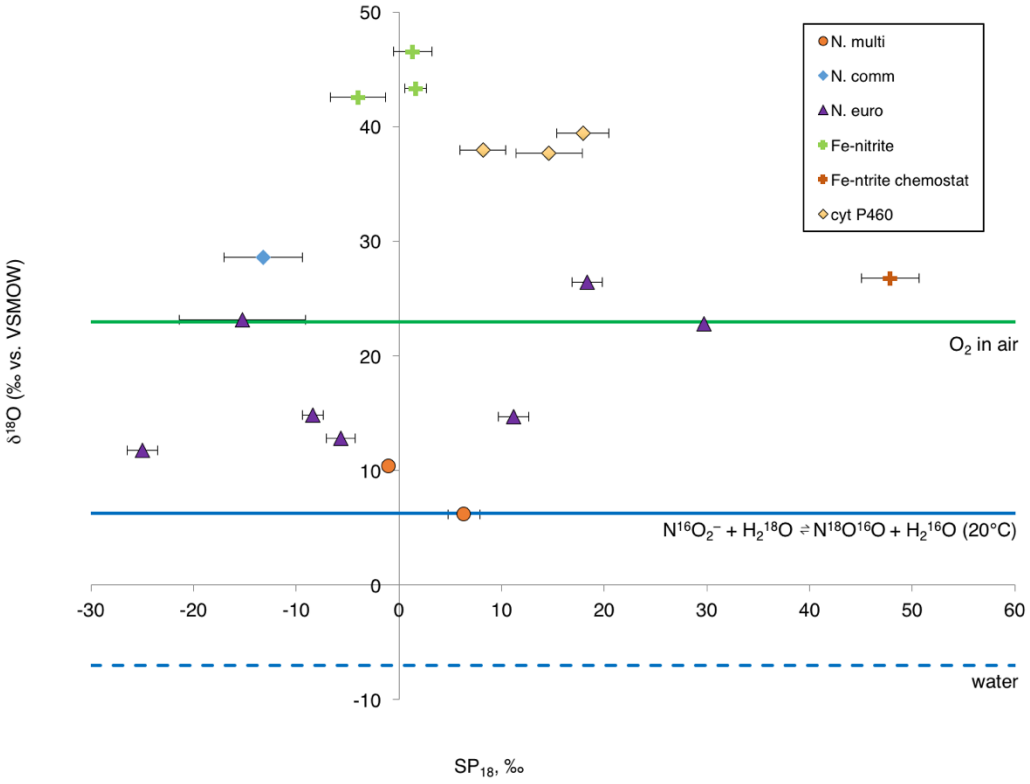

Figure 2. $\delta^{18}O$ vs. SP_{18}

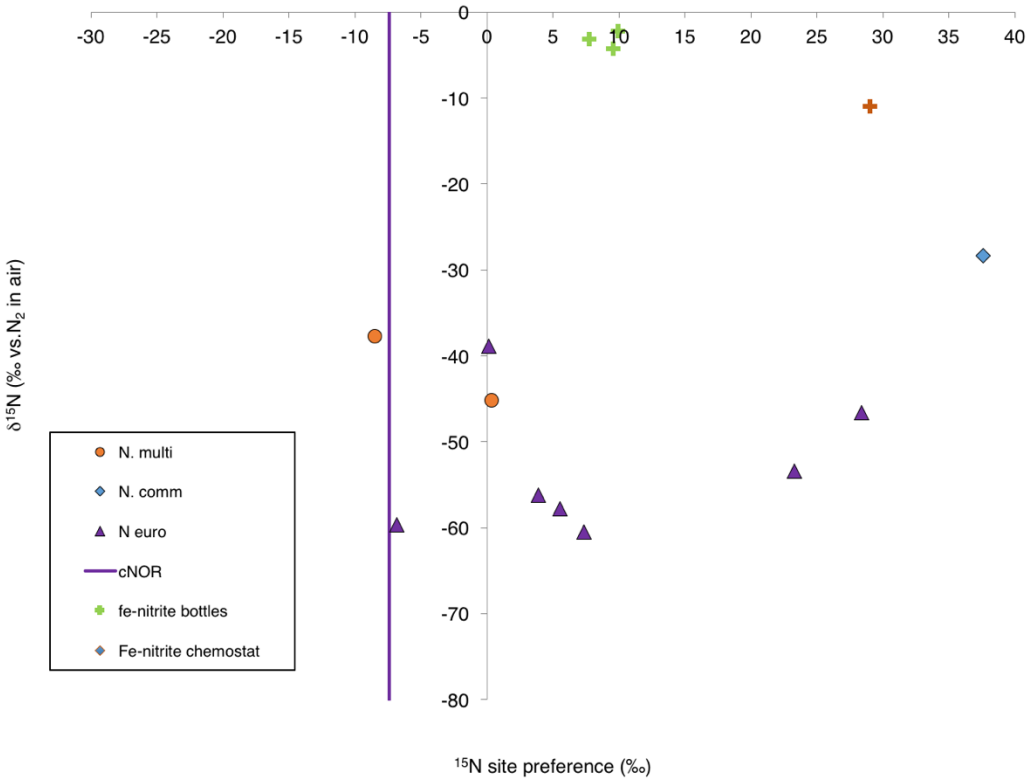

Figure 3. SP vs. $\delta^{15}N$

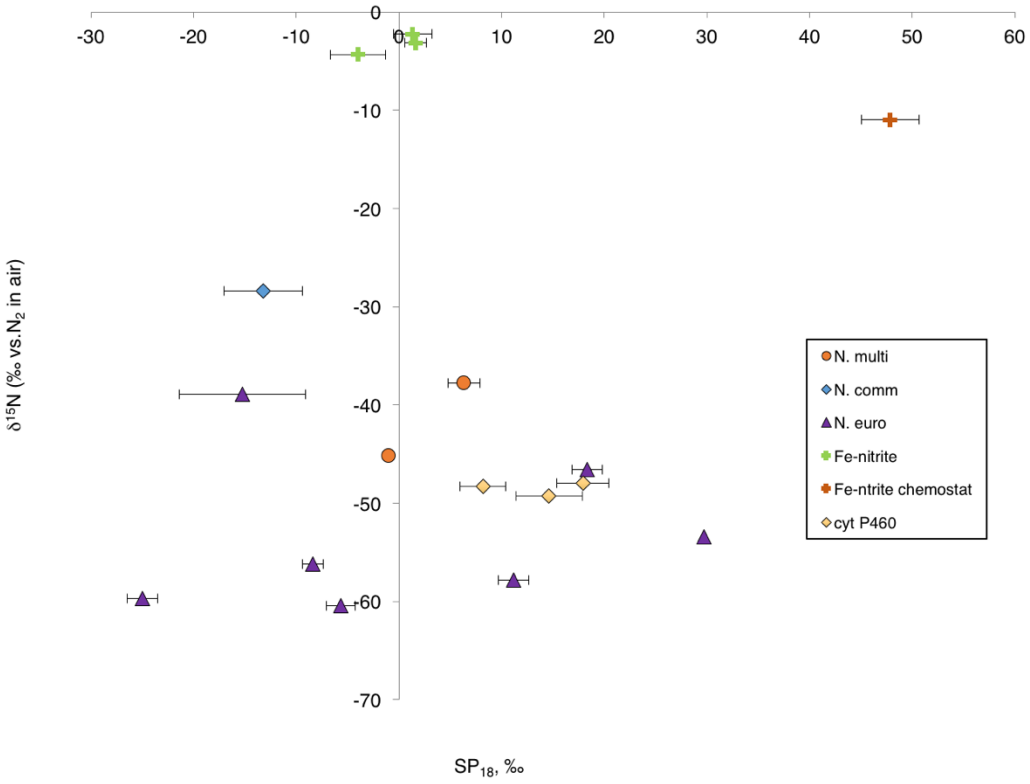

Figure 4. SP_{18} vs. $\delta^{15}N$

A p p e n d i x

NITROUS OXIDE FROM SEVERAL ENVIRONMENTAL SETTINGS

1. Nitrous oxide from worm castings.

To provide a first step towards evaluating nitrous oxide generation in a mixed environmental setting, we created incubations of worm castings. Commercially available earthworm castings (Encap, Green Bay, WI) and water were sealed into 250 mL and 1 L Pyrex bottles with a rubber stopper. The 250 mL incubation contained 113 g worm castings and 33 mL water; the 1 L incubation contained ~500 g worm castings and ~100 mL water. No additional nitrogen source was added. Equivalent dry incubations were also prepared, but were not observed to produce appreciable levels of N_2O. Using GC-TCD, as described in Chapter 4, the N_2O concentration and the N_2/O_2 ratio were monitored. The 250 mL incubation was sampled after 1 week, 2 weeks, and 2 years; the 1 L incubation was sampled at ~8 months and two years. By even the earliest sampling point no appreciable oxygen remained in the headspaces.

When measured after one week, the N_2O exhibited a strong imprint of nitrifier denitrification in bulk measurements ($\delta^{15}N$ = 55.18±0.02‰, 1 s.e.) and in clumped and position specific measurements (e.g., see Figure A1). After two weeks, the sample still reflects predominately nitrifier denitrification, but with contributions from a process that resembles abiotic iron oxidation by nitrite. After eight months the 1 L bottle matches well with this abiotic signature in SP, $SP_{18,}$ and $\delta^{18}O$. Finally, after two years both bottles have reached the highest values of ^{15}N site preference recorded in this study, approaching quite

close to equilibrium values (47‰ at 25°C). Yet, as shown in Figure A1, SP_{18} actually progress farther away from the equilibrium value. One important possibility to consider for these long-term results is that they reflect the storage of very high levels of N_2O in the presence of a complex soil matrix that may mediate either equilibrium or kinetic reaction.

2. Nitrous oxide from Lake Vida, Antarctica

We also measured N_2O from Lake Vida, Antarctica. Brine from Lake Vida was collected by N. Ostrom and coworkers (Ostrom et al., 2016) and stored in the laboratories at Michigan State University. Subsequently, N_2O was sparged and trapped from this brine and sent to us for analysis. We observed that all six isotopic parameters were consistent with mixing between two N_2O sources. This is illustrated in a plot of $\delta^{15}N$ vs. $\Delta^{17}O$ (Figure A2). Also shown are values from Savarino et al. (2007) for nitrate samples from Antarctica with exotic $\Delta^{17}O$; such materials have regularly been observed. These results support the conclusion of Ostrom et al. (2016) that chemodenitrification is responsible for the N_2O generation in these samples, but we are also able to draw the further conclusion that two different forms of chemodenitrification are occurring, one of which draws on a pool of $\Delta^{17}O$-enriched nitrate.

References

Ostrom N.E., Ganhdi H., Trubl G., and Murray A.E. (2016) Chemodenitrification in the cryoecosystem of Lake Vida, Victoria Valley, Antarctica. *Geobiology* **14,** 575–587.

Savarino J., Kaiser J., Morin S., Sigman D.M., Thiemens M.H. (2007) Nitrogen and oxygen isotopic constraints on the origin of atmospheric nitrate in coastal Antarctica. *Atmos. Chem. Phys.* **7,** 1925–1945.

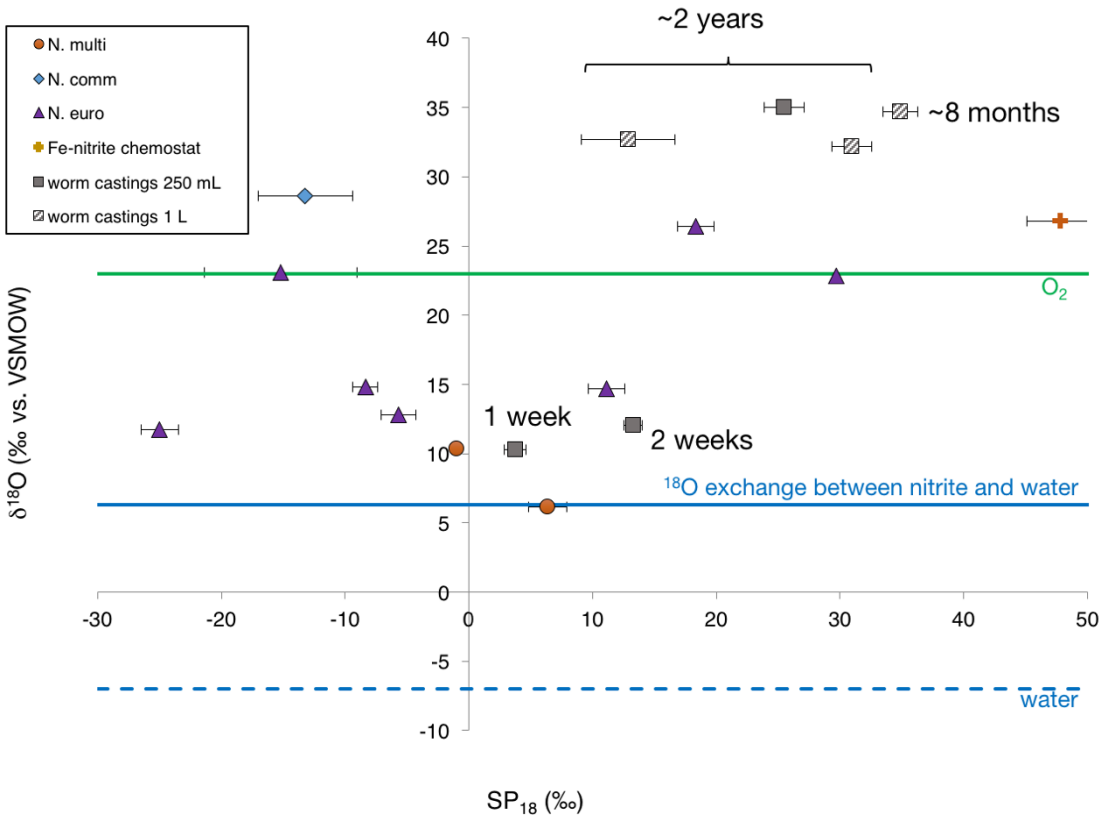

Figure A1. SP_{18}-$\delta^{18}O$ systematics of worm castings samples compared to ammonia oxidizing bacteria and abiotic nitrite reduction.

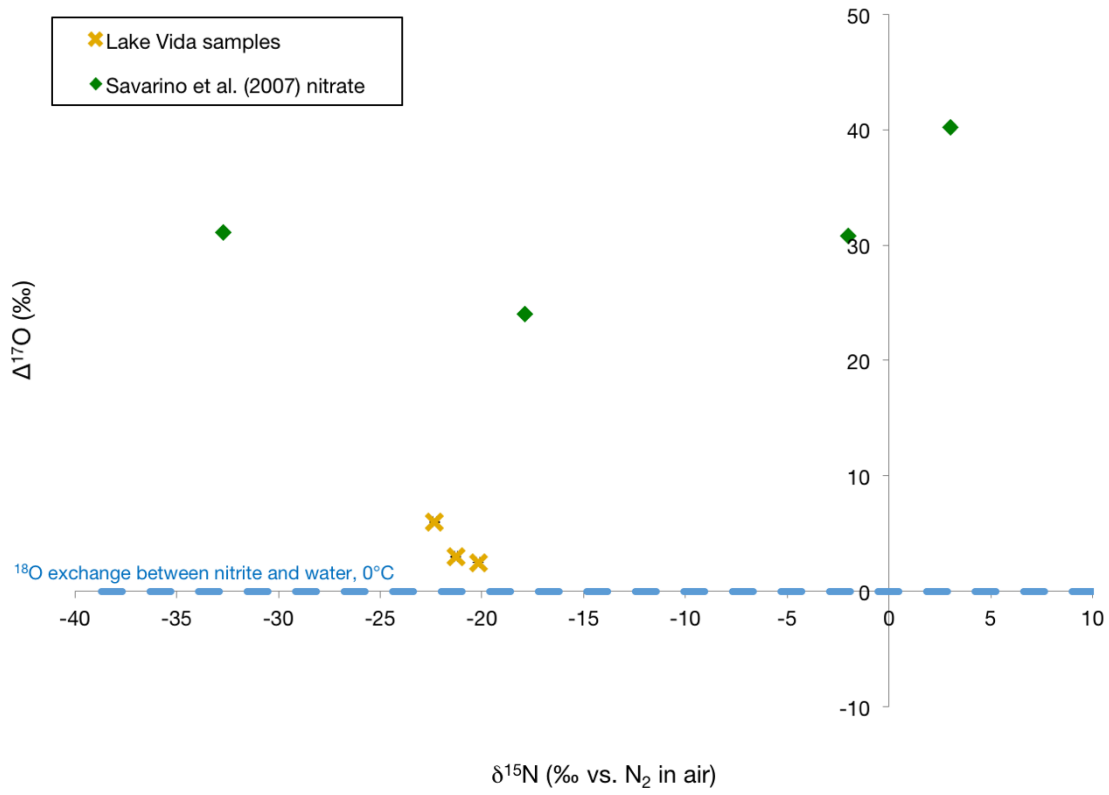

Figure A2. $\Delta^{17}O$ vs. $\delta^{15}N$ for nitrous oxide from Lake Vida brine, compared to Antarctic nitrate measurements from Savarino et al. (2007).